UNIVERSITY OF OKLAHOMA

GRADUATE COLLEGE

POLYVIOLOGEN-MODIFIED ANODES FOR CARBOHYDRATE BIOFUEL CELLS

A DISSERTATION

SUBMITTED TO THE GRADUATE FACULTY

in partial fulfillment of the requirements for the

Degree of

DOCTOR OF PHILOSOPHY

By

PINGMEI WANG
Norman, Oklahoma
2021

POLYVIOLOGEN-MODIFIED ANODES FOR CARBOHYDRATE BIOFUEL CELLS

A DISSERTATION APPROVED FOR THE
DEPARTMENT OF CHEMISTRY AND BIOCHEMISTRY

BY THE COMMITTEE CONSISTING OF

Dr. Daniel T. Glatzhofer, Chair
Dr. Steven P. Crossley
Dr. Wai Tak Yip
Dr. Yihan Shao

Acknowledgements

I would like to thank my Ph.D. Advisor, Dr. Daniel T. Glatzhofer. Prof. Glatzhofer has been an excellent mentor and advisor. I am deeply grateful for his patient and insightful guidance on my research and various academic activities. I would also like to thank my Ph.D. committee members, Dr. Steven P. Crossley, Dr.Wai Tak Yip, and Dr. Yihan Shao, as well as the former members Dr. Adam S. Duerfeldt, Dr. George B. Richter-Addo and Dr. Ann H. West. I thank my parents and husband for their love and support.

Contents

List of Figures

List of Tables

Abstract

Polyalkylviologens (PVC_n (n = 2 - 6)) were successfully deposited on glassy carbon electrodes (GCEs) by electropolymerization of α,Ω-bis(4-cyano-1-pyridino)-alkane dibromides (PyC_nBr_2 (n = 2 - 6)) as precursors. By studying the adsorption behavior of methyl, ethyl and propyl viologen in aqueous solutions, the polymerization pathway to form PVC_n (n = 2 and 3) is proposed to be reduction, coupling, eliminative viologen formation, and deposition, while PVC_n (n = 4, 5, and 6) are formed by reductive adsorption, coupling, and eliminative polyviologen formation. The electrochemical behaviours of PVC_5 and PVC_6 suggest they have relatively open, flexible structures.

PyC_5Br_2 was crosslinked by electrocopolymerization with 1,3,5-tris(4-cyanopyridinio-1-methyl)-2,4,6-trimethylbenzene tribromide ($PyBenMeBr_3$) to form viologen copolymers. The copolymer compositions were changed by using different concentrations of PyC_5Br_2 and $PyBenMeBr_3$ in the electropolymerization mixtures. Compared with no current response of PVC_5 after 50 successive scan cycles in pH 12 solution, the copolymer retained electrochemical activity. The copolymer, deposited onto three-dimensional carbon nanotube-modified GCE anodes, produced current densities up to 121.6 $\mu A/cm^2$ in fuel cells with a Pt/Nafion film cathode and in 5 mM glucose 0.1 M KCl solution at pH 9.7. On carbon felt anodes, the copolymer produced currents up to 587.9 μA and powers

up to 90.6 μW. Lowering the fuel cell solution to pH 8.1, the maximum current generated by the copolymer on carbon felt anodes decreased to 445.6 μA.

PyC_nBr_2 (n = 4, 5, and 6) was encapsulated by cucurbit[7]uril (CB[7]) to form PyC_nBr_2@CB[7] pseudorotaxanes. PyC_nBr_2@CB[7] were successfully polymerized to PVC_n@CB[7]. PVC_n@CB[7] showed slightly more negative redox potential shifts than PVC_n. PVC_5@CB[7]'s electrochemical activity is extremely stable in pH 12 aqueous solution. PVC_5@CB[7]-modified carbon felt anodes produced maximum currents of 585 μA and powers of 122 μW in a glucose fuel cell with a Pt/Nafion film cathode and in 5 mM glucose 0.1 M KCl solution at pH 9.7.

Chapter 1

Introduction

1.1 A Brief Introduction to Fuel Cells

1.1.1 Background

Since the Industrial Revolution, fossil fuels have become the most important energy source to meet human activities' growing demands. Fossil fuels, including coal, petroleum, and natural gas have been consumed in a way much faster than they were formed. For example, based on the U.S. Energy Information Administration, in 2019, the U.S. consumed around 8.5×10^{16} kJ of fossil fuels, which took millions of years to accumulate. Another problem of burning fossil fuels is the release of carbon dioxide (CO_2), which is the largest contributor to the greenhouse effect and global warming.[1] As both the energy demand and the effort on environmental protection grows, the topic of utilizing renewable energy has become more and more widespread.

Renewable energy devices, including solar cells, wind turbines, and fuel cells, have already played an important role in our daily life.[2] Among these devices,

fuel cells, which convert the chemical energy of fuels directly into electricity rather than through a combustion route, are widely studied and considered a promising alternative to traditional energy sources due to their simplicity, environmentally friendly nature, and efficient energy conversion rate. Similar to a battery, fuel cells supply power without a rotating generator. In addition, fuel cells generate electricity from various fuels and can be "refilled" or replenished continuously without any interruption to the system, while batteries such as lead-acid batteries have to store electricity with a long recharging time. Another advantage of fuel cells over an ordinary battery is that the fuel cells' size is flexible, making them suitable for many applications. For example, fuel cells have been used in engine scooters,[3] pacemakers,[4] drug delivery,[5] etc.

1.1.2 Working Principle of Fuel Cells

Though there exist various types of fuel cells, all of them work with the same principle. To better illustrate the working principle, a generalized schematic fuel cell is shown in Figure 1.1. Essentially a fuel cell consists of four parts: an anode (oxidation of fuels), a cathode (reduction of oxidants), an electrolyte (ionically conducting solutions), and an external circuit (passing electrons from anodes to cathodes). The driving force of a fuel cell is the potential difference between the anodic and cathodic reactions.

The fuel oxidation reaction occurs in the vicinity of the anode. In a typical fuel cell, catalysts or redox mediators modified on or around electrodes for both anodic and cathodic reactions are critical. The addition of catalysts or electron mediators improves the oxidation or reduction rate and accelerates the electron transfer efficiency between the reactant and electrodes, thereby improving the

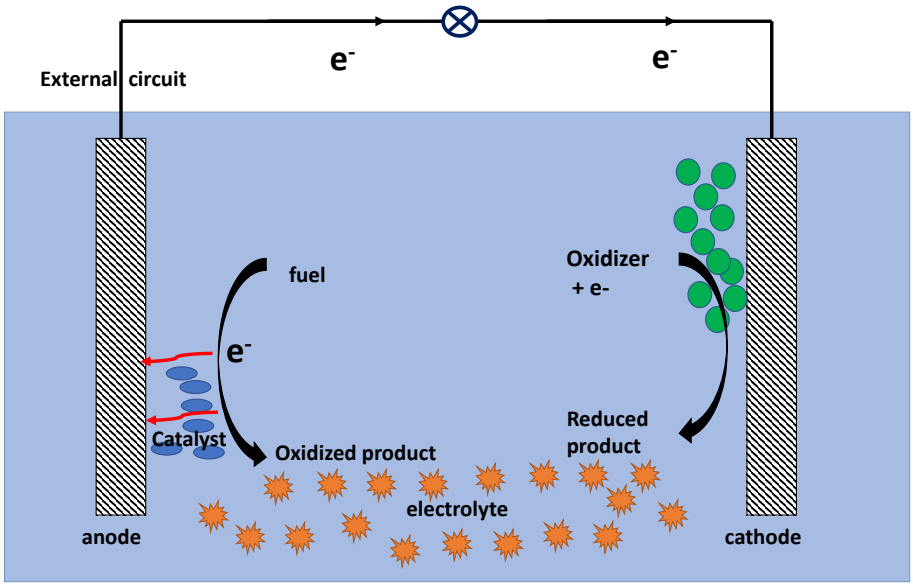

Figure 1.1: A simplified schematic representation of a fuel cell.

performance of a fuel cell.

For example, for a simple proton-exchange membrane fuel cell (PEMFC) as shown in Figure 1.2, platinum is used as the catalyst to absorb H_2, allowing its oxidation into 2 H^+ and transfers 2 e^- to the anode. The H^+s are transported to the cathode through the proton exchange membrane, which is typically a polymer. On the cathode, O_2 is reduced to H_2O after receiving protons and electrons. This simple H_2/O_2 fuel cell can produce a power density of 0.25 W/cm^2, with a current density around 0.5 A/cm^2 and an operating voltage of 0.5 V.[6]

The performance of a fuel cell is characterized by its output power P, output voltage E_{cell}, and current density J.[7] Power P is the product of cell voltage and current (current density J times effective area A). This relation can be expressed as

$$P = E_{\text{cell}} \times J \times A. \tag{1.1}$$

Usually, the maximum output voltage and the maximum current are measured as

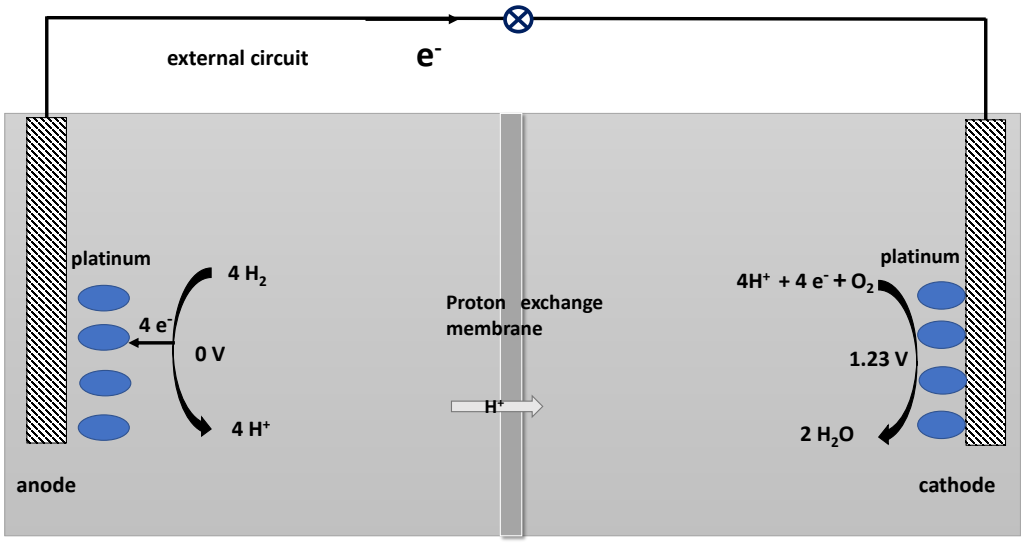

Figure 1.2: Schematic of a H_2/O_2 fuel cell that utilizes platinum as a catalyst. All redox potentials are vs. normal hydrogen electrode (NHE).

fuel cell performance indicators. Ideally, the maximum output voltage or open-circuit voltage (OCV) is the potential difference between the cathode reduction (E_C) and the anode oxidation (E_A). In practice, the OCV is considerably lower than the anodic and cathodic electrode potential difference due to overpotentials in the system. As an example, the theoretical OCV is 1.23 V for the fuel cell shown in Figure 1.2, while the measured OCV is ∼1.1 V. The maximum current or short circuit current (SCC) of a fuel cell is the peak current measured with a short external circuit (very low resistance). For the H_2/O_2 fuel cell fuel cell shown in Figure 1.2, the maximum current density is ∼0.8 A/cm^2.[6]

1.1.3 Types of Fuel Cells

Fuel cells are often categorized based on their fuels, electrolytes, etc. The most popular fuel cells include proton-exchange membrane fuel cells (PEMFCs), di-

rect methanol fuel cells (DMFCs), alkaline fuel cells (AFCs), biological fuel cells (BFCs), and carbohydrate fuel cells. Each category features its specific fuel, operating temperature & pH, and electrolyte.

PEMFCs are widely studied due to their relatively low operating temperature (80 °C), quick start without warming-up, and durability. They require pure hydrogen, oxygen, and water to operate and employ solid polymers that conduct protons but not electrons as electrolytes. Since PEMFCs are easily poisoned by carbon monoxide or sulfur impurities binding to the platinum catalyst at the anodes, much research has focused on finding alternative catalysts. A bibliometric analysis[8] showed that 1502 articles on this topic were published per year from 2008 to 2018. As reported,[9] PtV, PtCr, PtTi, and other Pt alloys enhance the activities of PEMFCs while maintaining output power densities as high as 0.91 W/cm^2.

An AFC is another type of fuel cell that oxidizes the substrate in an alkaline medium to achieve electricity production. Compared to PEMFCs, the advantages of AFC are that there is a wide range of fuel choices, including inorganic fuels, alcohols, and carbohydrates;[7,10] its catalysts are not limited to precious metals; and oxygen often shows high reaction kinetics in alkaline electrolytes. However, AFCs have relatively low power densities (0.32 W/cm^2 using hydrogen as fuel[11] and 9 mW/cm^2 using carbohydrate as fuel[12]).

BFCs are a different class of fuel cells that using living organisms or enzymes as catalysts to produce electricity,[13] though the broader definition would include using non-enzymatic catalysts as well. Bullen et al.[10] define BFCs as devices capable of transforming chemical energy into electrical energy *via* electrochemical reactions involving biochemical reactions. The advantage of enzymatic BFCs is that they operate at mild temperatures (typically 20 $\sim$ 40 °C) and mild pH

($6 \sim 7$). However, the low stability and high specificity for their substrates limit the application of enzymatic BFCs. In addition, low power densities (several hundred $\mu W/cm^2$) need to be improved for BFCs.

Carbohydrate fuel cells are a class of fuel cells where carbohydrates, such as glucose, are used as fuels. The advantages of carbohydrate fuel cells over H_2/O_2 fuel cells include that: (1) carbohydrates are abundant materials that can be used directly as fuels, and (2) the broader choices of catalysts for carbohydrate fuel cells reduce the costs in real-life applications. A broad range of catalyst types has been studied for use in carbohydrate fuel cells, including enzymes, precious metals, and organic electron mediators. This work focuses on developing a specific organic mediator system for use in carbohydrate fuel cells.

1.2 Carbohydrate Fuel Cells

1.2.1 Enzyme-Catalyzed Carbohydrate Biofuel Cells

As early as 1964, glucose oxidase (GOx) was employed as an anode catalyst to accelerate glucose oxidation in a glucose/O_2 fuel cell. Yahiro et al.[14] used an ion exchange membrane and platinum-foil electrodes to build the cell. After adding 0.34 g GOx and 0.92 g glucose in phosphate buffer (pH$\sim$6.7), the fuel cell generated a current density of 0.21 $\mu A/cm^2$. In this example, even though glucose oxidase has a high activity for glucose oxidation, it is hard for anodes to collect electrons from the GOx efficiently since GOx needs to diffuse to the electrode surface and the GOx active center (flavin adenine dinucleotide (FAD)), which produces electrons, is deeply buried in the enzyme, as shown in Figure 1.3. Given this, an electron mediator is required to transfer electrons from GOx to

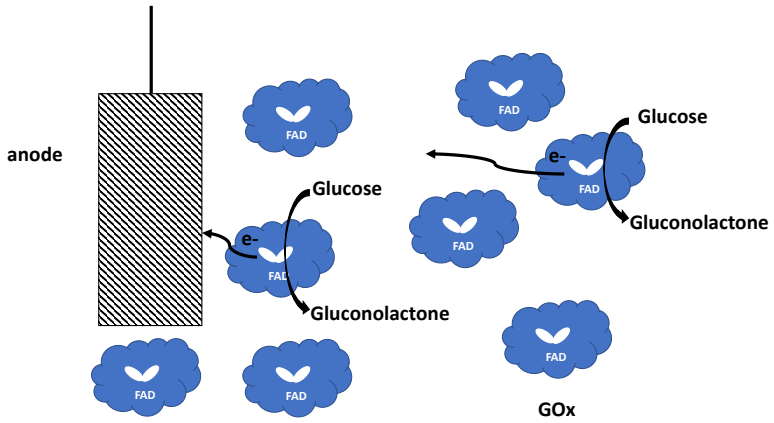

Figure 1.3: Schematic of electron transfer from glucose oxidase to an anode.

the anode.

In order to reduce the GOx diffusion effect on electron transfer, GOx was immobilized on the anode surface along with redox mediators, such as ferrocene analogs. For example, Glatzhofer's group[15] immobilized periodate-modified glucose oxidase (p-GOx) with cross-linked ferrocenylpropyl-modified linear poly(ethylenimine) (Fc-C_3-LPEI) film on a gold anode. At pH 7.0, the negative GOx and positive Fc-C_3-LPAEI were absorbed on the anode surface up to 16 bi-layers. The modified anode generated a maximum current density of 776 ± 3 μA/cm^2 using an air-breathing platinum cathode in a compartmentless biofuel cell.

To generate a high current density from GOx fuel cells, the anodes are typically treated with surface enhancing materials, such as graphite and carbon nanotubes, which provide a large surface area for GOx attachment. Chen et al.[16] demonstrated that with single-walled carbon nanotube-modified glassy carbon electrodes, crosslinked ferrocene-modified linear poly(ethylenimine) (Fc-C_6-LPEI)/fructose dehydrogenase films achieved a current density of 1.0 mA/cm^2, which is 4 times higher than with untreated glassy carbon electrodes. Kulkarni and Slaughter[17] coated multi-walled carbon nanotubes (MWCNTs) on a car-

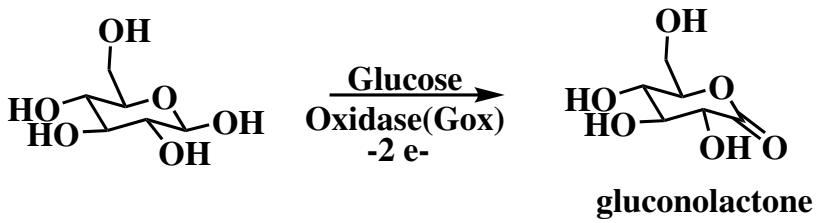

Figure 1.4: Glucose oxidase catalysed glucose oxidation.

bon electrode and immobilized pyrolloquinoline quinone glucose dehydrogenase (PQQ-GDH) on the MWCNT-modified anode. A short circuit current density of 352.5 μA/cm^2 was obtained.

Enzymatic carbohydrate fuel cells, however, have some limitations. For example, in a typical enzymatic glucose/O_2 biofuel cell, only two electrons per molecule are produced in the process of glucose oxidation, as shown in Figure 1.4. However, full glucose oxidation to carbon dioxide provides 24 electrons per molecule. Therefore, such enzymatic biofuel cells only convert 8% (2 electrons out of 24 available) of the chemical energy into electrical energy. Additionally, enzymes have a short lifetime and are sensitive to environmental changes, significantly limiting their real-world applications. Therefore, seeking a robust catalyst is necessary.

1.2.2 Metal-Catalyzed Carbohydrate Fuel Cells

Metal catalyzed carbohydrate fuel cells are a type of abiotic carbohydrate fuel cell that uses metals as catalysts instead of enzymes. Unlike enzyme-catalyzed carbohydrate biofuel cells, abiotic fuel cells do not have strict temperature and pH constraints to maintain the activity of enzymes. Different precious metal catalysts such as platinum, gold, and their alloys for glucose oxidation have been developed in past studies.[18–21]

Chen[22] fabricated and employed a three-dimensional Au/Ni foam as both anode and cathode materials. The fuel cell generated a maximum current density of 180 mA/cm^2 and power density of 26.6 mW/cm^2 using a 6 M KOH solution at a temperature of 70 °C. Torigoe et al.[23] developed a $Au_{80}Pt_{20}$ bimetallic nanoparticle catalyst and modified it on the carbon electrode. A current density as high as 100 mA/cm^2 and a power density of 95.7 mW/cm^2 were generated and with only 8% power dropping after 128 min. This fuel cell worked between 25 to 55 °C, a temperature range broader than most enzymatic catalysts allow.

Although platinum or gold-catalyzed carbohydrate fuel cells are able to produce electricity with less constrained conditions,[24] the scarcity and high cost of such precious metals restrict the large-scale applications of precious metal catalyzed carbohydrate fuel cells.

1.2.3 Organic Dye Catalyzed Carbohydrate Fuel Cells

Organic dye catalyzed alkaline fuel cells are another type of carbohydrate fuel cell that uses organic dyes such as methylene blue (MB), indigo carmine (IC), and viologens (Figure 1.5) to catalyze carbohydrate oxidation in fuel cell systems. Such dyes have been investigated as carbohydrate oxidation catalysts in the past decade due to their redox properties and also their lower cost compared to noble metal catalysts.

Though not as good as metal catalyzed carbohydrate fuel cells, organic dye catalyzed carbohydrate fuel cells exhibit performance comparable to enzymatic catalyzed carbohydrate fuel cells. Scott and Liaw[25] compared several organic dye fuel cells by dissolving 50 mM of MB, IC, methyl viologen (MV), etc. in a 2.5 M KOH solution. Carbon felt anodes were combined with an air-breathing

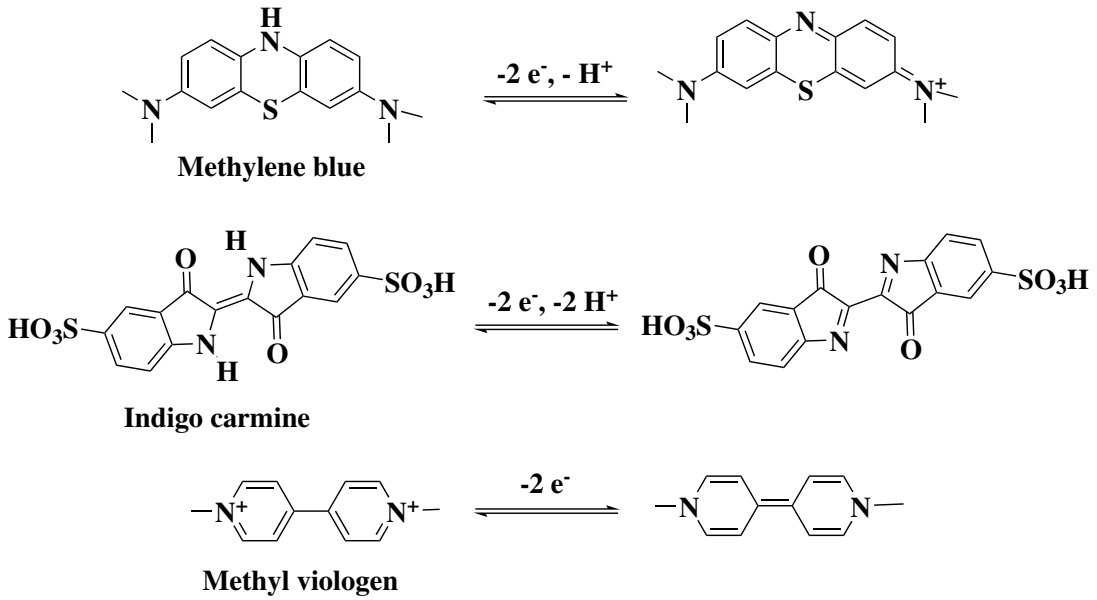

Figure 1.5: Structures of different dye catalysts.

Pt cathode using oxygen as the oxidant. By adding 0.5 M glucose to the solution, MV gave the best performance over other types of dyes, with a maximum power of 2.5 mW/cm^2, a cell voltage of 0.27 V, and a current density of 9 mA/cm^2. For comparison, the IC catalyzed fuel cell generated a maximum power of 1.5 mW/cm^2 with a cell voltage of 0.25 V and a current density of 6 mA/cm^2. Orton and Scott[26] observed similar results by testing those organic dyes at various operating temperatures. These cells used carbon felt anodes with air-breathing MnO_2 cathodes, operating in 3 M alkaline solution with 0.5 M glucose and 20 mM dyes as catalysts. MV and IC catalyzed cells showed better catalytic abilities, with the highest power densities of 2.39 mW/cm^2 and 2.31 mW/cm^2, respectively, at 32 °C.

To date, viologens have been much more extensively studied in the past decade than other dyes. One reason might be that a higher OCV is obtained when viologens are used as catalysts. Hansen et al.[27] calculated the OCV by using

various organic dyes as catalysts at different fuel cell pHs. They found that at pH 12, the OCV of the O_2-catalyst redox couple is 0.96 V when using MV as the catalyst; 0.81 V and 0.6 V for IC or MB as catalysts, respectively. In addition, viologen catalysts have a higher glucose oxidation efficiency. Formic acid, glycolic acid, and glyceric acid were detected for the viologen catalyzed glucose oxidation products. These oxidation products represent oxidation efficiencies of 50% (produce 12 electrons), 25% (produce 6 electrons) and 17% (produce 4 electrons), respectively,. while only gluconic acid (8%) is detected when MB or IC as the catalysts. Therefore, as carbohydrate oxidation catalysts, viologens are attractive candidates.

1.3 Viologen Catalyzed Carbohydrate Fuel Cells

Viologens, di-quaternized 4,4′-bipyridyl salts, have been well studied for optoelectronic and energy applications, such as electrochromic devices, field-effect transistors (FETs),[28] redox flow batteries (RFBs),[29] and dye-sensitized solar cells.[30] There are two types of viologens: monosubstituted viologens and disubstituted viologens. Disubstituted viologen, for example methyl viologen (MV), as shown in Figure 1.6, can exist in three stable redox states, MV^{2+}, $MV^{\bullet+}$, and MV^{0}. These three states are convertible through electron transfers, i.e., MV^{0} donating an electron gives $MV^{\bullet+}$, $MV^{\bullet+}$ donating another electron gives MV^{2+}. These three redox states are stable and highly reversible. Due to this property, disubstituted viologen derivatives have been widely studied in viologen-based charge-transfer complexes.[31–33] As a typical example of a monosubstituted viologen, monomethyl viologen (MMV) has only two stable redox states: $MMV^{\bullet}$ and MMV^{0}, which is shown in Figure 1.6.

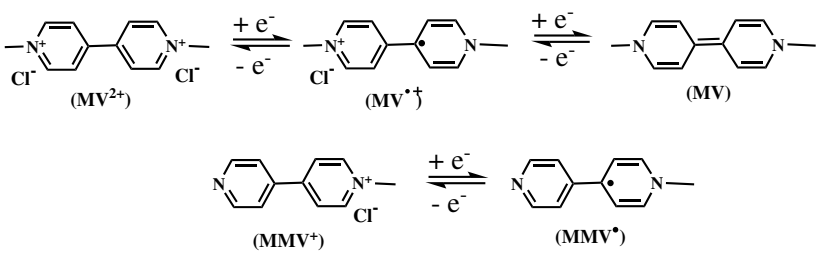

Figure 1.6: Examples of viologens in different states.

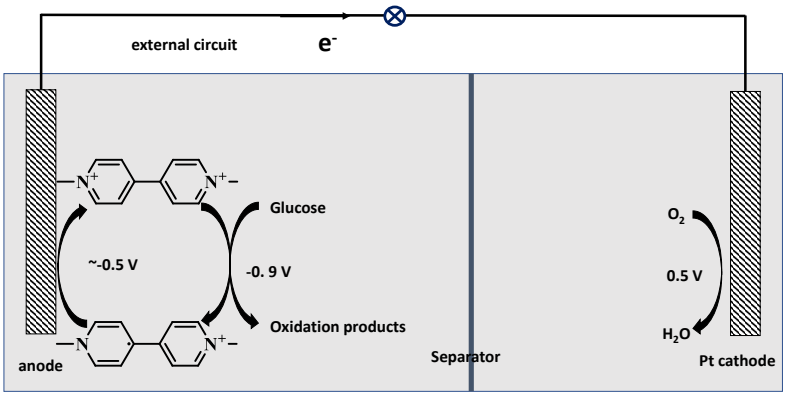

Figure 1.7: Schematic of a MV catalyzed glucose alkaline fuel cell. All redox potentials are vs. saturated calomel electrode (SCE).

1.3.1 Mechanism of Viologen Catalyzed Carbohydrate Fuel Cells

Viologen catalyzed carbohydrate fuel cells are a type of alkaline fuel cell. It is schematically shown in Figure 1.7. The potentials listed for each redox species in this scheme are based on a pH 12 solution.[34] Glucose as the fuel is oxidized to CO_2 on the anode with a potential of -0.9 V. The cathode redox species is O_2, which is reduced to H_2O with a potential of 0.5 V. $MV^{2+}/MV^{\bullet+}$, with a redox potential of -0.5 V, works as a catalyst for glucose oxidation. The detailed putative working mechanism is described below.

With a driving force of 0.4 V (a potential difference (ΔE) between glucose

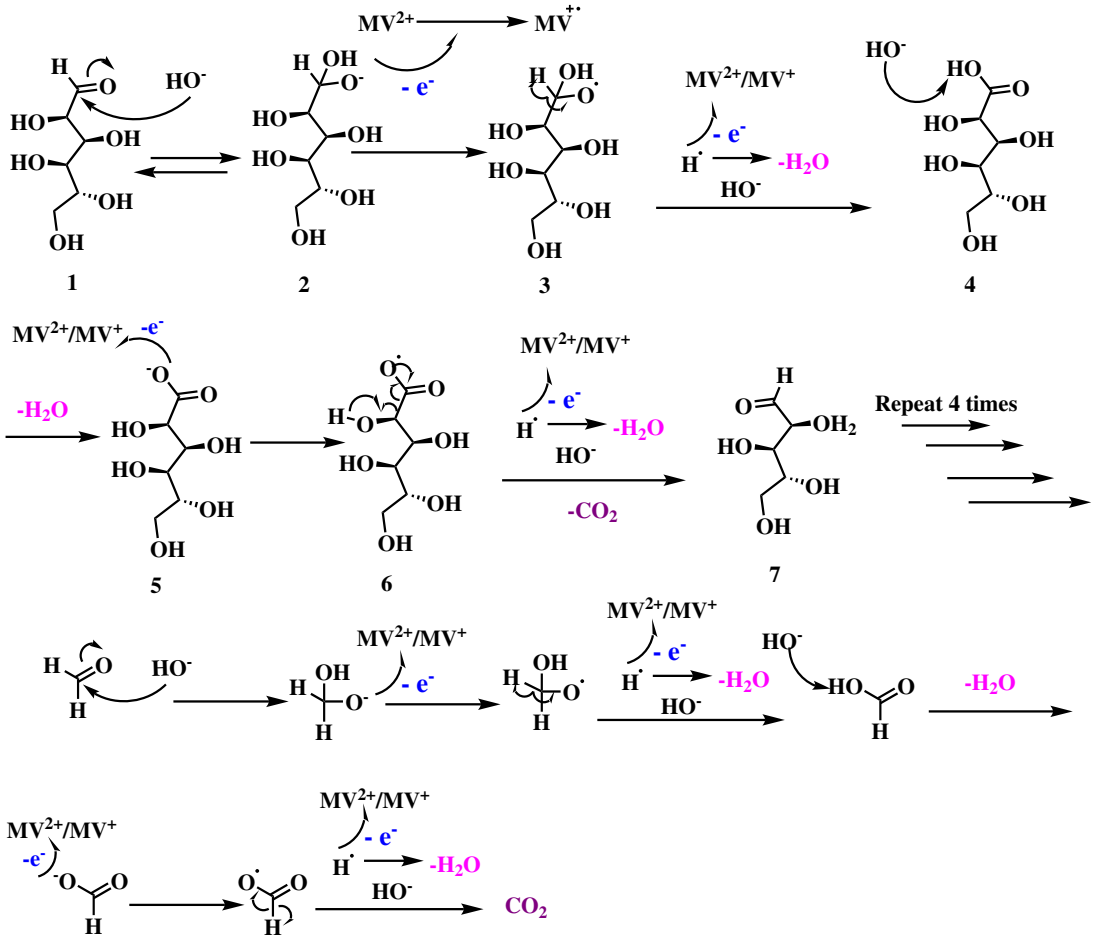

Figure 1.8: Simplified scheme for the alkaline oxidation of glucose to carbonate and water.

oxidation and MV^{2+} reduction), glucose donates its electrons to MV^{2+}. After receiving electrons, MV^{2+} is reduced to $MV^{\bullet+}$. The reduced $MV^{\bullet+}$ releases its electron to the anode and recovers its oxidation state. During the glucose oxidation process, carbonate, formic acid, glyceric acid, and glycolic acid were detected by ^{13}C NMR and MS analysis.[35] A cascading oxidative mechanism is proposed, which is shown in Figure 1.8. In alkaline solution, the aldehyde group is in equilibrium with its hemialkoxide (**2**), from which an electron is removed by MV^{2+} to form a hemialkoxy radical (**3**) ($BuO^- \longrightarrow BuO^\bullet + 1\,e^-$, $E^0_{ox} = 0.1$ V vs. SCE).[36] The radical is unstable and prefers to give its electron to MV^{2+} and form a carboxylic acid (**4**). The carboxylic acid is deprotonated to carboxylate (**5**) in the alkaline solution. The carboxylate then undergoes a Kolbe electro-oxidation in a step-wise dissociative electron transfer.[37] The electron is transferred to MV^{2+}, forming an acyloxy radical intermediate (**6**), **6** is not stable and decarboxylates to form an aldehyde (**7**). After four single electron transfers, six-carbon glucose is oxidized to a carbohydrate which is one carbon shorter. During this process, 4 OH^- are consumed, and at the same time, one CO_2, 3 H_2O, and 4 electrons are produced. After repeating this sub-process 5 times, the glucose is oxidized into carbon dioxide and the $MV^{2+}/MV^{\bullet+}$ couple transfers 24 electrons to the anode. The reactions are summarized as follows,

Anodic reaction:

$$C_6H_{12}O_6 + 24\,OH^- \longrightarrow 6\,CO_2 + 18\,H_2O + 24\,e^-$$

Cathodic reaction:

$$6\,O_2 + 24\,e^- + 12\,H_2O \longrightarrow 24\,OH^-$$

Overall fuel cell reaction:

$$C_6H_{12}O_6 + 6\,O_2 \longrightarrow 6\,CO_2 + 6\,H_2O$$

Even though no OH^- is present in the overall fuel cell reaction, it plays an impor-

tant role in both the anodic and cathodic reactions. During glucose oxidation, the hemialkoxide/hemialkoxide radical (**2**/**3**) intermediate has a standard redox potential (E^0) of 0.1 V,[36] which is much higher than that of $MV^{2+}/MV^{\bullet+}$ (-0.5 V). To have hemialkoxide donate an electron to MV^{2+}, based on the Nernst equation (below), the concentration of hemialkoxide needs to be high:

$$E = E^0 - \frac{RT}{F} \ln \frac{[\text{Red}]}{[\text{Ox}]} \tag{1.2}$$

where R is the universal gas constant, F is the Faraday constant, T is the temperature, and [Red]/[Ox] is the ratio of oxidized to reduced molecules. Since the aldehyde group is in equilibrium with its hemialkoxide (2), high glucose and OH^- concentrations are essential for a high hemialkoxide concentration. The increased hemialkoxide concentration([Red]) can lower its redox potential towards -0.5 V, making MV^{2+} able to remove an electron from it. In the fuel cell, OH^- essentially functions as a catalyst. Unfortunately, in high pH solution, the product CO_2 reacts with two OH^- to form carbonate, which reduces the solution pH as shown below,

$$6\,CO_2 + 12\,OH^- \longrightarrow 6\,CO_3^{2-} + 6\,H_2O$$

The overall reaction is:

$$C_6H_{12}O_6 + 12\,OH^- + 6\,O_2 \longrightarrow 6\,CO_3^{2-} + 12\,H_2O$$

To maintain the fuel cell performance, high concentration OH^- fuel cell solutions are essential.

1.3.2 Problems of Viologen Catalyzed Carbohydrate Fuel Cells

Water-soluble viologens, such as MV^{2+} and isopropyl viologen, were first used in solution as carbohydrate oxidation catalysts for fuel cells by the Watt group.[38] By adding 28 mM MV^{2+} in a 0.5 M glucose 3 M KOH solution, a current density as high as 9 mA/cm^2 and a power density of 2.6 mV/cm^2 were produced at 0.29 V. A higher current density of 20 mA/cm^2 was produced when 110 mM MV^{2+} was added into a 0.5 M glucose pH 11 $\sim$ 12 0.25 M potassium phosphate buffer solution.[38]

Based on the previous paper,[34] an important condition that impacts glucose oxidation efficiency (calculated by oxygen consumption) is the viologen/carbohydrate ratio. At ratios of 0.1 $\sim$ 2.0, the oxidation efficiency is 30 to 40% (7.2 $\sim$ 9.6 electrons/glucose). When MV^{2+}/glucose is 10, the catalytic oxidation efficiency increased to 80%. To reach such a high ratio, a high viologen concentration in the fuel cell solution is required. Further, having a high concentration of MV^{2+} is important to increase e^- transport to the electrode as in solution there are diffusion limitations. However, high concentrations are undesirable due to viologen's toxicity and effluent disposal.[39]

To achieve a high viologen/carbohydrate ratio as well as to avoid using such a high amount of viologen in solution, Rigby et al.[40] investigated water-soluble viologen polymers (shown in Figure 1.9) as glucose oxidation catalysts. Water soluble polyviologens increased the localized viologen concentration in the solution, along with a high viologen/carbohydrate ratio. A 5 mM water-soluble phenyl viologen polymer generated a current of 1.6 mA with 2.5 mM dihydroxyacetone (DHA). However, this was only partially successful as the reduced viologen poly-

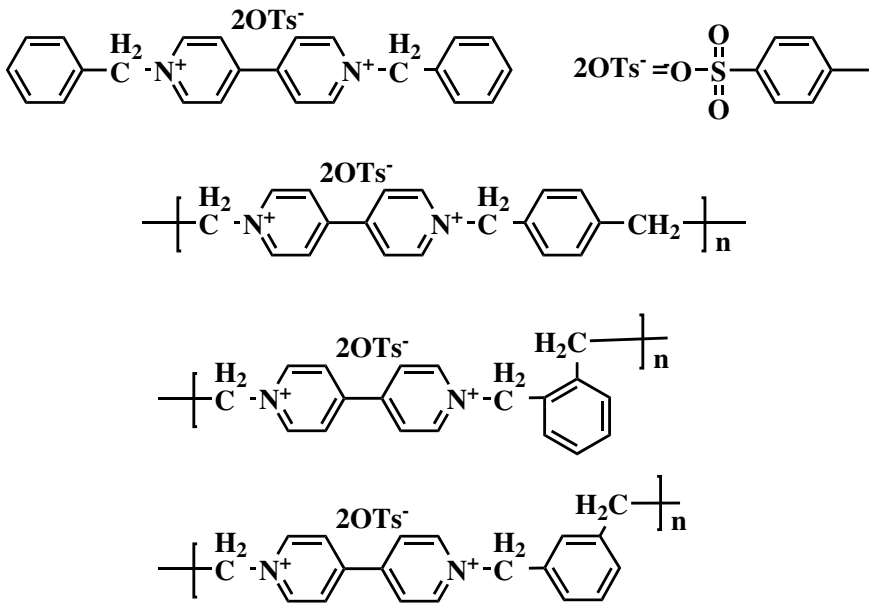

Figure 1.9: Chemical structures of a viologen and comparable water soluble polyviologens.

mer has low solubility and cannot transfer electrons to the anode efficiently and recover its oxidative state.

Immobilizing viologen polymers on the anode surface is a promising way to increase the local viologen unit concentration; at the same time improving the e^- transport rate from catalysts to the electrode. In addition, viologen polymers on the electrode achieve a high local viologen/carbohydrate ratio, which reduces the production of unreacted intermediates during glucose oxidation. One attempt at using polyviologen modified electrodes as the anode for fuel cells was reported by Pan et al.[41] They polymerized viologens on graphite disks by applying a constant potential of -1.297 V for 15 min to an aqueous solution containing 0.1 M monoviologen 1-(3-acrylamidopropyl)-[4,4′-bipyridin]-1-ium bromide (AAPB), as shown in Figure 1.10. The immobilized viologen polymer was used at a viologen/dihydroxyacetone (DHA) ratio of 13:1. By using an E-5 cobalt-based carbon

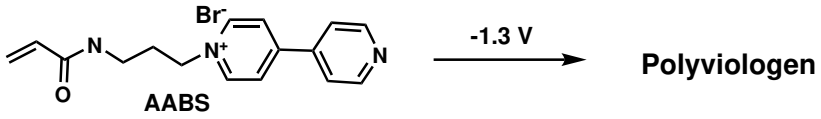

Figure 1.10: Polyviologen electrosynthesis from 1-(3-acrylamidopropyl)-[4,4′-bipyridin]-1-ium bromide (AAPB).

cathode, the modified polyviologen graphite disk (0.5 cm diameter) generated a 2.5 μA (within the background noise from the instrument) to 10 mM dihydroxyacetone in a pH 12 phosphate buffer fuel cell. The authors explained this low catalytic activity in two ways. After immobilization of the viologen monomer on the electrode surfaces, the viologen moieties may undergo some chemical changes that weaken its catalytic ability towards carbohydrates, or the way the viologen groups are oriented in the polymer makes the viologen moieties isolated and difficult for the carbohydrate molecules to reach. Therefore, developing better methods for polyviologen immobilization is necessary.

1.4 Immobilizing Polyviologens on Electrodes

To explore the chemistry of immobilizing polyviologens on electrode surfaces, the synthetic routes to form polyviologens should be reviewed. The synthetic strategies to form polyviologens mainly include Menshutkin reactions, reductive coupling reactions, and electrochemical methods.

A Menshutkin-type reaction converts a tertiary amine into a quaternary ammonium salt by S_N2 reaction with an alkyl halide. As shown in part A of Figure 1.11, both symmetric and asymmetric viologens,[42] as well as polyviologens,[43] have been synthesized using this method. The polyviologens obtained with this method are generally water-soluble.[44] To fabricate water-soluble viologens on

electrodes, dip or spin coating is usually used.[45] Polyviologen-modified glassy carbon electrodes have been prepared by spin coating for use in mercury detection. Spin coating is a quick and easy way to form uniform films on electrode surfaces. However, the actual material used in a spin coating process is typically very low (at around 10% or less), with the rest being flung off during processing and wasted. Polyviologen coated electrodes have not been used for application in carbohydrate fuel cells.

The reductive coupling reaction was first demonstrated by Kosower et al.[46] in 1964. As shown in part B of Figure 1.11, the reductive coupling reaction employs 4-cyano-1-alkyl-pyridinium salts as the starting materials, which are reduced by sodium dithionite in an alkaline aqueous solution. The 4-cyano-1-alkyl pyridinium salt receives an electron from sodium dithionite to form a radical intermediate. Two radical intermediates dimerize to form a precursor species. This precursor eliminates two cyano groups to synthesize the viologen.[47] A cross-linked polymeric membrane with viologen moieties incorporated was obtained by Kitamura et al.[48] In their work, a polymer containing 4-cyanopyridinium moieties was first synthesized and then cast on the electrode surface to form a coating. The 4-cyanopyridinium moieties in the membrane were then reductive coupled by adding sodium dithionite solution to form the viologen units. The formed viologen membrane has a cross-linked structure and showed reversible two-electron redox behavior, which might be used as carbohydrate oxidation catalysts. However, the preparation process was extremely complicated, and these electrodes were not used for carbohydrate fuel cells.

Electrochemical synthesis is an easy and efficient way to deposit insoluble polyviologens on electrodes.[49] There are two types of precursors that have been reported for polyviologen deposition on electrode surfaces. One type of precur-

A: Menshutkin reactions

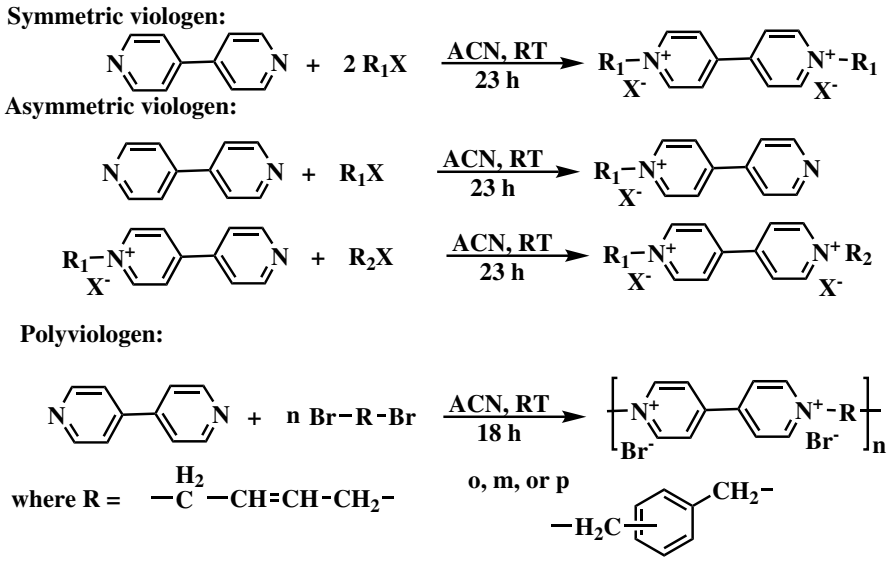

B: Reductive coupling reaction

C: Electro-dimerization

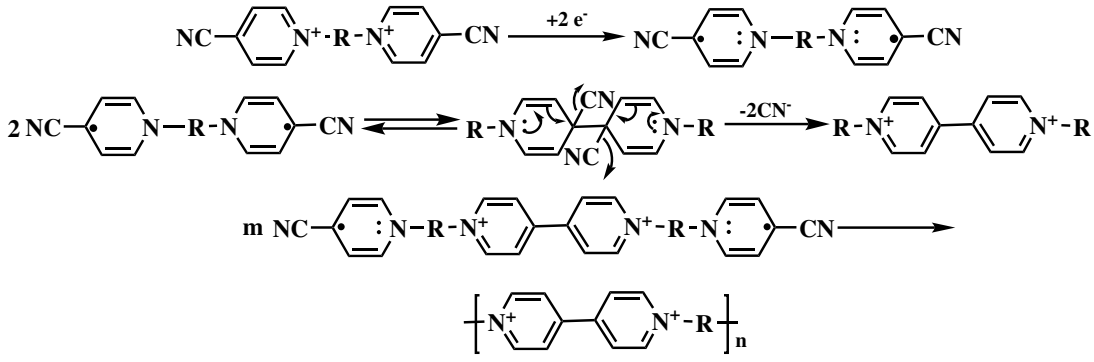

Figure 1.11: Viologen and polyviologen syntheses.

sor is viologen monomers or oligomers containing polymerizable vinyl groups. Using these types of monomers (as introduced in Pan's work[41] at the end of Chapter 1.3.2), the immobilized polyviologen didn't have a suitable structure for viologen/carbohydrate interaction. Another monomer type for polyviologen electrosynthesis is the bis(4-cyano-1-pyridino)alkane dibromides.[13] The synthetic mechanism is similar to the reductive coupling reaction, and is described in part C of Figure 1.11.[50] This mechanism consists of three steps. Firstly, pyridinium salts are reduced to their radical states at a specific potential. Secondly, after two radicals couple and the elimination of cyano groups, the corresponding viologen molecule forms. If the monomer contains more than one cyanopyridinium group, the other cyanopyridinium group can also be reduced and couple to form viologen units. Finally, viologen polymer films are formed on the electrode surfaces. The morphology of the formed film can be controlled by using different R groups in monomers. To the best of our knowledge, no one has used these electropolymerized polyviologens for fuel cell catalysts.

Zhidkova investigated α,Ω-bis(4-cyano-1-pyridino)alkane bromides (PyC_nBr_2) using various of alkyl chain length (n = 2 - 6), as monomers for polyviologen electrosynthesis.[51] The polyalkylviologens formed have a long linear structure and high flexibility. When the foldable polymers are reduced to cation radical viologen units $MV^{\bullet+}$), two cation radical units can form a dimer $2(MV^{\bullet+})$ through radical-radical interaction,[52] as shown in Figure 1.12. This dimerization inhabits electron transport from polyviologens to electrode surfaces. Furthermore, the viologen units can undergo oxidative degradation in alkaline solution as shown in Figure 1.13. The α-C in MV can be oxidized to form pyridinones, which gives a weak catalytic activity.[53,54] Therefore, these properties limit polyalkylviologens' application as carbohydrate fuel cell catalysts.

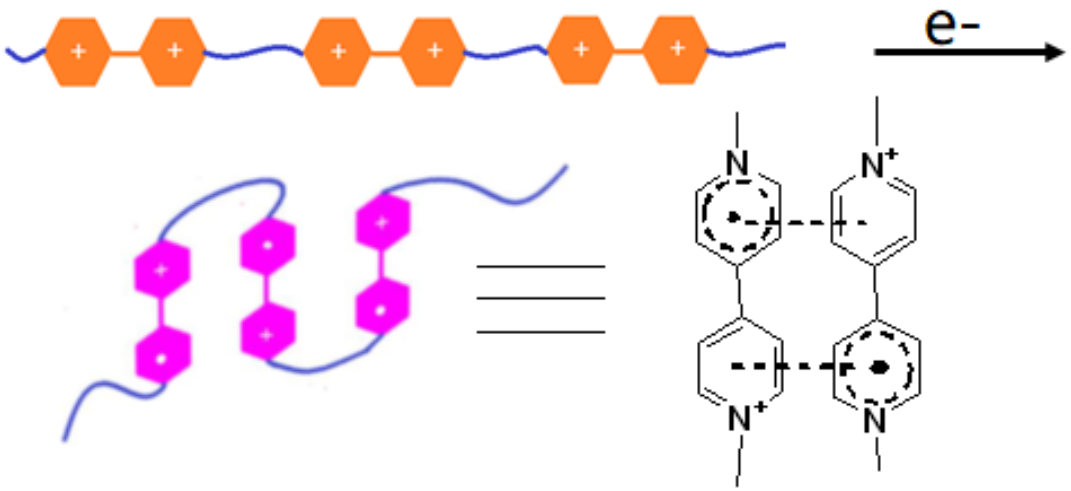

Figure 1.12: A model of a linear polyalkylviologen.

Viologen oxidation:

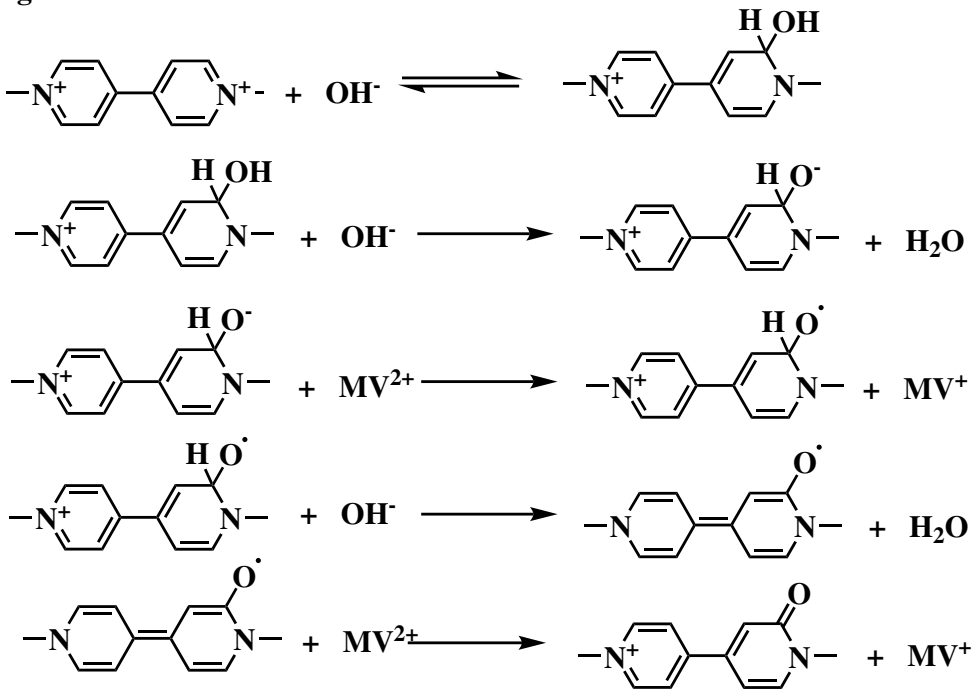

Figure 1.13: Viologen oxidation in the alkaline solution.

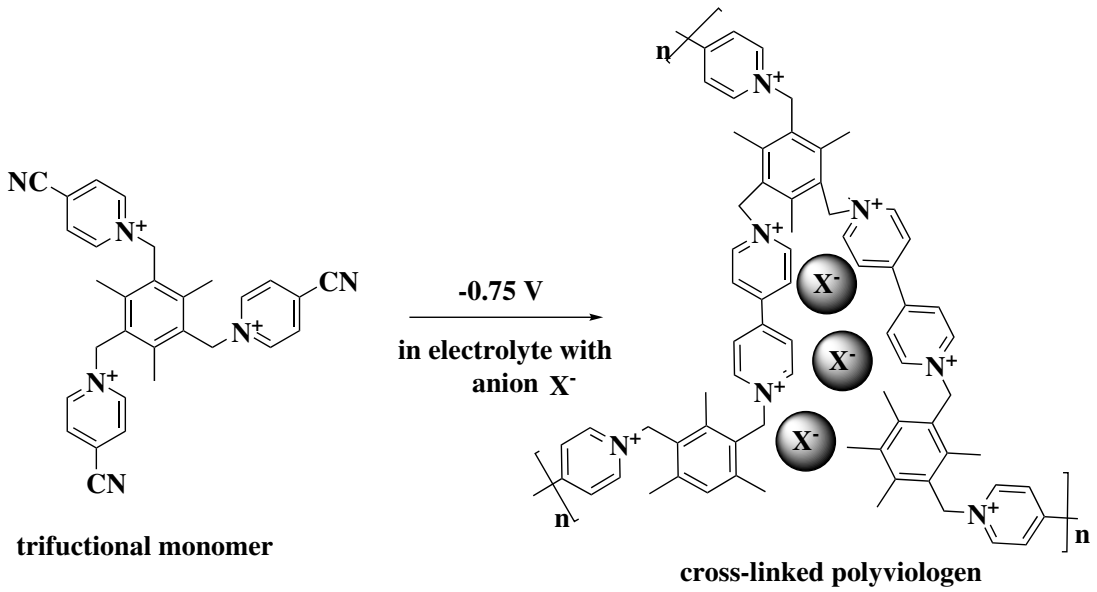

Figure 1.14: Electrosynthesis of crosslinked polyviologen films.

A crosslinked polyviologen modified electrode using 4-cyanopyridinium salts as precursors was reported by Kamata et al. in 2001.[55] As shown in Figure 1.14, the precursor, 1,3,5-tris(4-cyanopyridino-1-methyl)-2,4,6-trimethylbenzene tribromide, has a branched structure with three polymerizable groups. Through the successive reductive coupling of the cyanopyridinium moieties, a crosslinked polyviologen film was formed on the electrode. The film has a high voltammetric anion recognition ability. It shows typical redox peaks in an electrolyte with an anion size smaller than the anion used during polymerization. However, it shows no current response in an electrolyte with an anion size larger than the anion used during polymerization since the larger anions cannot enter the cavities of the polyviologens. To enlarge cavities of the polyviologen formed from this trifunctional monomer, Wang et al.[56] introduced a rigid linear cyanopyridinium monomer into a solution of the trifunctional monomer to form a copolyviologen on glassy carbon electrodes. The copolyviologens are able to host larger

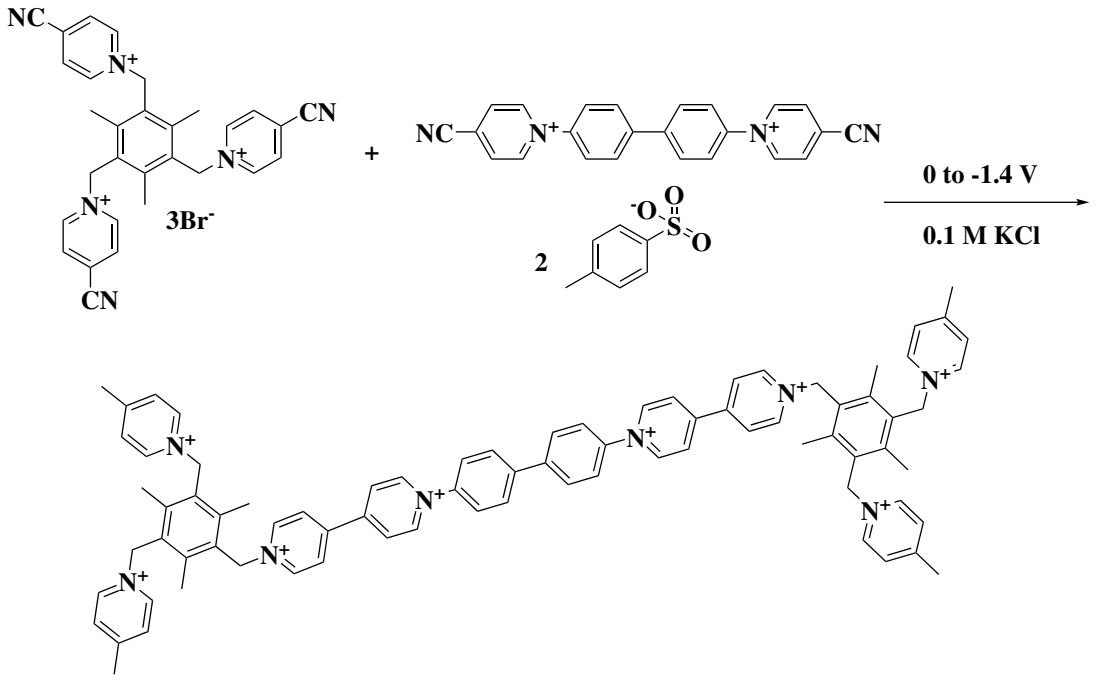

Figure 1.15: Electrosynthesis of crosslinked viologen copolymers.

molecules in oxidation/reduction, showing that the cavities are enlarged. However, as shown in Figure 1.15, the viologen units in the copolymer are surrounded by phenyl groups, which might have steric hindrance for large size carbohydrates interaction with viologen units, and lack flexibility.

1.5 Project Goals

This project aims to produce open, non-aggregated polyviologens on modified glassy carbon anodes for use as novel fuel cell catalysts. Compared with polyviologens deposited using viologen (AABS) as the monomer,[41] the novel polyviologen will show improved catalytic activity in glucose fuel cells.

To achieve this goal, α,Ω-bis(4-cyano-1-pyridino)alkane bromides (PyC_nBr_2) with various alkyl chain length (n = 2 - 6) were used to provide open structures to

allow facile diffusion of substrates, electrolytes, and products. The polymerization process to form polyalkylviologens electrosynthesis was discussed in more detail in Chapter 2.

However, to immobilize the polymers and to prevent the formed viologen units from forming aggregates and dimerization, a rigid spacer, 1,3,5-tris(4-cyanopyridino-1-methyl)-2,4,6-trimethylbenzene tribromide monomer was electrocopolymerized with α,Ω-bis(4-cyano-1-pyridino)alkane dibromides (PyC_nBr_2). The copolymer was formed on different anodes. Its catalytic activity was characterized in an alkaline glucose fuel cell as described in Chapter 3.

The macrocyclic molecule cucurbit[7]uril (CB[7]), which has a large cavity, can encapsulate the alkyl chains of α,Ω-bis(4-cyano-1-pyridino)alkane dibromides into its cavity. On electropolymerization, CB[7] encapsulated polyviologens may be formed. This encapsulation should prevent linear polyviologen aggregation and possibly protect the viologen moieties from degradation under basic conditions. In Chapter 4, CB[7] encapsulated α,Ω-bis(4-cyano-1-pyridino)alkane dibromides (PyC_nBr_2) were used as monomers for electropolymerization. To the best of our knowledge, no one has used such an approach for polypseudorotaxane synthesis. The CB[7]encapsulated polyviologen was modified on different electrodes and characterized as fuel cell catalysts in Chapter 4.

Chapter 2

Electrochemical Behavior of N,N′-Dialkylviologen Salts and Electrodimerization of N-Alkyl-4-cyanopyridinium Salts

2.1 Introduction

N,N′-Dialkylviologens are organic compounds comprised of pyridyl and alkyl groups. In the past decades, alkylviologen polymers have been of wide interest to researchers given their successful application in electrochromic devices (ECDs),[57] field-effect transistors (FETs),[28] redox flow batteries (RFBs),[29] molecular machines,[58] etc. (for a detailed review, see reference[59]).

Several groups have reported electrosynthesis of viologen polymers. The mechanism of polymerization is described in Chapter 1.4. 4-Cyanopyridine-based quaternary salts are the most commonly used precursors. The polymerization can

be carried out using either a potentiostatic or[51] a potentiodynamic process[13,60] in an electrochemical cell.

The properties of polyviologen films are determined in part by the alkyl group and counter ion types, as well as the polymerization methods. Therefore, by choosing different pyridinium salts or different electropolymerization methods, the polyviologen film growth and morphology can be controlled.[55] Zhidkova et al.[51] reported electrosynthesis of linear polyviologen polymers (PVC_n) from α,Ω-bis(4-cyano-1-pyridino)alkane dibromides (PyC_nBr_2) with different lengths of alkyl chain spacers (n = 2 - 6). They found that the polymerization efficiency increased with increasing the alkyl chain length by polymerizing 0.01 M precursors in 0.1 M phosphate buffer solution (pH = 7.55) at a constant potential -0.75 V. No polymer was formed using 1,2-bis(4-cyano-1-pyridino)ethane dibromide (PyC_2Br_2) as the precursor. The deposition current efficiency was about 1% by using 1,3-bis(4-cyano-1-pyridino)propane dibromide (PyC_3Br_2) as the precursor, and 10% by using 1,4-bis(4-cyano-1-pyridino)butane dibromide (PyC_4Br_2) as the precursor. It was hypothesized that the polymerization efficiency is related to the reduction behavior of the precursors. The reduction of PyC_2Br_2 or PyC_3Br_2 is diffusion-controlled, while PyC_4Br_2, PyC_5Br_2 and PyC_6Br_2 have adsorption-controlled reductions. To some degree, this explanation is reasonable. However, the reduced PyC_2Br_2 or PyC_3Br_2 radicals can couple and form viologen units in solutions. The viologen moieties corresponding to the repeat unit structure can be adsorbed on electrode surfaces. Tokuda group[60,61] reported the adsorption of methyl or ethyl viologen at a stationary mercury electrode or on a highly oriented pyrolytic graphite (HOPG) electrode. They found spike-like absorption processes for both anodic and cathodic peaks in cyclic voltammetry. In addition, if PyC_2Br_2 reduced and coupled to form polyviologens or viologen oligomers that

are soluble in the monomer solution, the products should have been detected in the precursor solution, but this was not investigated by the authors.

Potentiodynamic polymerization using cyclic voltammetry gives insight into the electrochemical and physical processes in going from precursors to products. It can monitor the formation of new species at any time. Because of our interest in understanding the electrochemical polymerization and deposition processes, potentiodynamic electropolymerization was chosen for the current studies. Glassy carbon electrodes (GCE) are commonly used for electrosynthesis and are the most commonly used for fuel cell anodes, but the adsorption behavior of dialkyl viologens at GCEs has not been reported. Therefore, investigating dialkyl viologen adsorption behavior on GCEs surfaces is necessary to understand the electropolymerization of PyC_2Br_2, and other bis(4-cyano-1-pyridino)alkane dibromide salts under the conditions used here.

In this chapter, methyl viologen, ethyl viologen, and propyl viologen's adsorption properties on GCEs have been studied. The electrosyntheses of methyl, ethyl, and propyl viologen from 4-cyano-N-alkylpyridinium salt precursors was investigated potentiodynamically, and finally, polyviologen PVC_2, PVC_4 and PVC_6 electrosynthesis were studied potentiodynamically.

2.2 Experimental

2.2.1 Synthesis of N,N′-Dialkylviologens

Methyl, ethyl, and propyl viologens are known compounds and were synthesized using 4,4′-bipyridyl (TCI, 98%) and methyl iodide (Sigma-Aldrich, 99%), bromoethane (Sigma-Aldrich, 98%), and bromopropane (Sigma-Aldrich, 99%), re-

spectively. The procedure is described as follows.[51] A reaction mixture of 5 mmol of haloalkane, 5 ml of acetonitrile, and 2 mmol of 4,4′ bipyridyl was heated at 60 °C for 6 h in a round bottom flask fitted with a reflux condenser. The mixture was cooled to room temperature. The precipitate that formed was collected by filtration and washed with diethyl ether to remove unreacted starting materials. The products were characterized by ^{1}H NMR (Appendix). The methyl viologen diiodide (MV) was obtained as an orange precipitate (85% yield). ^{1}H NMR (300 MHz, DMSO): 9.28 (d, 4H), 8.48 (d, 4H), 4.44 (s, 6H).[62] The ethyl viologen dibromide (EV) was obtained as a yellow precipitate (68% yield). ^{1}H NMR (300 MHz, DMSO): 9.42 (d, 4H), 8.80 (d, 4H), 4.72 (q, 4H), 0.93(t, 6H).[62] The propyl viologen dibromide (PV) was obtained as a yellow precipitate (56% yield). ^{1}H NMR (300 MHz, DMSO): 9.40 (d, 4H), 8.79 (d, 4H), 4.66 (t, 4H), 2.02 (4H), 1.59(t, 6H).[62]

2.2.2 Synthesis of N-Alkyl-4-Cyanopyridinium Halides

N-Methyl-4-cyanopyridinium iodide (PyC_1I), N-ethyl-4-cyanopyridinium bromide (PyC_2Br), and N-propyl-4-cyanopyridinium bromide (PyC_3Br) were synthesized using 4-pyridinecarbonitrile (Alfa Aesar, 98%) and iodomethane, bromoethane and bromopropane, respectively. All these compounds have been previously reported.[63] Mixtures of 3 mmol of haloalkane, 5 ml of acetonitrile, and 2 mmol of 4-pyridinecarbonitrile were heated to reflux solvent for 8 h. The reaction mixtures were cooled down to room temperature. The precipitate formed was collected by filtration and washed using diethyl ether to remove unreacted starting materials. The 4-cyano-N-alkylpyridinium halides were characterized by ^{1}H NMR (Appendix). N-Methyl-4-cyanopyridinium iodide ($C_7H_7N_2$)I (PyC_1I) was

isolated as a light orange precipitate (91% yield). ^{1}H NMR (300 MHz, D_2O): 9.30 (d, 2H), 8.80 (d, 2H), 4.50 (s, 3H).[63] N-Ethyl-4-cyanopyridinium bromide $(C_8H_9N_2)Br$ (PyC_2Br) was isolated as light yellow precipitate (63% yield). ^{1}H NMR (300 MHz, D_2O): 9.17 (d, 2H), 8.47 (d, 2H), 5.57(q, 2H), 1.65 (t, 3H).[64] N-Propyl-4-cyanopyridinium bromide $(C_9H_{11}N_2)Br$ (PyC_3Br) was isolated as light yellow precipitate (46% yield). ^{1}H NMR (300 MHz, DMSO): 9.37 (d, 2H), 8.75 (d, 2H), 4.63 (t, 4H), 1.96 (4H), 0.89 (t, 3H).[65]

2.2.3 Synthesis of α,Ω-Bis(4-cyanopyridino)alkane Dibromides

Bis(4-cyano-1-pyridino)alkane dibromides were synthesized using 4-pyridine carbonitrile (Sigma-Aldrich, 98%) and α,Ω-dibromoalkanes ($C_nH_{2n}Br_2$, where n = 2, 4, and 6) by the following procedure. All are known compounds.[51] The reaction mixture of 2 mmol of either 1,2-dibromoethane, 1,4-dibromobutane or 1,6-dibromohexane, 10 ml of acetonitrile, and 5 mmol 4-pyridinecarbonitrile was heated to reflux solvent for 8 h in a round bottom flask fitted with a reflux condenser. The mixture was cooled down to room temperature. After removing acetonitrile under reduced pressure, the precipitate was washed with diethyl ether to remove unreacted starting materials. The desired dibromide salts were characterized by ^{1}H NMR (Appendix). 1,2-Bis(4-cyano-1-pyridino)ethane dibromide $(C_{14}H_{12}N_4)Br_2$ (PyC_2Br_2) was obtained as dark brown precipitate (71% yield). ^{1}H NMR (300 MHz, D_2O): 9.17 (d, 4H), 8.35 (d, 4H), 5.33 (s, 4H).[51] 1,4-Bis(4-cyano-1-pyridino)butane dibromide $(C_{16}H_{16}N_4)Br_2$ (PyC_4Br_2) was isolated as a light yellow precipitate (55% yield). ^{1}H NMR (300 MHz, DMSO): 9.35 (d, 4H), 8.69 (d, 4H), 4.67 (s, 4H), 2.01 (s, 4H).[51] 1,6-Bis(4-cyano-1-pyridino)hexane di-

bromide ($C_{18}H_{20}N_4$)Br_2 (PyC_6Br_2) was isolated as a yellow precipitate (71%). ^{1}H NMR (300 MHz, DMSO): 9.35 (d, 4H), 8.70 (d, 4H), 4.62 (t, 4H), 1.87 (m, 4H), 1.26 (m, 4H).[51]

2.2.4 Electrochemical Studies of Alkylpyridinium Halides, Viologens and Polyviologens

Appropriate amounts of the 4-cyano-N-alkylpyridinium halides (PyC_nX, n = 1, 2, and 3) and α,Ω-bis(4-cyano-1-pyridino)alkyl dibromides ((PyC_2Br_2) n = 2, 4, and 6) were added to vials containing 0.1 M KCl solution. The solutions were sparged with nitrogen gas before use. The vial functions as a one-compartment cell, and the electrodes were connected to a CH Instruments 832 Bipotentiostat (Austin, TX). The working scheme of a three-electrode cell set-up is shown in Figure 2.1. A 3 mm diameter glassy carbon electrode (GCE) was used as a working electrode. A saturated calomel electrode (SCE) was used as the reference electrode, and a Pt wire was used as the counter electrode in this thesis. The GCE was polished successively on three alumina grades (1, 0.3, and 0.05 μm) and washed with distilled water before each use. Electrochemical experiments were carried out by potentiodynamic cycling from 0 to -1.2 V for 20 cycles using 50 mV/s as the scan rate unless otherwise noted. After dimerization or polymerization, the modified electrodes were rinsed with distilled water and cycled in a monomer-free 0.1 M KCl solution. All experiments were carried out at room temperature.

Electrochemical properties of viologens under different concentrations (0.5 to 2.0 mM) in 0.1 M KCl solutions and polyviologen on electrodes surfaces were studied by electrochemical experiments in a three-electrode cell as described above. The experiments were carried out by potentiodynamic cycling from 0 to -1.2 V

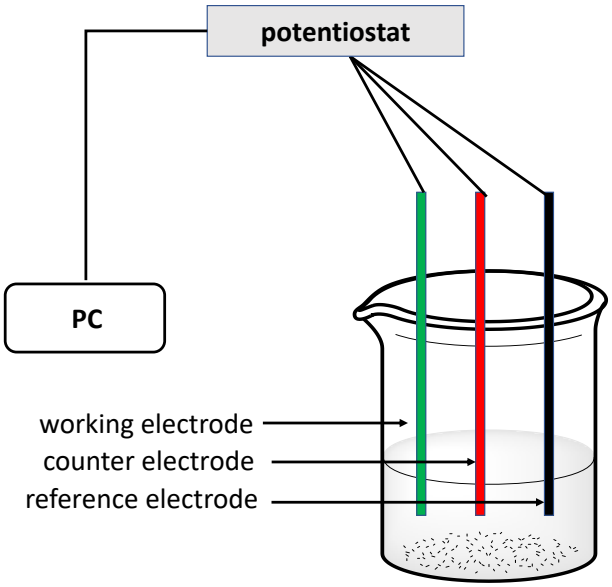

Figure 2.1: Working scheme of a three-electrode cell set-up for potentiodynamic experiments.

for 3 cycles using 50 mV/s as the scan rate unless otherwise noted.

2.3 Results and Discussion

2.3.1 Viologen Absorption and Dimerization on GCEs

The electrochemical behavior of methyl, ethyl, and propyl viologens on GCEs was explored using cyclic voltammetry. As shown in Figure 2.2, all viologens showed two redox couples (R1 and O1, R2 and O2). Scanning to more negative potentials, the first reduction (R1) is followed by a second reduction (R2). On the return scan to move positive potentials, a first oxidation process (O2) is followed by a second oxidation (O1). The designation scheme was chosen to reflect the pairing of the redox processes. At a concentration of 0.5 mM, MV showed normal diffusion-controlled redox waves, while both EV and PV show a spike-like

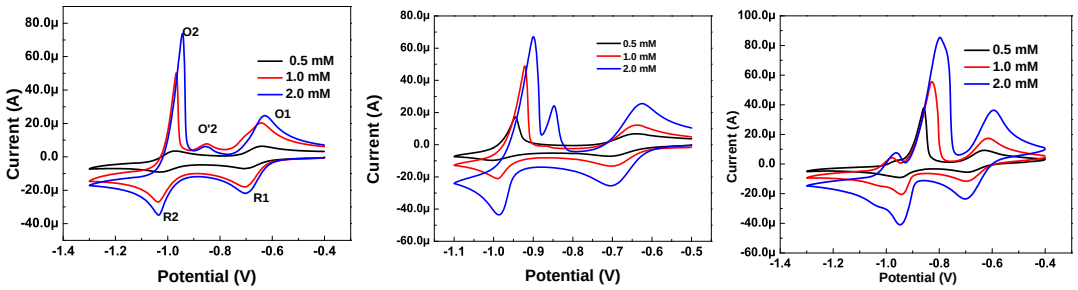

(a) (b) (c)

Figure 2.2: Cyclic voltammograms of MV (a), EV (b) and PV (c) at different concentrations, 0.5, 1.0, 2.0 mM, 0.1 M KCl solution.

oxidation peak O2. The spike-like oxidation peak O2 ($V^0 \longrightarrow V\cdot\equiv$) indicates the reductive desorption behavior of neutral viologens (V^0) adsorbed on GCE surfaces. This suggests that EV^0 and PV^0 are less soluble in aqueous solution than MV^0, and prefer to adsorb on the hydrophobic GCE surface. Increasing the concentration of viologens, the spike-like peak is more pronounced for all the viologens; even MV showed the adsorptive behavior on the GCE. At the same time, increasing the concentration results in a new anodic peak (O′2) between O1 and O2 for all viologens. A similar result has been reported by Hui et al. using Zeolite Y-modified electrodes when a low scan rate was applied in MV LiCl solutions.[66] They concluded that the new raised peak $O'2$ was a more stable crystalline deposit, while O2 results from the amorphous deposition of MV^0. When they lower the scan rate, the amorphous deposit can convert to a crystalline structure.

It appears that the putative crystalline deposit formation on GCEs is facilitated under high MV^0 concentration conditions. To confirm this conclusion, a potential holding experiment using MV at different scan rates and concentrations was conducted. As shown in Figure 2.3 (a) and (b), at 0.5 mM, MV showed normal redox peaks at the different scan rates. While at a concentration of 2 mM,

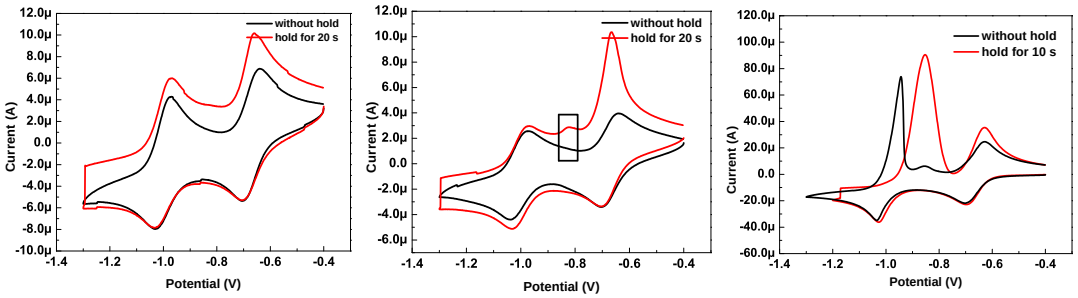

(a) (b) (c)

Figure 2.3: Cyclic voltammograms of MV at different scan rates and concentrations, (a) 20 mV/s, 0.5 mM; (b) 50 mV/s, 0.5 mM; (c) 50 mV/s, 2 mM, 0.1 M KCl. Holding potential at −1.3 V before scanning oxidatively.

MV showed the amorphous deposit (spike-like peak at −0.95 V) with a small amount of crystalline deposit (spike-like peak at −0.85 V) on the GCE surface. This is due to the higher concentration of hydrophobic MV^0 around the GCE surface. Holding the potential at about −1.3 V for a short time allowed more $MV^{\cdot +}$ to be converted into MV^0. This allowed a small crystalline deposit oxidation peak to appear at 20 mV/s, and almost all crystalline deposits dominate the GCE surface at 2 mM. The absence of spike-like peaks of MV at 0.5 mM and 50 mV/s, confirmed that crystalline deposition occurs when MV^0 concentration and deposition time are sufficient.

To further ascertain viologens' behavior in an aqueous solution, 0.5 mM of MV, EV, and PV were studied using cyclic voltammetry at different scan rates. The Randles—Ševčík equation and adsorption isotherm describe the effect of scan rate on the peak current respectively,[67] as follows,

$$i_p = 2.69 \times 10^5 \times n^{3/2} A D^{1/2} C v^{1/2} \tag{2.1}$$

$$i_p = -\frac{n^2 F^2}{4RT} A v \Gamma_0 \tag{2.2}$$

where i_p is the current, n is the number of electrons transferred in the redox event, A is the electrode area, D is the diffusion coefficient, C is the concentration, v is the scan rate, F is Faraday Constant, Γ_0 is the surface coverage. For diffusion-controlled behavior, i_p is proportional to $v^{1/2}$, and for absorption-controlled behavior, i_p is proportional to v. As shown in Figure 2.4, as scan rates increase, the redox responses increase. The influence of scan rate on redox responses was analyzed by plotting log(current) vs. log (scan rate). The slopes of the linear fitting are shown in Figure 2.4. Reductive peaks and oxidative peaks of MV viologens have a slope around 0.5, indicating that these redox processes are dominated by diffusion control. The first redox couple (R1/O1) of EV is diffusion controlled. Since a small amount of EV^0 absorption occurs on the GCE, the slopes of its second redox couple (R2/O2) deviates from 0.5. PV showed an absorption-controlled redox behavior as its first redox couple has slopes around 1.0. Because of the strong absorption of PV^0, the slopes of the second redox pair deviate even further from 1.0.

Based on MV, EV, and PV's absorption behavior, it is clear that, at low concentration, the electrochemical behavior of MV is diffusion-controlled in solution. To have MV^0 adsorption on GCE surfaces, a high concentration of MV is essential. EV^0 and PV^0 are adsorbed on the GC electrode even at a low concentration.

2.3.2 Viologen Electrochemical Synthesis from Dimerization of N-Alkyl-4-cyanopyridinium Halides

After studying the electrochemical behavior of MV, EV, and PV on GCE surfaces, the electrosynthesis of alkyl viologens from 4-cyano-N-alkylpyridinium halides could be investigated. Cyclic voltammograms for PyC_1I, PyC_2Br, and PyC_3Br

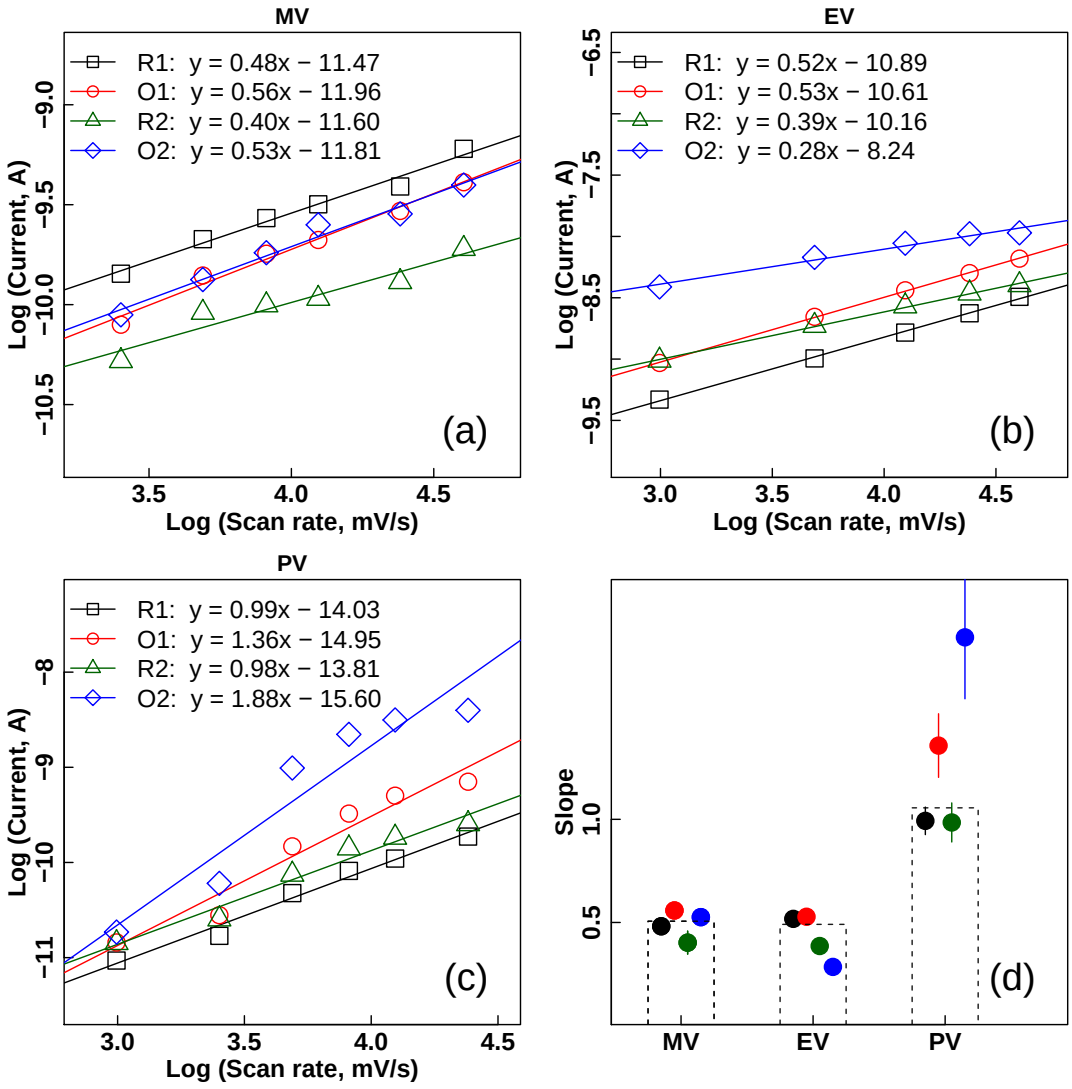

Figure 2.4: Log (oxidation/reduction peak currents) vs. log (scan rate) of 0.5 mM MV (a), EV (b), and PV (c) in 0.1 M KCl solution from 0 to 1.2 V, at scan rates 20, 40, 60, 80 and 100 mV/s. The slopes of each log-log plot fitting (d).

are shown in Figure 2.5; the first scan cycles are shown as inserts. During the MV formation process (Figure 2.5 (a)), the precursor, PyC_1I is initially reduced to its radical state at approx. −0.85 V. The formed radicals can couple, and the cyano groups eliminated to form a viologen dicationic unit. The peaks that developed slowly due to the higher solubility of MV are at −0.7 V (R1), −0.95 V (R2), −0.9 V (O2) and −0.62 V (O1), and are characteristic of MV redox behaviors, referring to the MV in 0.1 M KCl solution as shown in Figure 2.2 (a). The process for the formation of EV is shown in Figure 2.5 (b). PyC_2Br was reduced at −0.88 V. EV was formed after PyC_2Br reduction during the first scan cycle. The peaks at potential −0.95 V and −0.6 V were EV oxidation peaks O2 and O1, referring to the EV redox behavior in 0.1 M KCl solution, as shown in Figure 2.2 (b). A similar result was observed for PV electrochemical synthesis. PyC_3Br was reduced at −0.88 V. The peak at −1.0 V is $PV^{\bullet+} \longrightarrow PV^0$. The peak at −0.95 V indicates the PV deposition on the GCE surface, and the peak at −0.58 V is $PV^{\bullet+}$ to PV^{2+}. All CVs revealed that with more scans, the viologen redox peaks grow along with the redox peaks of PyC_nX decreasing, indicating slow deposition of increasing amounts of viologens.

Different precursor concentrations (0.5, 2.5, and 5.0 mM) were investigated for MV, EV, and PV electrosynthesis. Figure 2.6 shows the 1st (a, c, and e) and 20th (b, d, and f) scan cycles. MV was not detected even after 20th cycles at 0.5 mM of PyC_1I. On increasing the precursor concentration from 0.5 to 5.0 mM, the MV redox peaks were detected at the 1st scan cycle. This confirmed that the diffusion behavior of MV predominates at low concentration and adsorptive deposition occurs at high concentration. At low precursor concentration, the amount of MV^{2+} formed from cyanopyridinium salt reductive coupling is low. MV^{2+} dissolves into the precursor solution, and almost no MV adsorption occurs

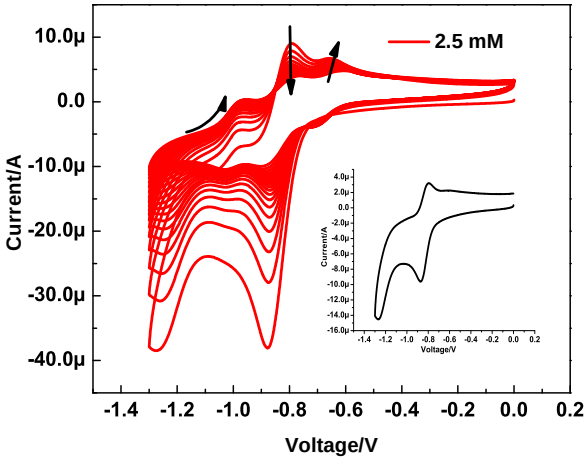

(a)

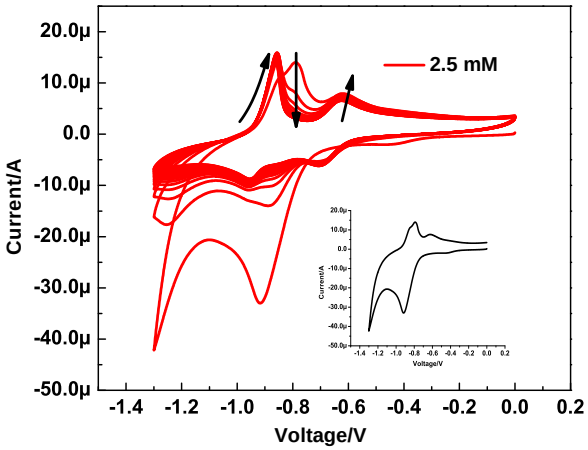

(b)

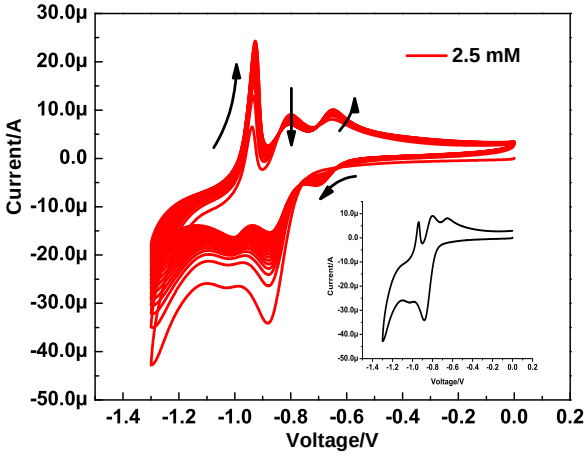

(c)

Figure 2.5: Cyclic voltammograms for the electrosynthesis of viologens in 0.1 M KCl aqueous solution, scan rate 50 mV/s, 20 cycles. The inset shows the first cycle of the electrodimerization from 2.5 mM PyC_1I (a), PyC_2Br (b), and PyC_3Br (c).

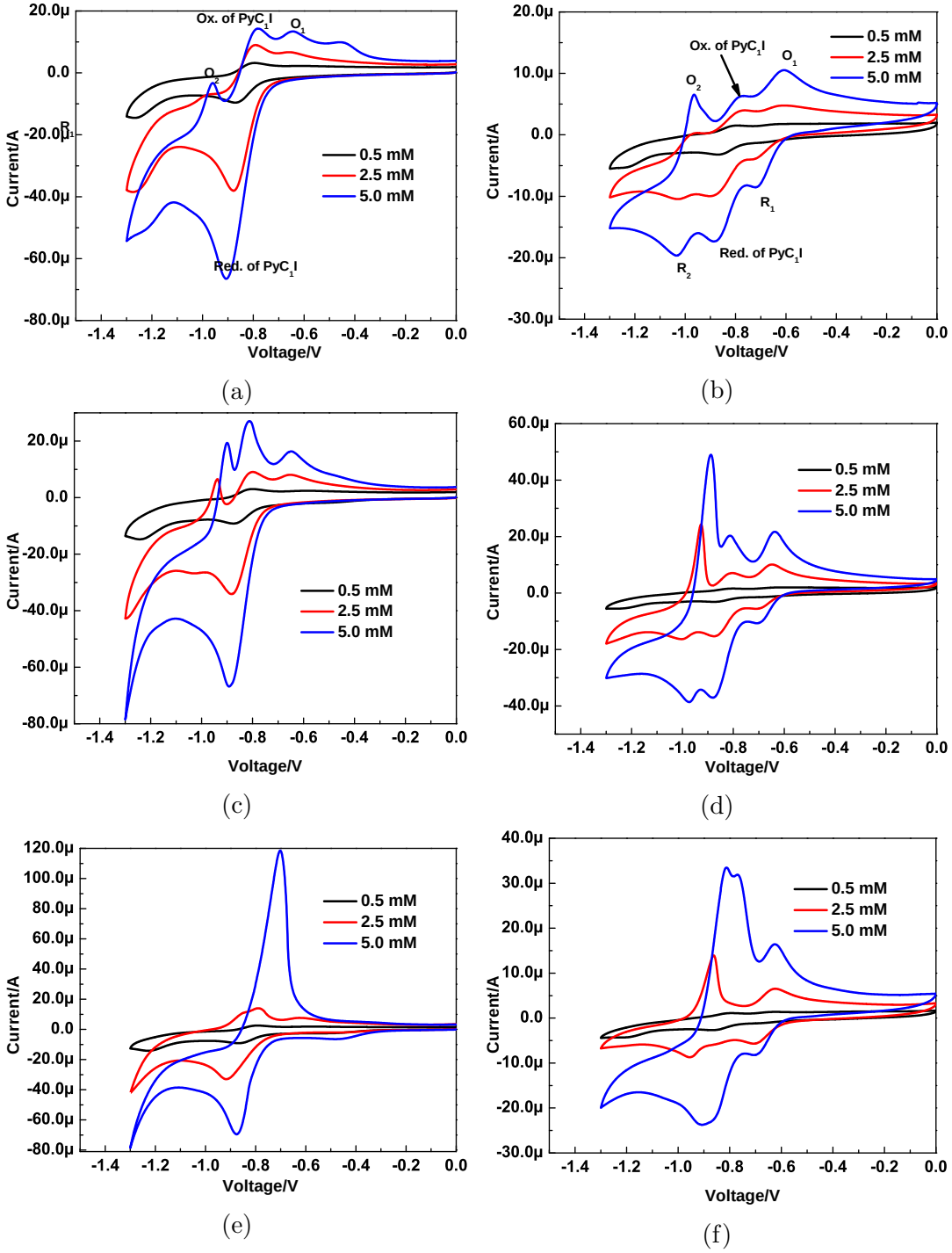

Figure 2.6: Cyclic voltammograms for the electrosynthesis process at different precursor concentrations in 0.1 M KCl solution, 1st scan cycle of PyC_1I (a), PyC_2Br (c), PyC_3Br (e) and 20th scan cycle of PyC_1I (b), PyC_2Br (d), PyC_3Br (f).

on the GCE surface. At a high precursor concentration (5.0 mM), more MV can be formed. The spike-like oxidation peak O2 at about -0.95 V indicates the amorphous deposit of MV on the GCE surface.

After electrodimerization, the GCEs were taken out and washed with distilled water. No viologen film was found on the GCE surfaces, and no viologen current response or UV-Vis absorption peaks were detected by testing the monomer solutions, suggesting that the amounts of formed viologen in the solutions are extremely low. Since high viologen current responses were observed during the electrodimerization process, especially the 20th scan cycle, it indicates that the formed viologens have a high local concentration in the vicinity of GCE surfaces. Therefore, electrosynthesis is an efficient way to achieve a high local viologen concentration with a small amount of viologen.

2.3.3 Polyviologen Electrochemical Synthesis

Based on the electrosynthesis of N,N′-dialkyl viologens and the absorption behavior of these viologens, the electrochemical formation of polymeric analogs of methyl viologen (PVC_2), ethyl viologen (PVC_4) and propyl viologen (PVC_6) was studied under potentiodynamic conditions. The electropolymerization conditions are similar to those of the electrodimerization conditions, scanning 20 cycles from 0 V to -1.3 V. The only difference is using α,Ω-bis(4-cyanopyridino)alkane dibromides precursors. Figure 2.7 shows the precursor polymerization process, and the first scan cycles are shown as inserts. The cyanopyridinium groups on PyC_2Br_2 were initially reduced to form radicals at approx. -0.68 V. The radicals couple intermediately, and the cyano groups eliminate from the precursors, leaving a viologen unit. The newly formed viologen reduces from the dication state to a

radical cation and a neutral state at about −0.4 V and −0.8 V. By reversing the scan, the neutral polyviologen can be reoxidized to the radical cation and the dication at about −0.7 V and −0.3 V. This result is inconsistent with the result reported by Zhidkova et al.,[51] which reported almost no redox signal after electropolymerization of 10 mM $(PyC_2)_2[Fe(CN)_6]$ or PyC_2Br_2 in 0.1 M phosphate buffer solution at a constant potential −0.75 V.

The electrosyntheses of polyviologens PVC_4 and PVC_6 exhibited similar behavior to PVC_2 synthesis. As shown in Figure 2.7 (b) and (c), the reductive peaks of PyC_4Br_2 and PyC_6Br_2 were around −0.75 V which is more negative than that of PyC_2Br_2, since the close proximity of two pyridinium groups in PyC_2Br_2 makes it slightly easier to reduce.

Comparing the polymerization processes of these three precursors (the inserted figures in Figure 2.7), the reduction peak of PyC_2Br_2 is asymmetric, while PyC_4Br_2 and PyC_6Br_2 have narrow and symmetric peaks; Additionally, the response of PyC_2Br_2 is 70 μA which is smaller than the reduction currents of PyC_4Br_2 and PyC_6Br_2, even though the concentrations of the precursors were all 2.5 mM. This is consistent with PyC_4Br_2 and PyC_6Br_2 being adsorbed. Therefore, PyC_4Br_2 and PyC_6Br_2 undergo a polymerization process of reductive deposition, coupling, and eliminative polyviologen formation. However, the broad reductive peak for PyC_2Br_2 suggests it is a diffusion-controlled process that is slightly different: reduction, coupling, eliminative viologen formation, and deposition.

During the polymerization process, the PVC_2 and PVC_4 second oxidation peak (O1) first increased, and then decreased. This suggests that electrodeposition of polyviologen reaches a limit, possibly due to a tight morphology hindering the diffusion of new monomers. Whereas, O1 of PVC_6 increases during the polymerization process since the polymers formed from PyC_6Br_2 are more flexible

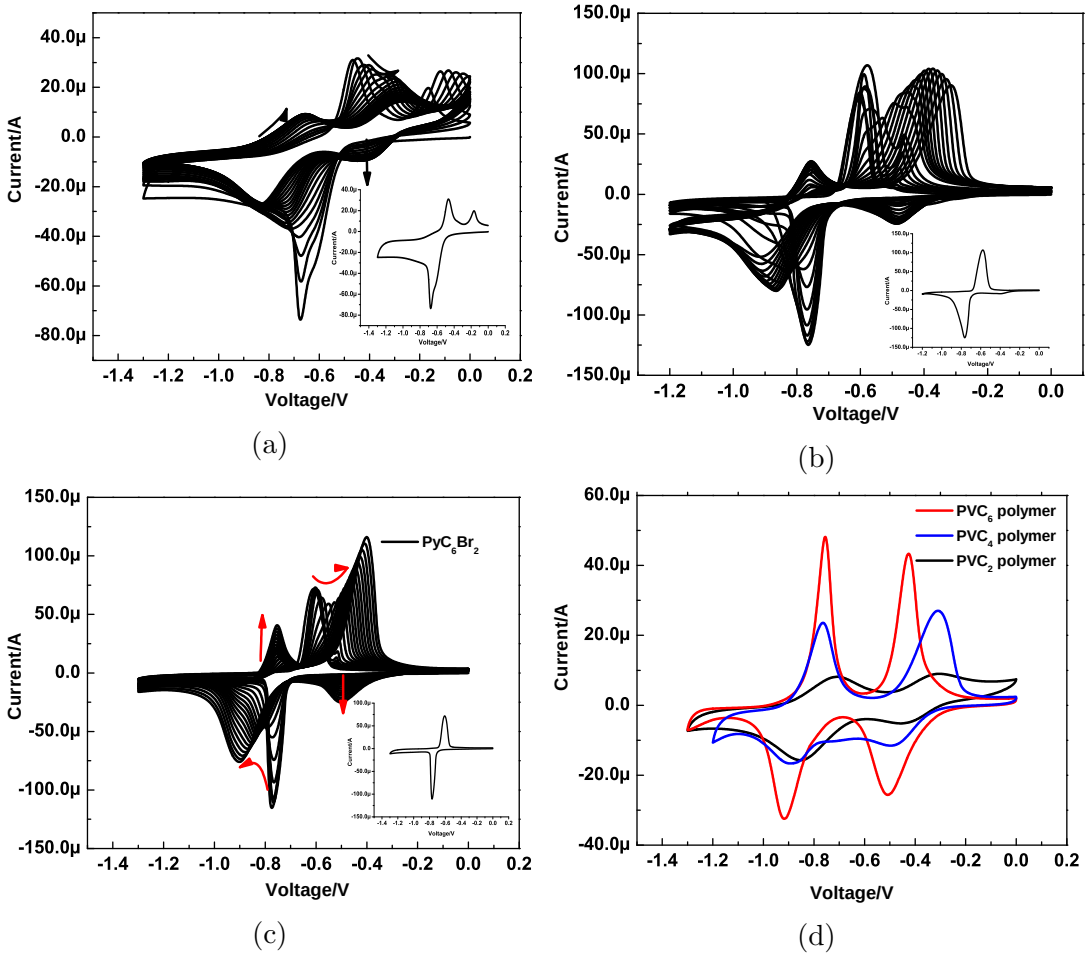

Figure 2.7: Cyclic voltammograms of the electropolymerization of α,Ω-bis(4-cyanopyridino)alkane dibromides in 0.1 M KCl aqueous solution, scan rate 50 mV/s, 20 cycles. The inset shows the first cycle of the polymerization from 2.5 mM PyC_2Br_2 (a), PyC_4Br_2 (b), PyC_6Br_2 (c). The formed PVC_2, PVC_4 and PVC_6 films in monomer-free 0.1 M KCl solution, 50 mV/s (d).

and "open" due to the longer chain.

Figure 2.7 (d) shows a comparison of the films PVC_2, PVC_4 and PVC_6 from 2.5 mM precursor solutions. Since the polymers are adsorbed on the surfaces of the electrodes, their $E1_{1/2}$ and $E2_{1/2}$ values are -0.45 V and -0.85 V, which are more positive than that of alkyl viologens with $E1_{1/2}$ and $E2_{1/2}$ values of ca. -0.67 V and -0.98 V. As expected, PVC_6 shows the highest current response, indicating PyC_6Br_2 has the highest polymerization/deposition efficiency. This is because both PyC_6Br_2 and PV prefer to adsorb on the GCE surface, even at a low concentration, and PVC_6 is less soluble in an aqueous solution. However, MV does not deposit well at low concentrations, and its polymer analog PVC_2 is prone to solvate in an aqueous solution instead of attaching to the electrode surface.

In order to find the optimal polymerization condition for PVC_2, different polymerization scan rates from 30 to 60 mV/s, and different precursor concentrations from 0.25 mM to 5 mM of PyC_2Br_2, were investigated using cyclic voltammetry for 20 scan cycles. After polymerization, the films were obtained by rinsing the electrode with distilled water and scanned in monomer-free 0.1 M KCl solution. The results are shown in Figure 2.8. The polymer formed at 50 mV/s or 60 mV/s scan rates showed the highest redox currents. Low scan rates resulted in low deposition efficiency. PyC_2Br_2 reduction is diffusion-controlled and does not absorb strongly on the electrode surfaces. To form a polymer, PyC_2Br_2 needs to be reduced and coupled into viologen moieties first, which then adsorbs on GCE surfaces more strongly at high concentrations. Since the reduced viologen units are soluble in water, slow scans may allow the diffusion of oligomers away from electrodes. Similar results occurred at low PyC_2Br_2 concentration, which is shown in Figure 2.8 (b). At 0.25 mM, almost no redox response means a tiny

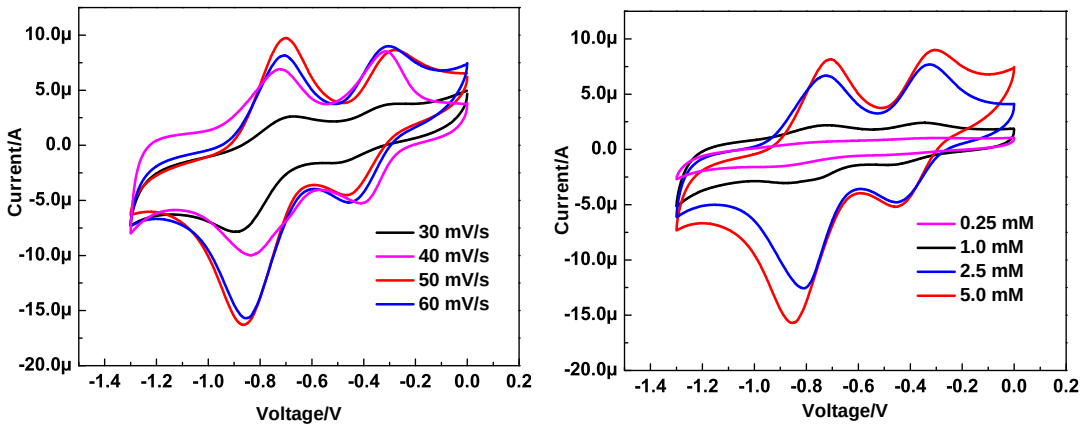

(a) (b)

Figure 2.8: Cyclic voltammograms for PVC_2 in monomer-free 0.1 M KCl solution, scan rate 50 mV/s. (a) PVC_2 formed at 2.5 mM PyC_2Br_2, scan rate from 30 to 60 mV/s for 20 cycles; (b) PVC_2 formed at different PyC_2Br_2 concentrations from 0.25 to 5 mM, scan rate 50 mV/s for 20 cycles.

amount of PVC_2 remains on or near the surface. Increasing the concentration of PyC_2Br_2 leads to a high concentration of viologen moieties on the electrode that then deposits on the GCE surface.

After deposition on GCE surfaces, the redox behavior of these polymers was studied by varying scan rates. The influence of scan rate on the redox responses of these polymers are plotted as log (current) vs. log (scan rate), and is shown in Figure 2.9. For PVC_2, the redox processes are absorption controlled since the slopes of log (current) vs. log (scan rate) are near 1.0, except the reductive peak R1, which is far away from 1.0 with R^2 of 0.646. This might be because the formed PVC_2 is not stable on the electrode surface. The log (current) of PVC_4 show a linear relationship to log (scan rate) with high $R^2 > 0.974$, which indicates the electron transfer in this film is absorption controlled. The slopes of log (current) of PVC_6 vs. log (scan rate) are all 0.5 with $R^2 > 0.999$, indicating the film has an open, cross-linked structure and electron transfer in this film is diffusion-controlled.

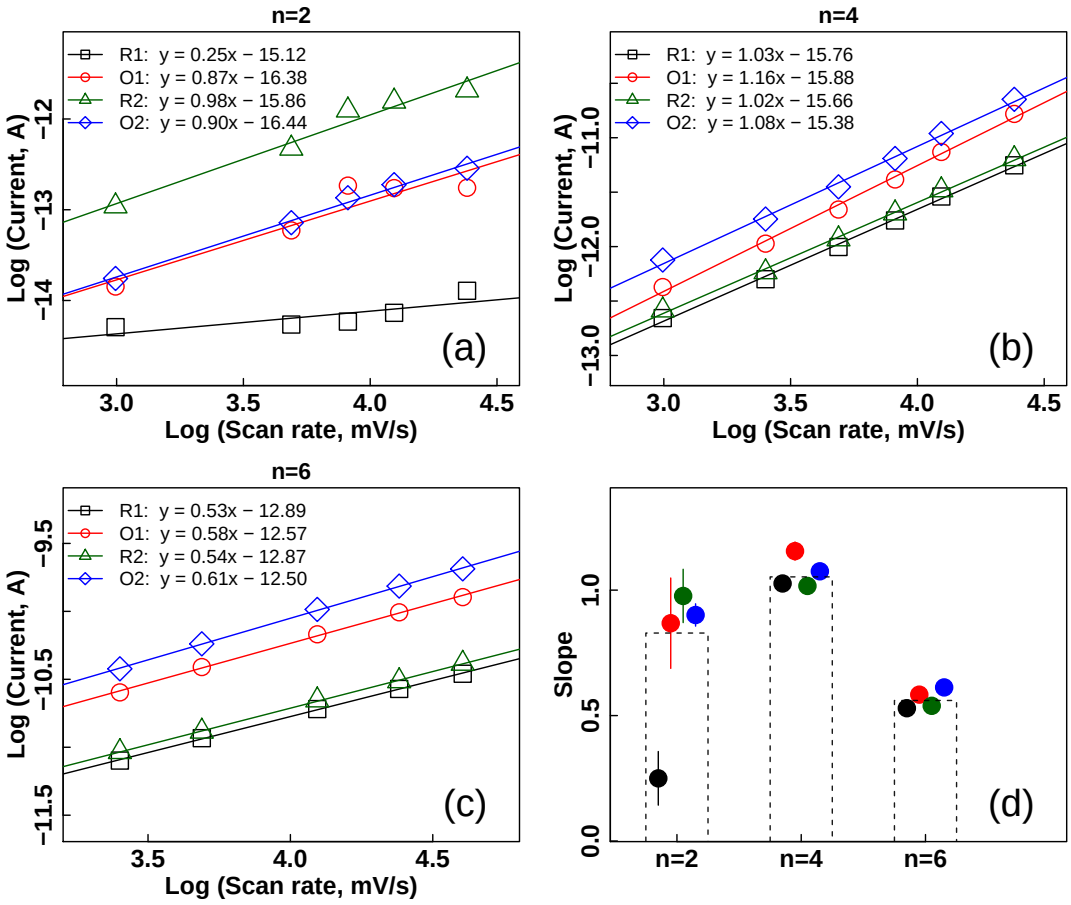

Figure 2.9: Plots of log (oxidation/reduction peak currents) vs. log (scan rate) of polyviologens. PVC_2 (a), PVC_4 (b), PVC_6 (c), the slopes of each log-log plot fitting (d). The polyviologen film deposited on GCE was scanned three times from 0 to 1.2 V consecutively, at different scan rates of 20, 40, 60, 80 and 100 mV/s in monomer free 0.1 M KCl solution. The redox currents measured for the third scan at each scan rate were used for plotting.

2.4 Conclusions

The electrochemical behavior of MV, EV, and PV in 0.1 M KCl solutions has been studied in this chapter. At high concentrations, all show amorphous or crystalline deposition on the GCE surface. At low concentration, MV showed a diffusion-controlled behavior and did not show any adsorption, while EV shows amorphous deposition and PV shows crystalline deposition on GCE surfaces.

MV, EV, and PV have been formed by electrodimerization of 4-cyano-N-alkylpyridinium halides in 0.1 M KCl solutions using the potentiodynamic method. The spike-like adsorption peaks of the resulting viologens were detected. Because of the high solubility of dialkyl viologens, all products ultimately diffused into the solution, and no residue viologen was detected on the electrode surfaces.

PVC_2, PVC_4 and PVC_6 were formed by electropolymerization from 1,2-bis(4-cyano-1-pyridino)ethane dibromide, 1,4-bis(4-cyano-1-pyridino)butane dibromide and 1,6-bis(4-cyano-1-pyridino)hexane dibromide, respectively. Two polymerization path ways are proposed. For PVC_2 synthesis, PyC_2Br_2 undergoes reduction, coupling, eliminative viologen formation, and deposition. For PVC_4 and PVC_6 synthesis, PyC_4Br_2 and PyC_6Br_2 undergo reductive deposition, coupling, and eliminative polyviologen formation. The polymerization conditions for PVC_2 synthesis was optimized. All three polyviologens were characterized as films by CV. PVC_6 polymers has a more open structure, which is beneficial if used as a component in fuel cell catalysts.

Chapter 3

Electrosynthesis and Characterization of Novel Copolyviologens as Carbohydrate Fuel Cell Catalysts

3.1 Introduction

Viologens, di-quaternized 4,4′-bipyridyl salts, exhibit useful, reversible redox properties due to their three stable states: dication, radical cation, and neutral states. As a result, and because of its redox potentials, viologen-based charge transfer complexes have been investigated to catalyze the fuel oxidation process in fuel cells.[35,68,69] For example, Read et al.[34] employed small molecular viologens, such as methyl viologen and ethyl viologen, as catalysts for glyceraldehyde oxidation and reached a carbohydrate oxidation efficiency of 80%. To minimize the formation of unreactive intermediates, a viologen/carbohydrate ratio no less than 8 is

typically required, which means a concentration of 8 mM viologen in a fuel cell solution is necessary when the carbohydrate is 1 mM. There are certain problems with such a high amount of viologens in aqueous solutions due to their toxicity. To achieve high viologen/carbohydrate ratios, water-soluble polyviologens were investigated as electron catalysts in alkaline fuel cells.[40] Since they give high local concentrations, the glucose oxidation efficiency is reportedly improved. However, the neutral or radical cation forms of these polyviologen are less soluble than the dication state, limiting their capability in transferring electrons.

Immobilizing viologens on electrode surfaces is an efficient way to increase the local viologen/carbohydrate ratios, improve the carbohydrate oxidation efficiency, avoid catalyst effluent, and prevent catalysts from migrating to the cathode. To immobilize viologens on fuel cell anodes, Pan et al.[41] used a highly flexible viologen monomer (as shown in Chapter 1 Figure 1.10) as the precursor for electropolymerization to form a monoalkylviologen polymer on a graphite anode. Using an E-5 cobalt-based carbon cathode, the modified polyviologen graphite anode (0.5 cm diameter) generated a 2.5 μA to 10 mM dihydroxyacetone in a pH 12 phosphate buffer fuel cell. This is a fairly low current, possibly due to an undesirable morphology.

Cyanopyridinium salts are another type of precursor that has been used to electrosynthesize polyviologens. The detailed mechanism of polyviologen electrosynthesis was discussed in Chapter 1, Figure 1.11. Kamata et al. reported a branched precursor, 1,3,5-tris(4-cyanopyridino-1-methyl)-2,4,6-trimethylbenzene tribromide ($PyBenMeBr_3$) as a precursor to prepare polyviologen films. The film has a highly cross-linked structure and was used to recognize specific anions electrochemically.[70] However, these branched phenyl polyviologens were not suitable for glucose oxidation catalysts as the film lacks large cavities for glucose

to enter and react with the viologen units. Wang et al. copolymerized a conjugated 4,4′-bis(4-cyanopyridinium-1-yl)biphenyl bis-tosylate with $PyBenMeBr_3$ to increase the film cavity size.[56] The viologen units in this film are surrounded by bulky biphenyl groups, which cause some steric hindrance. This problem has been confirmed by Watt et al.,[31] who used benzyl viologen or phenyl viologen as carbohydrate fuel cell catalysts. These catalysts needed to be heated to a temperature of 40 °C to optimally function in fuel cell operation.

Zhidkova et al. investigated (PyC_nBr_2) with different lengths of alkyl chain spacers (n = 2 - 6) as monomers for polyviologen electrosynthesis.[51] Under a potentiostatistic condition, the electron polymerization efficiency increases as the alkyl chain length grows. The monomer with six carbons showed the highest polymerization efficiency. The electropolymerization of PyC_nBr_2 (2, 4 and 6) under potentiodynamic conditions was discussed in Chapter 2. The formed PVC_6 films appear to have an open and flexible structure. We hypothesized that the longer, and more flexible alkyl spacers provide a more open network that allows ions and/or substrate diffusion into and out of the films more easily.

Based on the above hypothesis, this novel class of copolyviologens was developed further as oxidative catalysts for glucose fuel cells and was the focus of this work. Such copolymers were electrochemically synthesized using PyC_nBr_2 (n = 2 - 6) as the linear precursors to create more open structures and $PyBenMeBr_3$ was used as the branched rigid precursor to provide immobilizing crosslinks, as shown in Figure 3.1. Copolyviologen films including linear and branched polyviologens, were electrochemically produced on the surface of GCEs from appropriate precursors dissolved in 0.1 M KCl solution. The coupling sequence of these two monomer units was controlled by varying the relative concentrations of monomers in solutions. The polyviologen films were characterized using cyclic voltamme-

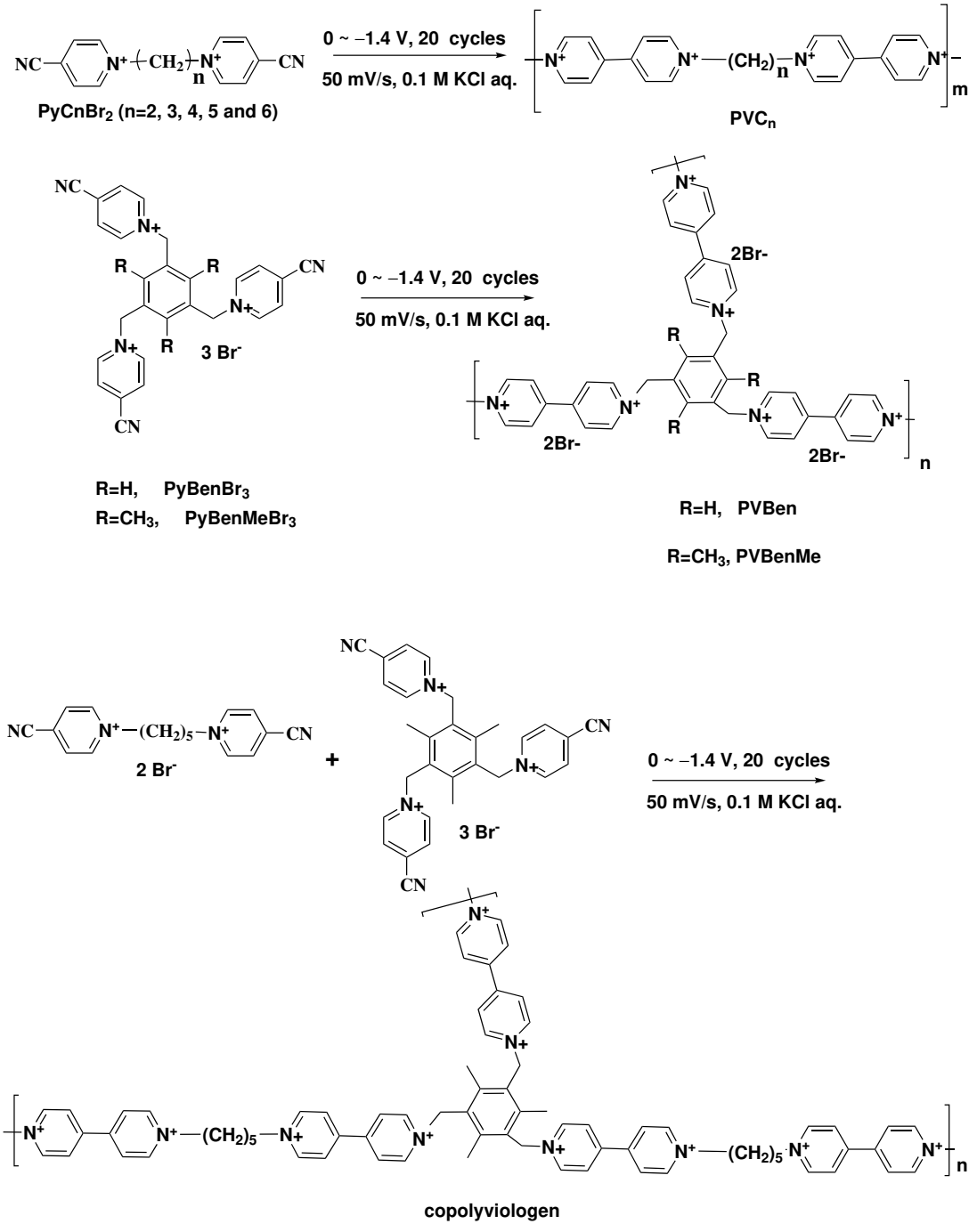

Figure 3.1: Electrosynthesis of PVC_n, PVBen, PVBenMe and copolyviologen from PyC_nBr_2 and $PyBenMeBr_3$, respectively.

try, IR spectroscopy, and the AFM technique. The performance of copolyviologen catalyzed glucose fuel cells fabricated on multiwall carbon nanotube (CNT) modified GCEs (CNT@GCE), and carbon felt electrodes was evaluated against an air-breathing standard Pt/Nafion cathode.

3.2 Experimental

3.2.1 Synthesis of Linear Precursors

α,Ω-Bis(4-cyano-pyridino)alkane dibromides (PyC_nBr_2) were synthesized as discussed in Chapter 2.2.3. The desired bromide salts were characterized by ^{1}H NMR (Appendix) and matched known spectra. 1,2-Bis(4-cyano-1-pyridino)ethane dibromide $(C_{14}H_{12}N_4)Br_2$ (PyC_2Br_2) was obtained as dark brown precipitate (71% yield). ^{1}H NMR (300 MHz, D_2O): 9.17 (d, 4H), 8.35 (d, 4H), 5.33 (s, 4H).[51] 1,3-Bis(4-cyano-1-pyridino)propane dibromide $(C_{15}H_{14}N_4)Br_2$ (PyC_3Br_2) was obtained as light yellow precipitate (71% yield): ^{1}H NMR (300 MHz, DMSO): 9.41 (d, 4H), 8.82 (d, 4H), 4.80 (t, 4H), 2.69 (m, 2H).[51] 1,4-Bis(4-cyano-1-pyridino)butane dibromide $(C_{16}H_{16}N_4)Br_2$ ((PyC_4Br_2) was isolated as a light yellow precipitate (55% yield): ^{1}H NMR (300 MHz, DMSO): 9.35 (d, 4H), 8.69 (d, 4H), 4.67 (s, 4H), 2.01 (s, 4H).[51] 1,5-Bis(4-cyano-1-pyridino)pentane dibromide $(C_{17}H_{18}N_4)Br_2$ (PyC_5Br_2) was obtained as yellow precipitate (71% yield): ^{1}H NMR (300 MHz, D_2O): 9.40 (d, 4H), 8.76 (d, 4H), 4.67 (t, 4H), 1.98 (m, 4H), 1.31 (m, 2H).[51] 1,6-Bis(4-cyano-1-pyridino)hexane dibromide $(C_{18}H_{20}N_4)Br_2$ (PyC_6Br_2) was isolated as a yellow precipitate 2 (71%). ^{1}H NMR (300 MHz, DMSO): 9.35 (d, 4H), 8.70 (d, 4H), 4.62 (t, 4H), 1.87 (m, 4H), 1.26 (m, 4H).[51]

3.2.2 Synthesis of Branched Precursors

1,3,5-Tris(4-cyanopyridino-1-ylmethyl)-benzene tribromide ($PyBenBr_3$) and 1,3,5-tris(4-cyanopyridino-1-methyl)-2,4,6-trimethylbenzene tribromide ($PyBenMeBr_3$) were synthesized using the following procedures. 1,3,5-Tribromomethylenebenzene (1.5 mmol, Sigma-Aldrich) was dissolved in 10 mL acetonitrile. 4-Pyridinecarbonitrile (5 mmol) was added to the solution. The mixture was heated to reflux solvent in a round bottom flask fitted with a condenser for 8 h. The acetonitrile was removed under reduced pressure and the residue was washed with diethyl ether to extract unreacted materials. The $PyBenMeBr_3$ synthesis procedure was the same as that used for $PyBenBr_3$ except that 2,4,6-tris(bromomethyl)mesitylene (Sigma–Aldrich, 98%) was used. The purified products were characterized by ^{1}H NMR and matched known spectra. $PyBenBr_3$ was obtained as yellow solid (56% yield): ^{1}H NMR (300 MHz,DMSO) 9.49 (d, 6H), 8.79 (d, 6H), 7.66 (s, 3H), 5.97 (s, 6H).[71] $PyBenMeBr_3$ was obtained as a solid precipitate (88% yield): ^{1}H NMR (300 MHz, DMSO) 9.20 (d, 6H), 8.71 (d, 6H), 6.16 (s, 6H), 2.24 (s, 9H).[56]

3.2.3 Electropolymerization and Electrocopolymerization

PVC_n, PVBen, PVBenMe and copolymers (Figure 3.1) were prepared using cyclic voltammetric (CV) methods. A CH Instruments 832 Bipotentiostat (Austin, TX) and a three-electrode system were employed. Glassy carbon electrodes (GCE) with 3 mm-diameter or 2×1 cm, indium tin oxide (ITO) glasses, or carbon felts (3.18 mm, Alfa Aesar) were used as the working electrodes. GCEs were polished using 0.3 μm alumina and washed thoroughly using distilled water. CNT@GCEs were made by dropping 5 μL CNT suspension (0.1 mL polysorbate 20 as a surfactant dissolves in 1 mL water) on GCE surfaces and drying at room temperature.

ITO glass was immersed into a solution of distilled water, hydrogen peroxide, and ammonia in a 5:2:2 ratio for 1 h, then sonicated with DI water, ethanol, acetone for 5 min successively. A carbon felt electrode was cut in size of $1 \times 0.5 \times 0.318$ cm. A saturated calomel electrode (SCE) was used as the reference electrode, and a platinum wire functioned as the counter electrode. Electropolymerization to form linear polymers, branched polymers, and copolymers were carried out in 0.1 M KCl solution, using the working electrode potential beginning at 0 V and ending at $-0.8 \sim -1.4$ V for 15 cycles, at a scan rate of 50 mV/s. All solutions were sparged with nitrogen before the experiments.

3.2.4 Polyviologen Film Characterization

Cyclic voltammetry measurements were performed to characterize the electrochemical properties of each polymer and copolymer coated on GCE in 0.1 M KCl solution.

IR spectra were recorded using a Bruker Tensor 27 spectrometer ranging from 3,500 to 370 cm^{-1}. The monomers were dried and mixed with 200 mg KBr and pressed into pellets. The viologen films were polymerized on the ITO glass and scraped off. After drying, the polymers were mixed with 200 mg KBr and pressed into pellets for measurement.

In UV-Vis experiments, the polymers were electrodeposited on ITO glass. The measurements were made by placing the ITO electrode in a 1 cm path length quartz cuvette with water. The UV-Vis spectra were recorded between 270 to 900 nm on an Implen NanoPhotometer with a CCD array detector (1024 pixels). The background spectrum was measured using an ITO glass blank in water.

In atomic force microscopy (AFM) experiments, the viologen films were electropolymerized on the ITO glass surface. The AFM images were taken using a BioScope Catalyst AFM instrument (Bruker) under ambient conditions in the contact mode with a vertical range of 2.5 μm.

3.2.5 Copolyviologen Modified Anode Characterization in Carbohydrate Fuel Cells

Copolyviologens were electrodeposited on GCE, CNT@GCE, or carbon felt electrodes and used as anodes in fuel cells. A one-compartment cell was used with 5 mM glucose in pH 9.7, 0.1 M KCl solution. As shown in Figure 3.2, the fuel cell was connected to a CH Instruments 832 potentiostat. The anode was connected as both the reference and the auxiliary electrodes. The air-breathing Pt/Nafion cathode was connected as the working electrode. Linear sweep voltammetry experiments were performed on the fuel cell by sweeping from 0.005 V to the open-circuit voltage at 2 mV/s.

3.3 Results and Discussion

3.3.1 Linear Alkyl and Branched Monomer Polymerizations

Solutions of different chain length PyC_nBr_2 monomers were prepared in 0.1 M KCl solution at a concentration of 2.5 mM. Their electropolymerization was carried out between 0 to -1.4 V as shown in Figure 3.3 (a) - (e). The first scan cycle is shown as an insert. Initially, all PyC_nBr_2s were reduced at about -0.75 V with a current of about 60 μA except PyC_2Br_2, which is reduced below -0.7 V and

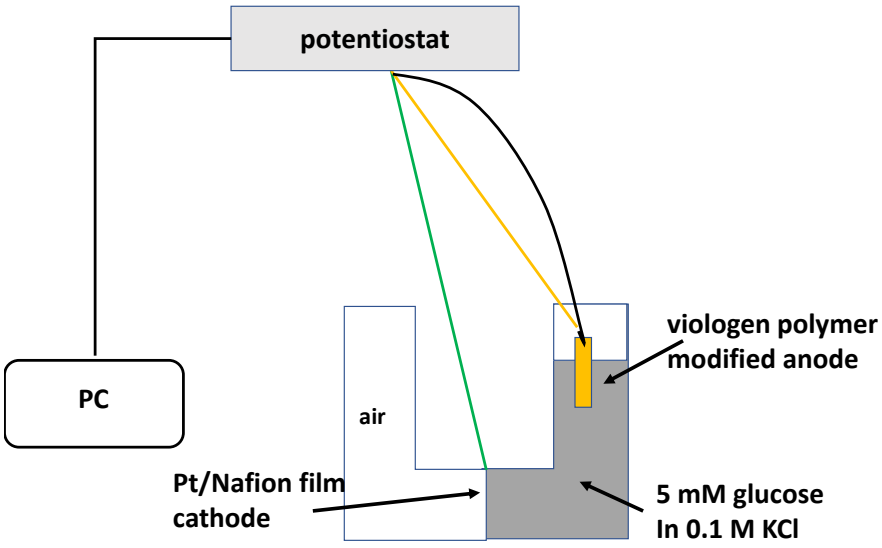

Figure 3.2: Working scheme of a glucose fuel cell set-up.

with a lower reductive current and a shoulder. After 15 scanning cycles, all those monomers formed their corresponding polymers on GCEs.

To compare each precursors' polymerization efficiency, the current efficiency (**CE**) of polymerization was calculated based on the following equation:[51,70]

$$\mathbf{CE} = \mathrm{Q_1/Q_2} \times 100\% \tag{3.1}$$

where Q_1 is the charge passed in polyviologen reductions (R1 and R2 in Figure 3.3 (f)), and Q_2 is the charge spent for cyanopyridinium salt reduction during 15 scan cycles. In cyclic voltammetry, $Q = \frac{1}{v}\int_{\text{onset}}^{\text{offset}} i\,\mathrm{d}V$, where v is the scan rate (50 mV/s), i is the current, and V is the potential. The onset and offset potentials of $\mathrm{PyC_2Br_2}$ are -0.5 V and -0.8 V, $\mathrm{PyC_nBr_2}$ (3 - 6) are -0.7 V and -0.8 V, polyviologens are -0.3 V to -1.1 V. From Figure 3.4, the CE increases as the alkyl chain length of $\mathrm{PyC_nBr_2}$ increases, suggesting that the oligomers from short

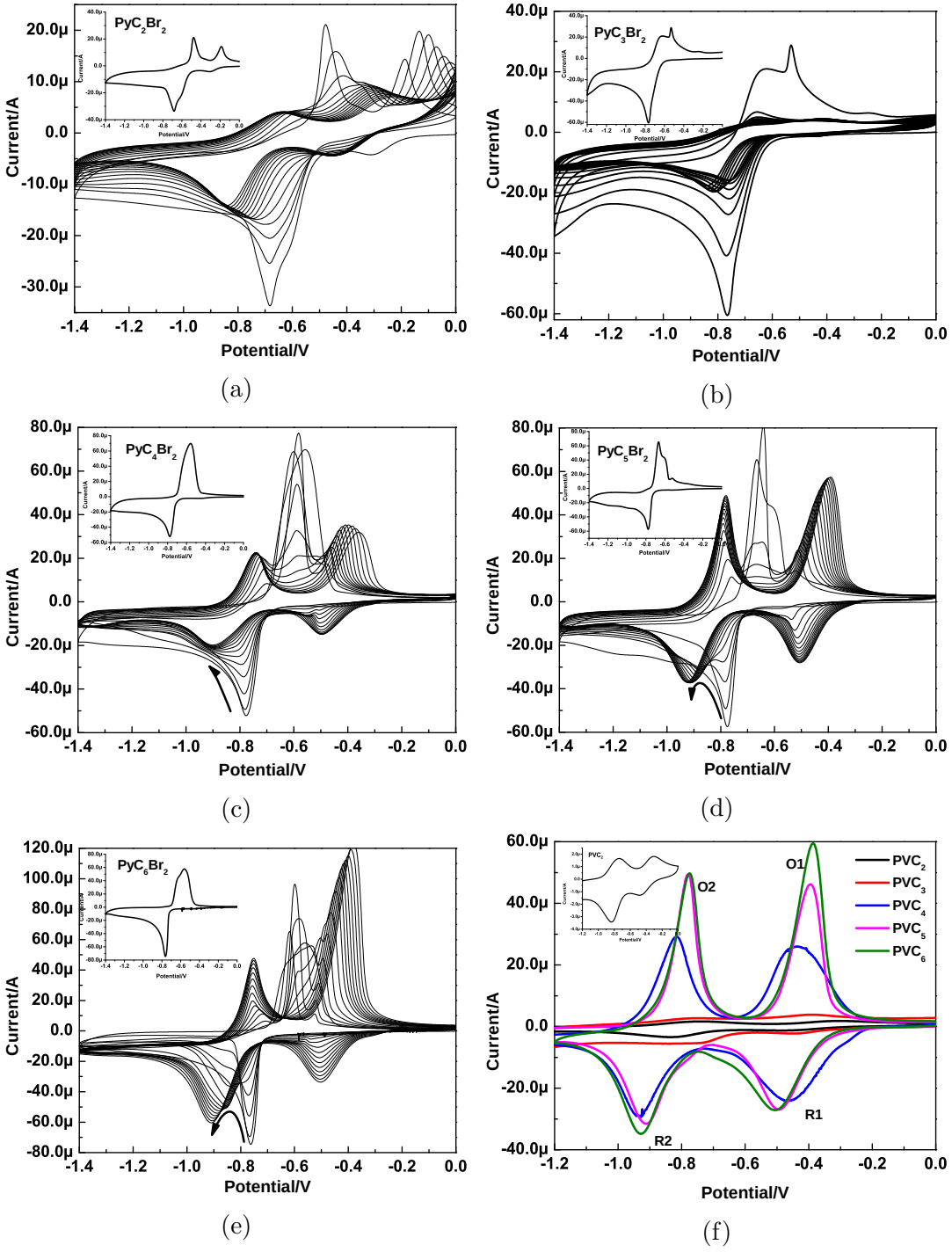

Figure 3.3: Cyclic voltammograms of the electropolymerization of 2 mM PyC_nBr_2 (a - e: 2 - 6) and their corresponding polymers in 0.1 M KCl electrolyte at a scan rate of 50 mV/s (f).

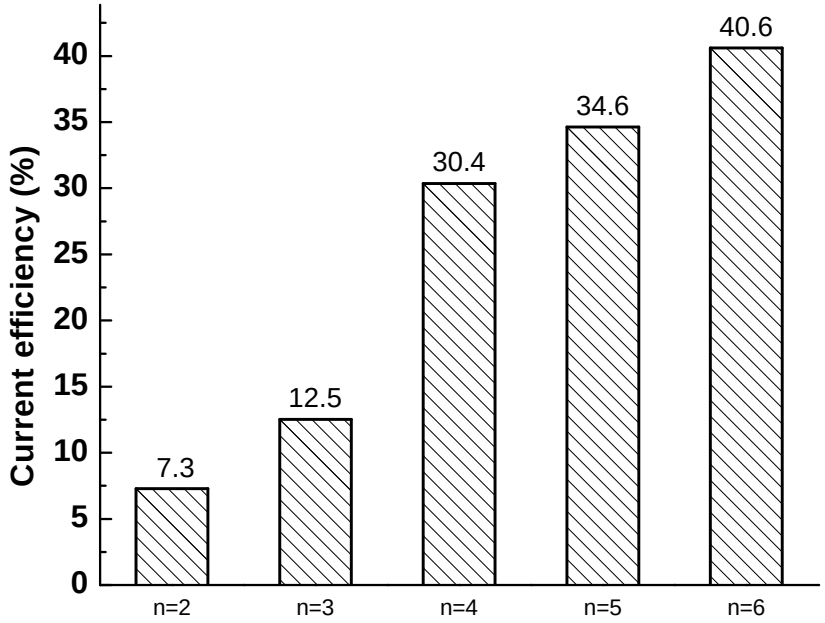

Figure 3.4: Polymerization current efficiencies (CEs) for precursors PyC_nBr_2 with different alkyl chain length (n = 2 - 6).

length alkyl PyC_nBr_2 are more soluble in aqueous solution and diffuse away. The result is in accordance with the work reported by Zhidkova et al.,[51] who using a potentiostatic process (a constant potential at -0.75 V), even though PyC_2Br_2 was not polymerized to PVC_2 in their work.

The newly formed polyviologens were characterized using cyclic voltammetry in monomer-free 0.1 M KCl solution, as shown in Figure 3.3 (f). Their cyclic voltammograms (CV) have two redox pairs, R1/O1 and R2/O2. R1/O1 indicates the reaction between dication states and radical cations state; R2/O2 indicates the reduction and oxidation between radical cations and neutral compounds. These CVs confirmed that PyC_nBr_2 precursors successfully polymerized and formed viologen films on the GCEs.

After polymerization, the redox properties in each PVC_n film were studied by varying scan rates ($0 \sim 100$ mV/s) in 0.1 M KCl solution using cyclic voltamme-

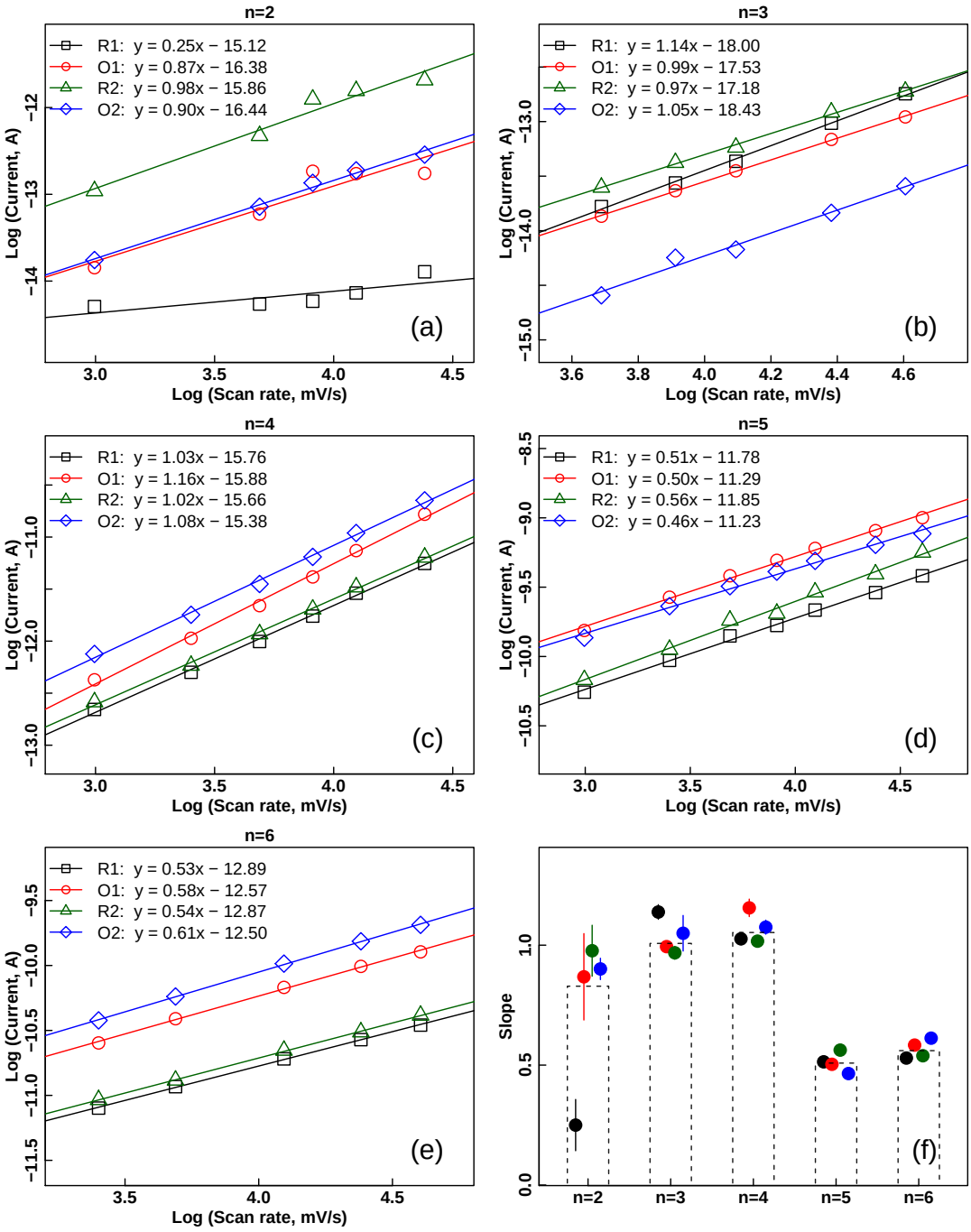

Figure 3.5: Plots of log (oxidation/reduction peak currents) vs. log (scan rates) of PVC_n (2 - 6) (a - e). The slopes of each log-log plot fitting (f). The polyviologen film deposited on GCE was scanned three times from 0 to 1.2 V consecutively, at different scan rates of 20, 40, 60, 80 and 100 mV/s in monomer free 0.1 M KCl solution. The redox currents measured for the third scan at each scan rate were used for plotting.

try. Figure 3.5 (a) - (e) show the linear relationship of Log (current) vs. Log (scan rate). The slopes of each fitting are shown in Figure 3.5 (f). For PVC_2, PVC_3 and PVC_4 their slopes are around 1.0, indicating the surface-controlled redox processes. All the fitting slopes from PVC_5 and PVC_6 are around 0.5, indicating that the redox processes are diffusion-controlled and the polyviologen films have a more open structure. This suggests PVC_5 and PVC_6 to be good candidates for use as glucose oxidation catalysts in fuel cells. In this work, PVC_5 was chosen as the linear polyviologen for further study.

3.3.2 Polymerization Condition Study

In order to optimize the polymerization conditions, PVC_5 films were synthesized using different potential ranges starting at 0 V and ending at $-0.8 \sim -1.5$ V. The result is shown in Figure 3.6. The polymer cannot be formed at the potential range of $0 \sim -0.8$ V or $0 \sim -0.9$ V. With the ending potential more negative, the film formed on the electrode has a higher redox response. This might because as the scans go to a further negative potential, PyC_5Br_2 has enough time for the radicals to couple, eliminate, and reduce to form viologen polymer on GCE surfaces.

PyC_5Br_2 and its polymer PVC_5 were characterized using IR spectroscopy. The IR spectra are shown in Figure 3.7. Since the monomer is cyanopyridine-based, PyC_5Br_2 has an absorption at 2200 cm^{-1}, which is caused by the C≡N triple bond vibration. Compared to the spectrum of the monomer, the polyviologen film has no absorption at approx. 2200 cm^{-1}, which indicates that the cyanopyridinium groups in the polymer were reductively coupled into viologens.

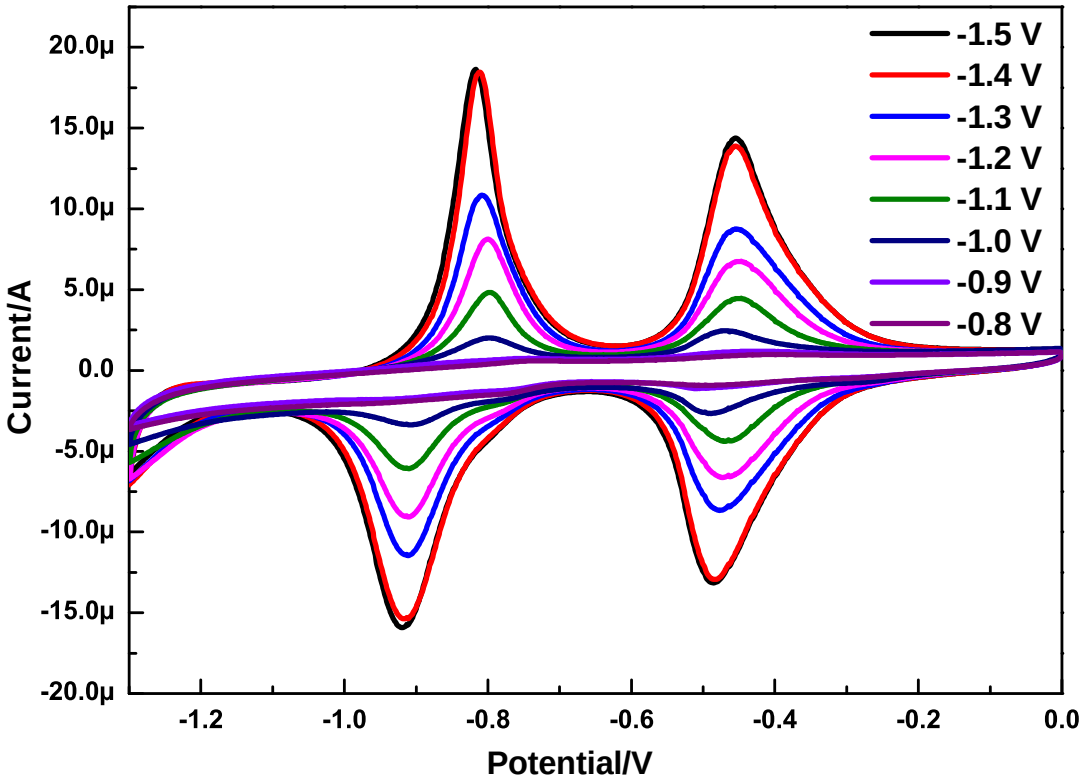

Figure 3.6: Cyclic voltammograms of PVC_5 film formed on GCE surface from 1.0 mM PyC_5Br_2 at different potentials from 0 V to $-0.8 \sim -1.5$ V, 15 scan cycles. The formed PVC_5 was tested in monomer-free 0.1 M KCl solution, scan rate: 50 mV/s.

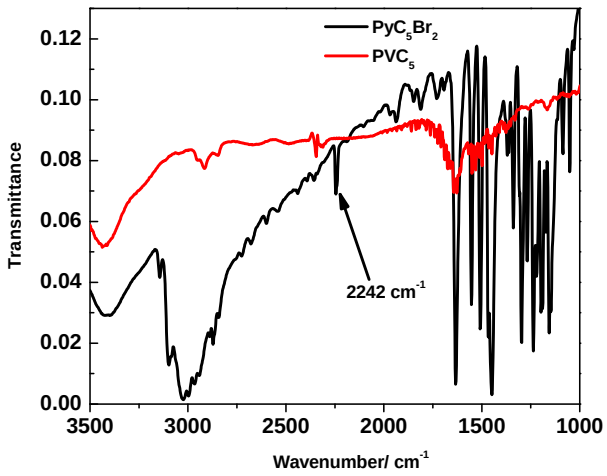

Figure 3.7: IR spectra of PyC_5Br_2 and PVC_5.

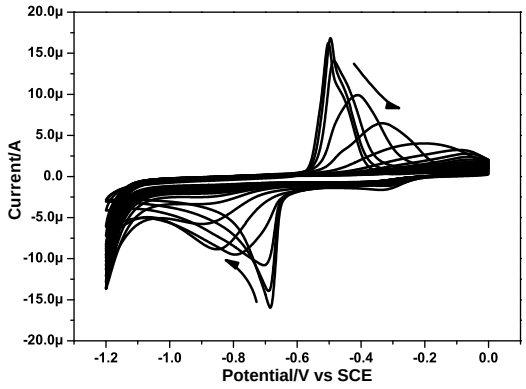

(a)

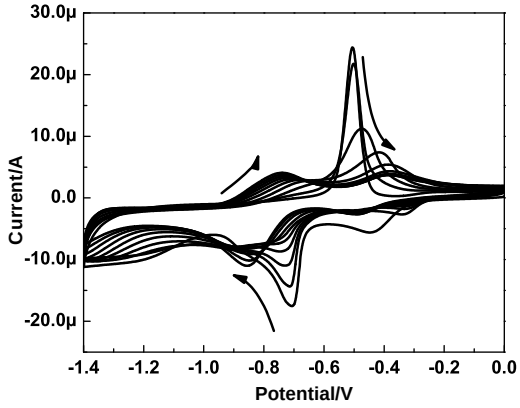

(b)

Figure 3.8: Cyclic voltammograms of the electropolymerization of 0.5 mM PyBenBr$_3$ (a) and PyBenMeBr$_3$ (b) in 0.1 M KCl solution, scan rate 50 mV/s, 15 scan cycles.

3.3.3 Electrosyntheses and Characterization of Crosslinked Polyviologens

Two different trifunctional branched cyanopyridinium salts, PyBenBr$_3$ and PyBenMeBr$_3$, were studied as monomers for polymerization. As shown in Figure 3.8 (a), PyBenBr$_3$ can be reduced at -0.7 V. However, a deficient viologen redox response was observed. In contrast, PyBenMeBr$_3$ can be reduced at -0.7 V, and the polyviologen has formed with redox peak potentials at -0.43 V (O1), -0.52 V (R1), -0.80 V (O2), and -0.97 V (O2).

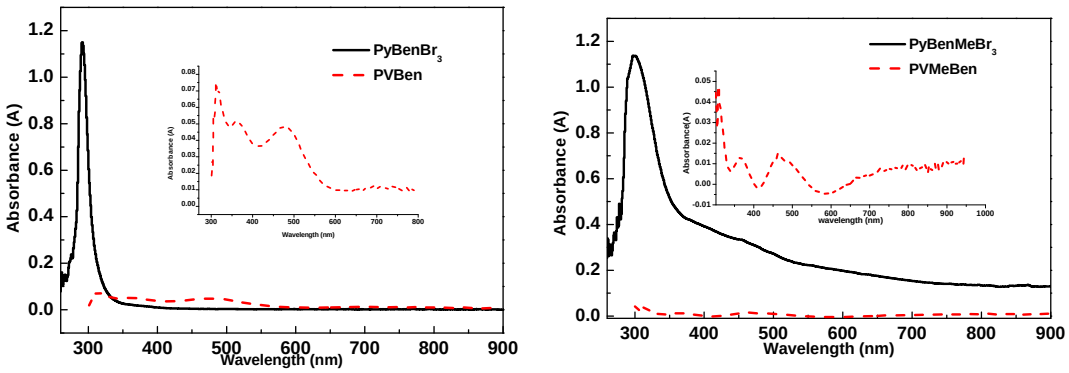

(a) (b)

Figure 3.9: Absorption spectra of PVBen (a) and PVBenMe (b). The solid lines are their precursors $PyBenBr_3$ and $PyBenMeBr_3$.

The trifunctional monomers were dissolved in distilled water for UV-Vis absorption studies and polyviologen films were electrodeposited on ITO electrodes for UV-Vis absorption measurements. The UV-Vis spectra are shown in Figure 3.9. Compared with the monomers, both of which have an absorption peak at 290 nm, the polyviologens exhibit $\pi - \pi^*$ absorptions at about 310 nm for dication state and 380 nm for radical cation state.[59,72]

To investigate surface morphology, PVBen and PVBenMe films were electrodeposited on ITO glass surfaces. The AFM images of PVBen and PVBenMe are shown in Figure 3.10. The surface roughness was analyzed using Gwyddion software.[73] The matrix ITO glass has a roughness value of $R_a = 0.96$ nm, suggesting it has a smooth surface and has a little morphological effect on the polymerized films. PVBen has a smooth surface with a roughness value of $R_a = 2.03$ nm. This material was investigated in 2015.[71] Even though its redox response grows with increasing scan rate, a non-linear relationship between currents and scan rates, or the square root of the scan rates, were observed. These observations suggest a condensed, non-open structure. In contrast, PVBenMe has a coarse texture with $R_a = 10.01$ nm due to its open cross-linked structure, which has also been

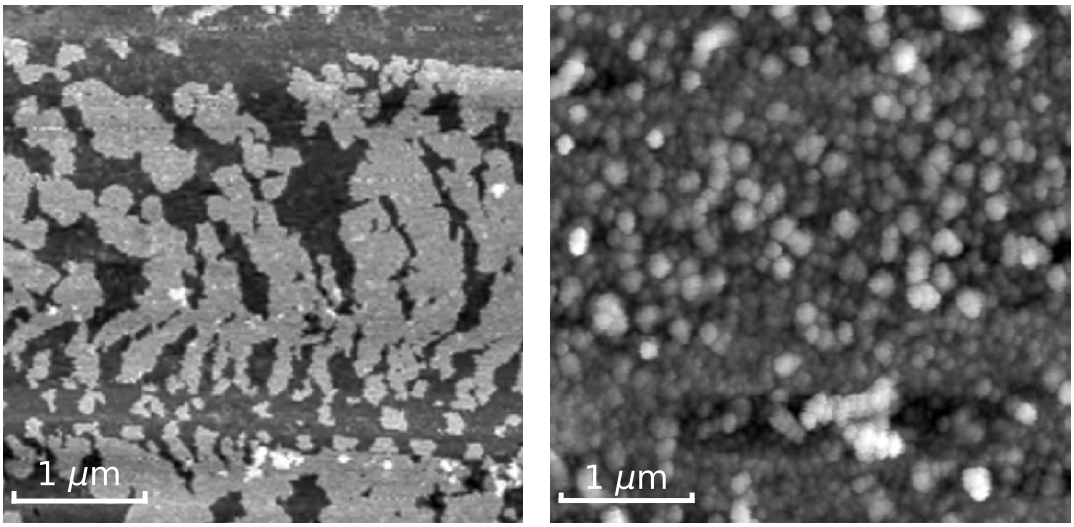

(a) (b)

Figure 3.10: AFM images of PVBen (a) and PVBenMe (b).

reported by Wang et al.[56] Therefore, $PyBenMeBr_3$ was used as the comonomer for copolymerization.

3.3.4 PyC_5Br_2 and $PyBenMeBr_3$ Electrocopolymerization

In order to determine efficient copolymerization concentrations for PyC_5Br_2 and $PyBenMeBr_3$, a series of experiments were repeated with various concentrations (0.5, 1, 2, 3, and 5 mM) of linear and branched phenyl monomers. The viologen polymers formed on the GCE surface were evaluated electrochemically in monomer free 0.1 M KCl solution. As shown in Figure 3.11, linear viologen film, PVC_5, shows increasing redox current responses by increasing the concentration of PyC_5Br_2. This means that the monomer radical keeps polymerizing on the viologen film surface. The formed film has an open structure that allows monomers and ions and electrons to be transferred to the electrode. $PyBenMeBr_3$ shows quite different behavior. Figure 3.11 (b) indicates that with increasing $PyBenMeBr_3$ concentration, PVBenMe formed on the electrode surface shows increasing

redox current responses, indicating more polyviologen deposition on the GCE surface. However, the viologen film cannot be polymerized when the concentration reaches 2.0 mM or higher. Instead, the films show little redox current response in cyclic voltammetry. This might be caused by more monomers being reduced and absorbed on the electrode surface, saturating the polymerization area of the electrode surface. As a result, the formed film may be very dense and lack permeability; electrolytes or electrons to the electrode then cannot transfer in and out of the film efficiently.

In Figure 3.11 (b), R_1 represents $PVBenMe^{2+}$ to $PVBenMe^{\bullet+}$ reduction and is lower than R_2 which represents $PVBenMe^{\bullet+}$ to neutral PVBenMe. The asymmetry of the areas under the peaks suggests that not all viologen dication moieties are accessible for easy reduction, but are reduced at higher potentials, blending into the R2 reduction. The poor electrochemical accessibility of PVBenMe indicates it is not suitable for fuel cells, since only the out layer is in contact with the fuel cell solution, and the inner viologen moieties are less available to participate. Compared with PVC_5 and PVBenMe formed at a concentration of 1.0 mM, the redox currents of PVC_5 are more than 20 μA, while the redox currents of PVBenMe are less than 10 μA. This indicates a higher amount of PVC_5 was coated on the GCE surface than PVBenMe.

Copolymerization was performed using the potentiodynamic method from 0 V to -1.2 V at a scan rate of 50 mV/s in 0.1 M KCl aqueous solution. Figure 3.12 (a) shows the cyclic voltammogram for the copolymerization of 3 mM PyC_5Br_2 and 2 mM $PyBenMeBr_3$. The reduction peaks at approx. -0.7 V and -0.8 V show that the cyanopyridinium groups of the monomers PyC_5Br_2 and $PyBenMeBr_3$ were being reduced. The voltammogram shows additional redox peaks at approx. -0.95 V and -0.5 V after several scans, which correspond to the reduc-

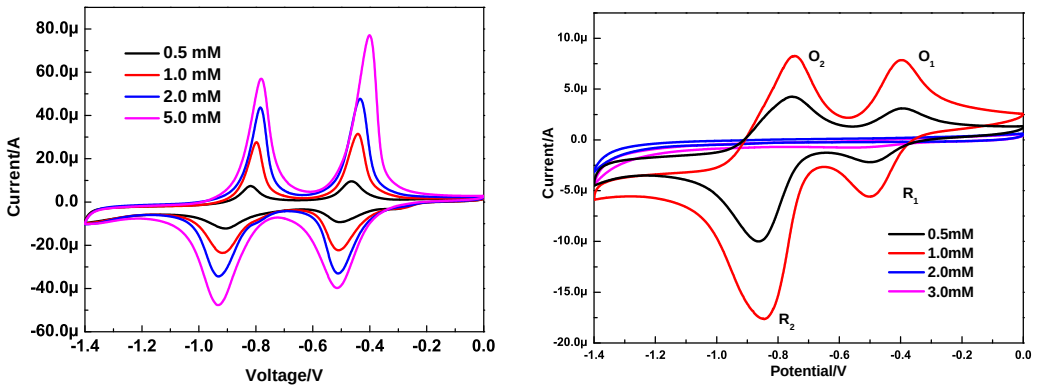

(a) (b)

Figure 3.11: Cyclic voltammograms from PVC_5 (a) and PVBenMe (b) in 0.1 M KCl solution, scan rate 50 mV/s. (The films were polymerized at different monomer concentrations in 0.1 M KCl solution scan rate 50 mV/s, 15 scan cycles.)

tion peaks of PVC_5 and PVBenMe. The oxidation peaks at approx. -0.75 V and -0.4 V in the reverse scan are from the neutral viologen to its radical cation and dication form. All these indicate the formation of polyviologen deposited onto the electrode surface. Copolyviologen films were synthesized at four different monomer concentration ratios to optimize conditions. A comparison of the redox responses in monomer free 0.1 M KCl solution for these copolyviologens is shown in Figure 3.12 (b). The copolymers formed at PyC_5Br_2/$PyBenMeBr_3$ concentration ratio of 1:4 showed lowest redox current responses. Increasing the component ratio of PyC_5Br_2 in the monomer mixture, the copolymers redox responses increased. Since the copolymer synthesized at the concentration ratio of 3 mM PyC_5Br_2 and 2 mM $PyBenMeBr_3$ showed slightly higher redox responses, this copolymer was chosen for further study and development.

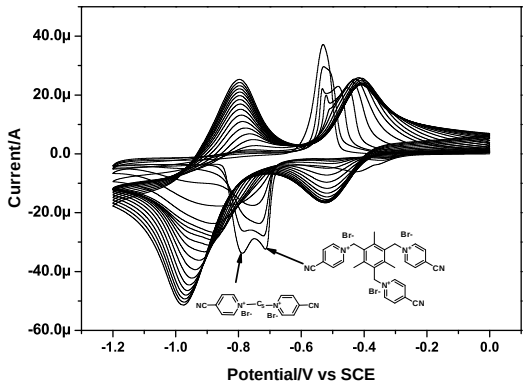

(a)

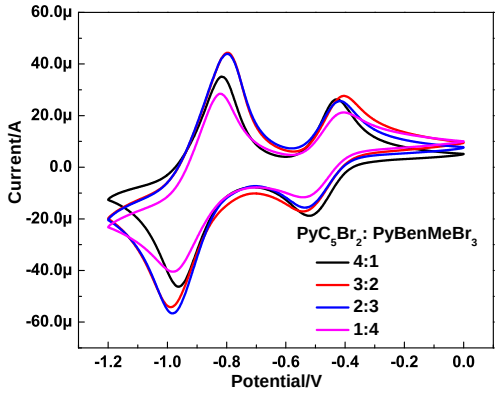

(b)

Figure 3.12: A cyclic voltammogram from the copolymerization of PyC_5Br_2 and $PyBenMeBr_3$ in 0.1 M KCl solution at a scan rate 50 mV/s on the GCE (a) and cyclic voltammograms of copolyviologens formed at different monomer ratios, tested in 0.1 M KCl solution, scan rate 50 mV/s (b).

3.3.5 Stability of Copolyviologen in Alkaline Solution

Since the polyviologen films must function in alkaline solution, polyviologen modified electrodes were immersed in 0.1 M KCl solution at different pHs. After 50 voltammetric cycles from 0 to −1.3 V, the modified electrodes were put into neutral 0.1 M KCl solution to test its electrochemical activity. Of the viologen's three redox forms, PolyV^{2+} is used as the carbohydrate oxidation catalyst. Therefore, the main focus of the viologen stability evaluation is the O_1 (oxidation of PolyV$^{\bullet+}$ to PolyV^{2+}) current response. As shown in Figure 3.13 (a) or (c), the redox peak currents of PVC_5, especially the first redox peak current which represents the PolyV^{2+} to PolyV$^{\bullet+}$ couple, decreased dramatically with increasing solution pH. This is permanent damage to the film and the currents cannot be recovered when putting this film into lower pH again. In comparison, even though the redox currents decrease, the copolyviologen still has two prominent redox peaks (Figure 3.13 (b) or (d)), which indicate its improved retention of catalytic activity. The higher stability of the copolymer is expected due to some steric protection from the methyl groups on the crosslinking moiety. With methyl groups blocking the oxidation site on the neighboring pyridinium cation, the rigid structure reduces the undesirable oxidation. The lost catalytic activity might also be caused by some dealkylation, shown in Figure 3.14 using MV as an example. In this dealkylation process, the methoxide formed on dealkylation is a reducing agent and reduces MV^{2+} into MMV^{+}.[54] Some papers reported that monoalkyl viologen (such as MMV) has a high stability in alkaline solutions,[34] but this would have a decreased catalytic activity due to losing one active pyridinium center.

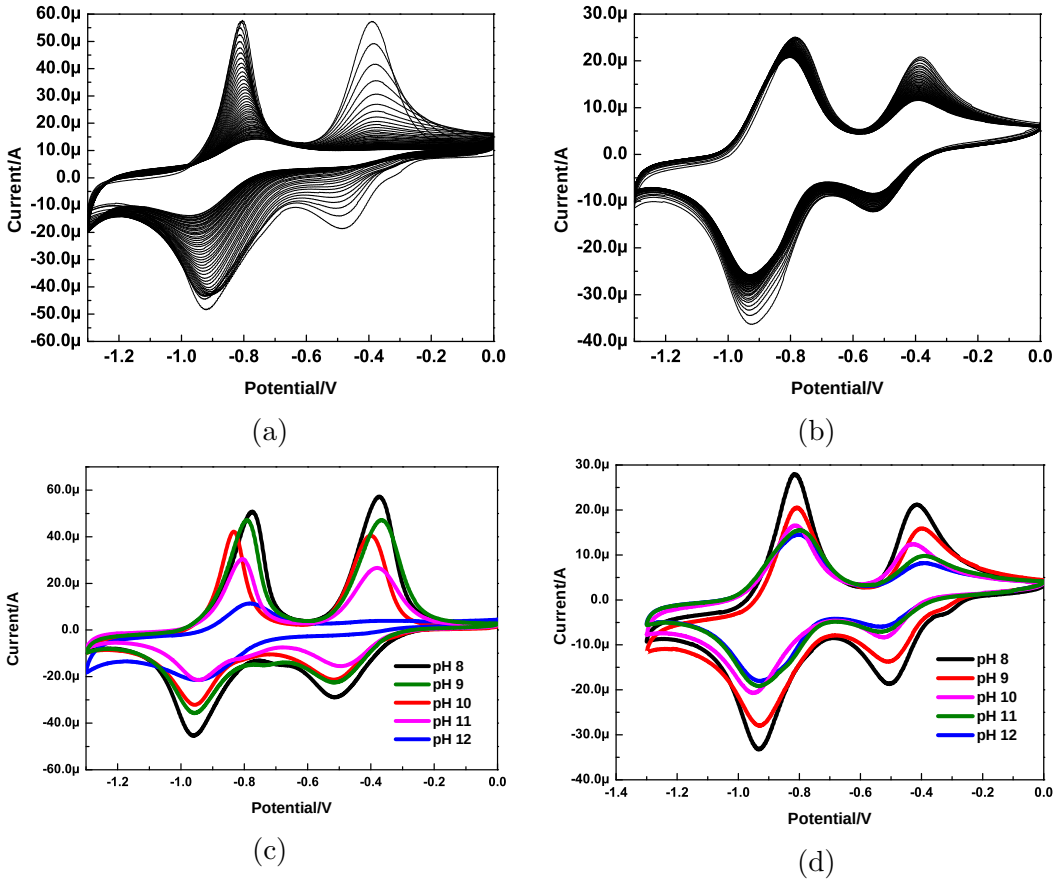

Figure 3.13: Cyclic voltammograms of PVC_5 (a) and copolyviologen (b) in pH 12 0.1 M KCl solution, scan rate 50 mV/s, 50 scan cycles, the 50^{th} scan cycle of PVC_5 (c) and copolyviologen (d) in different alkaline solutions.

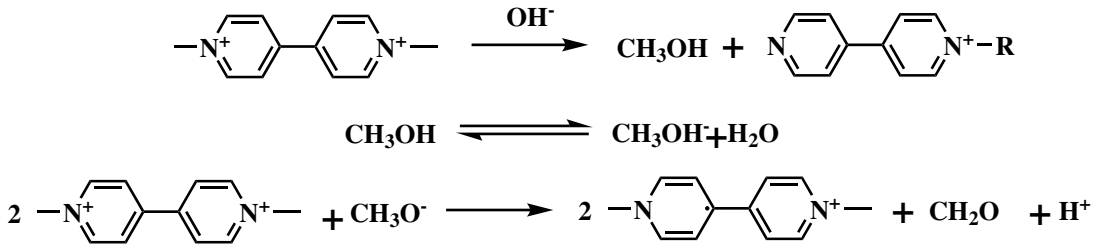

Figure 3.14: MV dealkylation in the alkaline solution.[54]

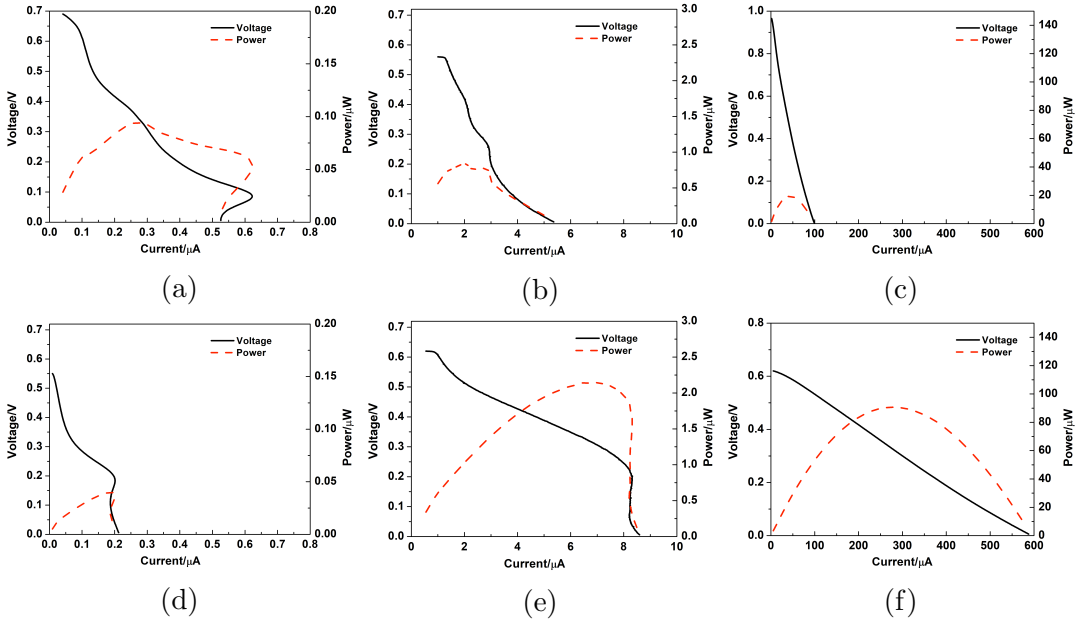

Figure 3.15: Power curves for fuel cells with Pt/Nafion film as the cathode and PVC_5 On GCE (a), CNT@GCE (b), carbon felt (c), and copolymer on GCE (d), CNT@GCE (e), carbon felt (f) as the anode. The fuel cell solution is 5 mM glucose pH 9.7 0.1 M KCl.

3.3.6 Copolyviologen Catalyzed Glucose Fuel Cells

To determine the effectiveness of the copolyviologen films in glucose/O_2 alkaline fuel cells, PVC_5 and copolymer were electropolymerized on GCE, CNT@GCE, and carbon felt electrodes for use as anodes in glucose/air fuel cells. A commercially available air-breathing Pt/Nafion film electrode was chosen as the cathode to ensure that it would not be the limiting electrode in the fuel cell. The results are shown in Figure 3.15 and summarized in Table 3.1. As expected, without polyviologen modification, the GCE, CNT@GCE, and carbon felt electrodes show extremely weak open-circuit voltage (OCV) and short circuit current (maximum current). With PVC_5 modification, the GCE anode showed an SCC of 0.52 μA, and an OCV of 0.7 V; the CNT@GCE anode showed an improved SCC of 5.25 μA. The maximum currents for copolymer on GCE and CNT@GCE an-

Table 3.1: Comparison of glucose/air fuel cells composed of an air-breathing Pt/Nafion cathode with different anodes. The units for current, voltage, and power are μA, V, and μW, respectively. Experiments were performed using 5 mM glucose in 0.1 M KCl solution with a pH 9.7, at 25 °C

	OCV	i_{max}	Starting		$Power_{max}$
			Voltage	Current	(voltage, current)
Blank GC	0.06	0.046	0.05	0.023	0.003 (0.11, 0.23)
Blank GC CNT	0.05	0.08	0.06	0.06	0.003 (0.05, 0.06)
Blank Carbon felt	0.06	0.8	0.06	0.69	0.04 (0.062, 0.71)
PVC5 GC	0.7	0.52	0.7	0.03	0.08 (0.36, 0.2)
Copolymer GC	0.56	0.21	0.56	0.013	0.056 (0.312, 0.18)
PVC5 GC@CNT	0.57	5.25	0.57	1.3	0.33 (0.16, 2.13)
Copolymer GC@CNT	0.62	8.59	0.62	0.55	2.15 (0.316, 6.79)
PVC5 carbon felt	0.965	98.5	0.965	1.7	19.3 (0.413, 46.6)
Copolymer carbon felt	0.62	587.9	0.62	5.6	90.6 (0.325, 278.9)

odes were as 0.21 μA and 8.59 μA, and the current densities for copolymer on GCE and CNT@GCE are calculated as 10.76 $\mu A/cm^2$ and 121.6 $\mu A/cm^2$ (geometrical surface area of GCE). Up to now, the highest current density 20 mA/cm^2 was reported when 110 mM MV^{2+} was added into a 0.5 M glucose pH 11 $\sim$ 12 0.25 M potassium phosphate buffer solution.[38] However, this system used high MV^{2+} and glucose concentration in solutions. The only reported immobilized polyviologen on graphite used as an anode only generated 2.5 μA (without the anode area), using 10 mM DHA in a pH 11 0.25 M potassium phosphate buffer solution.[74] Compared with this system, the copolymer on CNT@GCE produced a much higher current.

To increase the fuel cell performance further, a carbon felt anode, which has a large polymerization surface area, was chosen for modification. Without modification, carbon felt anodes showed a weak current response, as listed in Table 3.1. After electropolymerization, carbon felt electrodes showed improvement in SCCs and output powers. With PVC_5 modification, the fuel cell SCC was increased to 98.5 μA, with an OCV of 0.96 V. However, the fuel cell solution turned light yellow in 5 min after putting PVC_5-modified carbon felt into the fuel cell solution, indicating the PVC_5 falling off from the carbon felt. The copolymer showed the highest SCC of 597.8 μA with an OCV of 0.62 V. Compared with 2.5 μA produced by viologen polymer on graphite electrode,[74] PVC_5 and copolyviologen modified carbon felt anodes showed highly improved performance. Unfortunately, the exact polymerization surface area of the carbon felt electrodes were not obtained in this study, and so the current densities were not calculated.

The fuel cell performance was also characterized in 0.1 M KCl solution with 5 mM glucose at a pH of 8.1. As shown in Figure 3.16, increasing the fuel cell solution pH increases the catalytic performance of copolyviologen. However, since the Pt/Nafion cathode has proton exchange membranes that can be damaged in alkaline solution, the copolyviologen was not characterized using a higher pH fuel cell solution, and the lifetime stability of the copolyviologen was not characterized.

3.4 Conclusion

Different linear polyviologens (PVC_n) with various alkyl length spacers were synthesized electrochemically using α,Ω-bis(4-cyano-pyridino)alkane dibromides as precursors. The longer the alkyl chain on alkylcyanopyridinium salts, the higher

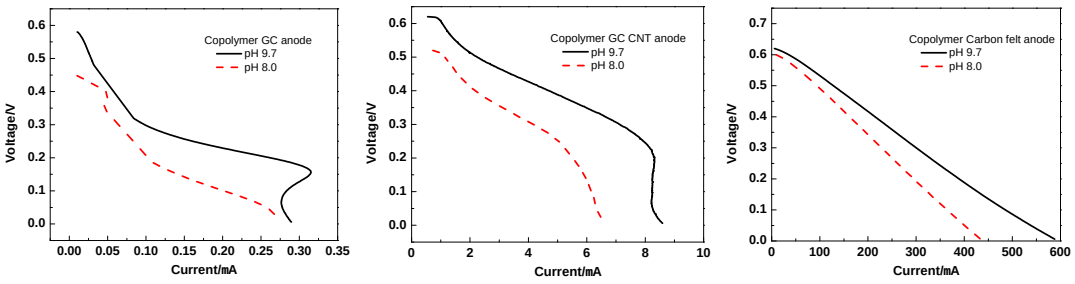

(a) (b) (c)

Figure 3.16: Polarizations curve for fuel cells with Pt/Nafion film as the cathode and copolyviologen on GCE (a), CNT@GCE (b), carbon felt (c) as the anode. The fuel cell solution is 0.1 M KCl at pH 9.7 (black solid line), 8.1 (red dash line).

the polymerization efficiency. The polymers formed were characterized by CV and IR. PVC_5 and PVC_6 demonstrate an open, cross-linked structure, while PVC_2, PVC_3, or PVC_4 have adsorption controlled redox behavior. In this work, PVC_5 was chosen for further study. The electropolymerization conditions for PVC_5 was optimized, and films formed by cycling between $0 \sim -1.4$ V have higher redox currents than those cycled beginning at 0 V and ending at $-0.8 \sim -1.3$ V.

Branched polyviologens PVBen and PVBenMe were also successfully electropolymerized on GCE's and characterized by CV, UV-Vis, and AFM. Since the methylated branched polyviologen was shown to have a more open structure, it was chosen for copolymerization with PVC_5.

To increase the stability of linear polyviologens in alkaline solution, copolyviologen was carried out by mixing linear PyC_5Br_2 and branched $PyBenMeBr_3$ into one solution. The copolymerization ratio was controlled by changing the concentrations of these two monomers. With 3:2 of linear:branched monomer ratio, the formed copolymer showed the highest redox currents. In a pH 12 solution, the copolymer is more stable than PVC_5.

The copolyviologen were also coated on CNT@GCE and carbon felt elec-

trodes. PVC_5 and copolymer deposited electrodes were investigated as glucose alkaline fuel cell anodes. The copolymer on carbon felt produced a current of 587.9 μA, which is much higher than 2.5 μA produced by the polyviologen modified graphite anode reported in the literature.[74]

Chapter 4

CB[7]-Polyviologen-modified Electrodes for Glucose Fuel Cells

4.1 Introduction

Viologens as homogeneous carbohydrate alkaline fuel cell catalysts have been reported in several studies.[35,68,69] With methyl viologen as a catalyst, a dihydroxyacetone fuel cell was able to generate a current density up to 20 mA/cm^2 (geometric area). However, water-soluble viologens, which are toxic to humans, can result in environmental problems. An approach to overcome this problem is to immobilize viologens on the fuel cell electrodes. Several methods have been used to immobilize viologen polymers on electrodes. Among them, electropolymerization is an efficient way that can also allow some control of the polyviologen morphology on the electrodes. Two types of immobilized viologen (as shown in Chapter 3 Figure 3.1), linear polyalkylviologens (PyC_n) and branched polyviologens (PVBen and PVBenMe) have been electropolymerized on electrodes by different groups.[51,70] However, none have been used as catalysts for carbohy-

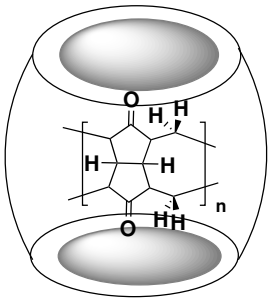

Figure 4.1: Structure of cucurbit[n]uril (CB[n]).

drate fuel cells. Since branched polyviologens (PVBen and PVBenMe) have rigid structures and large benzyl groups around the viologen units, which hinder the diffusion of carbohydrates and electrolytes, they are not good candidates to be carbohydrate oxidation catalysts. As discussed in Chapter 1.4, some alkyl-based polyviologens have flexible chains and can form more accessible structures, which allows them to interact with carbohydrates and electrolytes more efficiently. However, these long-chain polymers might swell and delaminate from the electrode surface. Moreover, viologens units in a polyalkylviologen are unstable in alkaline solution due to the oxidation with OH^-, which has been discussed in detail in Chapter 1.4.

Pseudorotaxanes are a class of supra-molecule that has a linear molecule as the inner axle and a macrocyclic molecule as the outer wheel. Cucurbit[n]uril (CB[n]) (as shown in Figure 4.1) is a type of macrocyclic wheel, which consists of n (5 - 10) glycoluril units and 2n methylene bridges. CB[n]s have exo-carbonyl groups and a hydrophobic cavity that binds various guests via ion-dipole and hydrophobic interactions. After being encapsulated, guest properties (i.e., diffusion coefficient, solubility) are highly altered. Given this, supramolecular host-guest complexes have been widely investigated for drug delivery,[75] fluorescence spectroscopy,[76] catalysis,[77] and nanotechnology.[78] CB[7] as an effective host not only has a

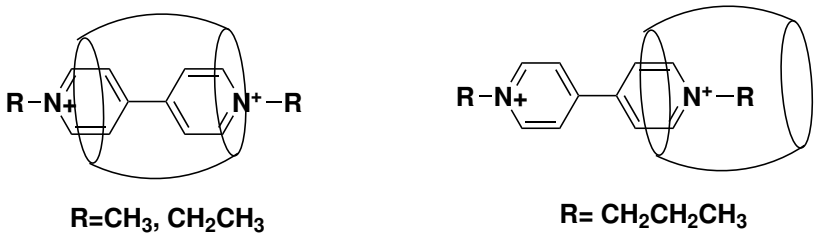

Figure 4.2: Interaction of alkyl viologens and CB[7].

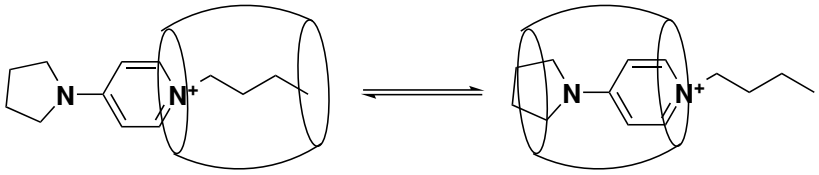

Figure 4.3: Interaction of 4-pyrrolidinopyridinium salt and CB[7].

suitable cavity to encapsulate more sizable guest molecules but also has a greater solubility in aqueous solutions (as high as 10 mM) than other CB[n] analogs (0.01 mM for CB[8] or CB[10]).[79] This makes CB[7] widely studied.

CB[7] hosted viologens have been studied systematically.[62] As shown in Figure 4.2, it was found that CB[7] included the nucleus of methyl viologen (MV^{2+}) and ethyl viologen (EV^{2+}) to form pseudorotaxane complexes, while CB[7] encapsulates the aliphatic moieties of propyl viologen or other viologens with chains longer than three carbons.

A series of alkyl substituted 4-pyrrolidinopyridinium salts guests with different alkyl chains' lengths has been studied with CB[7] (Figure 4.2).[80] The binding behavior between CB[7] and the molecules containing pyridinium and alkyl units is highly dependent on the length of the alkyl chain. If the alkyl chain has more than four carbons (butyl), CB[7] is able to shuttle between the pyridine and pyrrole rings, and the alkyl chain, in a dynamic equilibrium, as shown in Figure 4.3.

Since polyviologens (PVC_n) can be electrosynthesized from cyanopyridinium

salts (PyC_nBr_2), which have been discussed in Chapter 2, it was hypothesized that PVC_n@CB[7] (guest@host, the symbol "@" indicates the formation of an inclusion complex.)[81] can be electrosynthesized from PyC_nBr_2@CB[7] as precursors. To our best knowledge, no one has reported the use of electropolymerization to form this type of polypseudorotaxane. Since CB[7] encapsulates the pyridinium group or alkyl chains of viologen, we predict that CB[7] can protect the α-C on the pyridine rings from oxidation and hinder dealkylation in alkaline solution.

In this work, electropolymerization to form PVC_n@CB[7] from PyC_nBr_2@CB[7] is discussed. The binding of PyC_nBr_2 with CB[7] was studied qualitatively using ^{1}H NMR. These pseudorotaxane systems were used to provide the monomers to form CB[7]-threaded polyviologens on glassy carbon electrodes (GCE), carbon nanotube modified glassy carbon electrodes (CNT@GCE), and carbon felt electrodes electrochemically. The effect of CB[7] on PyC_nBr_2 electropolymerization is also discussed. The stability and electrochemical characters of PVC_n@CB[7] complexes were investigated. Polypseudorotaxane-modified anodes were used to fabricate glucose alkaline fuel cells.

4.2 Experimental

4.2.1 PyC_nBr_2@CB[7] Pseudorotaxane Complexes

CB[7] is available commercially but we are grateful to Prof. Ronald L. Halterman and Dr. Justin Garrett at the University of Oklahoma for providing a sample. PyC_nBr_2 (n = 2 - 6) were prepared as described in Chapter 3. Pseudorotaxane PyC_nBr_2@CB[7] systems were formed in a series of CB[7]:PyC_nBr_2 0.1 M KCl solutions containing different concentrations (1 mM, 2 mM, 3 mM, 4 mM) of

CB[7] as the host and 2 mM PyC_nBr_2 (n = 2 - 6) as guests. The PyC_nBr_2@CB[7] complexation was confirmed and studied by ^{1}H NMR. PyC_nBr_2 (5 mM) was prepared in D_2O solution, and CB[7] (0.5 equivalent) was added into aliquots of the PyC_2Br_2 and PyC_3Br_2 guest solutions. Four aliquots of CB[7] (0.5 equivalent) were added into PyC_4Br_2, PyC_5Br_2 and PyC_6Br_2 guest solutions in succession. After each addition, the mixture was incubated for 24 h before ^{1}H NMR measurements.

4.2.2 PVC_n@CB[7] Polypseudorotaxane Synthesis

PVC_n@CB[7] were electrosynthesized from monomers PyC_nBr_2@CB[7] using cyclic voltammetry (CV) and a CH Instruments 832 potentiostat. The polymerization process was described in Chapter 2.

4.2.3 PVC_n@CB[7] Characterization

Cyclic voltammetry measurements were performed to characterize the electrochemical properties of each PVC_n polymer and PVC_n@CB[7] polyseudorotaxane polymer coated on GCEs in 0.1 M KCl solution.

IR spectra were measured using a Bruker Tensor 27 spectrometer ranging from 3,500 to 370 cm^{-1}. The monomer PyC_5Br_2 was dried and mixed with 200 mg KBr and pressed into pellets. The PVC_5@CB[7] films were polymerized on the ITO glass and removed by scraping. After drying, the polymers were mixed with 200 mg KBr and pressed into pellets for measurement.

4.2.4 Polyviologen@CB[7] Modified Anode Characterization

PyC_5Br_2 and PVC_5@CB[7] coated GCE, CNT@GCE, and carbon felt electrodes were used as the anodes in glucose/air fuel cells. One compartment cells were made using 5 mM glucose as the fuel, which was dissolved in 0.1 M KCl solution at pH 9.7. As shown in Figure 3.2, the fuel cell was connected to a CH Instruments 832 potentiostat. The anode was connected as both a reference and auxiliary electrode. The air-breathing Pt/Nafion cathode was connected as the working electrode. Linear sweep voltammetry experiments were performed on the fuel cell from 0.005 V to open circuit voltage at 2 mV/s.

4.3 Results and Discussion

4.3.1 PyC_nBr_2@CB[7] ^{1}H NMR Spectroscopy

The host-guest binding interactions between CB[7] and PyC_nBr_2 (n = 2 - 6) were characterized qualitatively using ^{1}H NMR spectroscopy. Figure 4.4 (a) shows the chemical shift changes of PyC_2Br_2 protons on adding CB[7]. Without CB[7], the chemical shifts detected at 9.31 and 8.61 ppm are assigned as the pyridyl proton peaks **b** and **a**. The alkyl proton peak **c** is at 5.48 ppm. Adding 0.5 equivalent or 1.0 equivalent of CB[7] results in the alkyl proton peak **c** merging into the CB[7] proton peaks. The broad peaks at 9.31 and 8.61 ppm indicated the included PyC_2Br_2 and free PyC_2Br_2 dynamic equilibrium exchange on the ^{1}H NMR time scale.[82,83] The peaks associated with CB[7] can be found at 4.1 ppm, 5.5 ppm, and 5.8 ppm, which are the 14 outer methylene protons, the 14 methylene protons, and the 14 inner methylene protons, respectively. Since PyC_2Br_2 has a similar

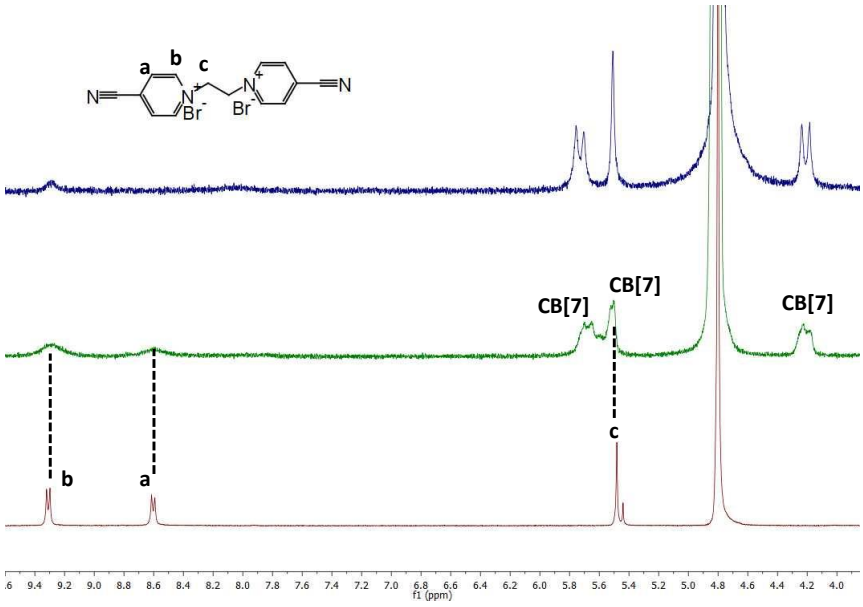

(a)

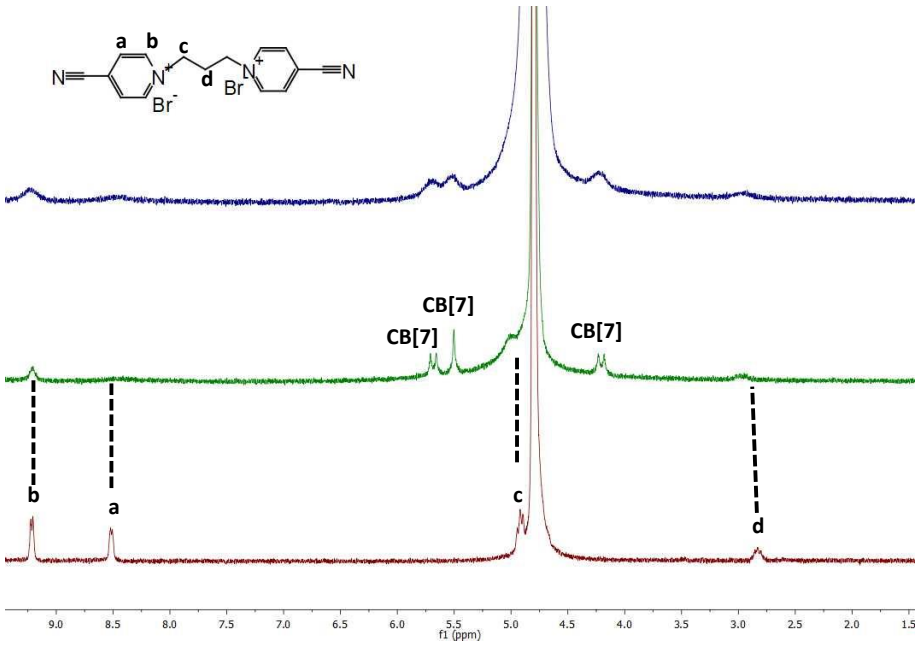

(b)

Figure 4.4: Interactions of PyC_2Br_2@CB[7] (a), PyC_3Br_2@CB[7] (b): ^{1}H NMR spectra (300 MHz, D_2O) of PyC_nBr_2 (5 mM) from bottom to top: 0, 0.5, and 1.0 equivalent of CB[7].

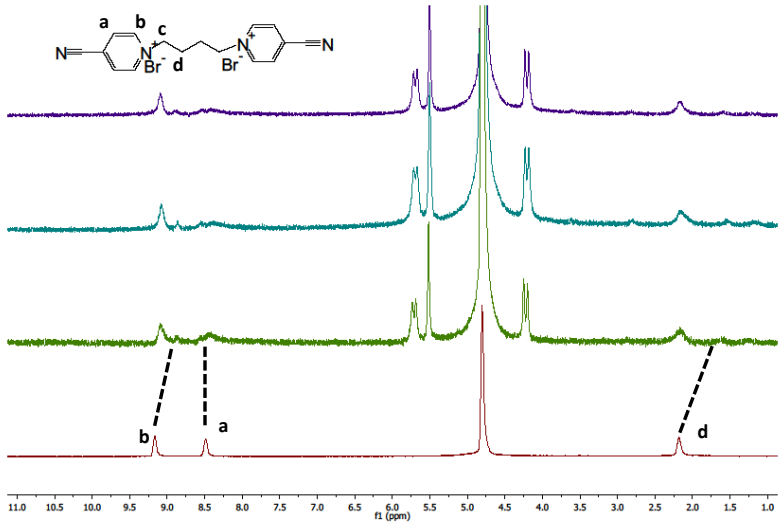

Figure 4.5: Interaction of 5 mM PyC_4Br_2 and CB[7]. ^{1}H NMR data, from bottom to top: 0, 0.5, 1.0 and 2.0 equivalents of CB[7].

length to methyl viologen, which was reported to be entirely included in the cavity of CB[7];[84] it was expected that the whole of PyC_2Br_2 is encapsulated by CB[7].

As Figure 4.4 (b) shows, a similar result was obtained using PyC_3Br_2 as the guest. After adding 0.5 or 1.0 equivalent of CB[7], peaks at 9.2, 8.5, and 2.8 ppm became broader due to the dynamic equilibrium exchange of encapsulated PyC_3Br_2 and free PyC_3Br_2. The aromatic proton b is somewhat more distinct, suggesting it is less sensitive to the complexation effects. Proton **c** from PyC_3Br_2 is merged into CB[7] peaks.

As shown in Figure 4.5, after adding 0.5 equivalent of CB[7] into PyC_4Br_2, the peak at 8.49 ppm became broadened due to dynamic equilibrium exchange of encapsulated PyC_4Br_2 and free PyC_4Br_2. After adding 2.0 equivalents of CB[7], this broad peak begins to split into two peaks indicating more PyC_4Br_2 was

encapsulated by CB[7]. The aromatic protons **b** are again, more distinct, and less affected by broadening. It is assumed that the shielding region of CB[7] is 6.2 Å, which is the interatomic distance between carbonyl oxygens axially spanning the cavity of CB[n] and has been determined by using a series of n-alkane diamine as guests and CB[6] as the host.[85] This distance is approximately 4.5 methylene units.[85] The length of the butyl group from PyC_4Br_2 is less than 4.5 methylene units, confirming the butyl group can be encapsulated by CB[7].

In the case of PyC_5Br_2, the pentyl group's length on PyC_5Br_2 is 4.935 Å as reported in the literature.[51] Since in the CB[7] shielding region, the protons in the pentyl group begin to have upfield shifts after adding CB[7] in PyC_5Br_2 solution, which was shown in Figure 4.6 (a). Since the aromatic proton **b** is positioned in the shielding region, it begins to shift from 9.13 to 8.80 ppm. Similarly, proton **a** is positioned out of the cavity and begins to show a downfield shift from 8.44 to 8.61 ppm due to the deshielding effect of the carbonyl group from CB[7].

As reported, all the alkyl protons in the 1,6-hexanediamine@CB[6] complex shift upfield.[85] Therefore, the hexyl protons on PyC_6Br_2@CB[7] are expected to show upfield shifts. As Figure 4.6 (b) shows, the alkyl proton **d** and **e** begin to shift from 2.03 to 1.16 ppm, and 1.40 to 0.51 ppm, respectively. The peak of proton **c** on PyC_6Br_2 is submerged in the solvent peak and is not detected even after adding CB[7]. The peak of aromatic proton **a** shifts from 8.44 to 8.57 ppm, indicating that the proton **a** on PyC_6Br_2 is located out of the carbonyl-laced rim. The other aromatic proton **b** shifted from 9.10 to 8.87 ppm, indicating **b** is affected by CB[7] shielding region. However, the protons (on the carbons adjacent to amino groups) on 1,7-diaminoheptane have been reported to be out of the CB[6] shielding region and showed slightly deshielded shifts (-0.08 ppm) on CB[6] inclusion.[85] Since the aromatic proton **b** has a large $\Delta\delta$ ($+0.13$ ppm),

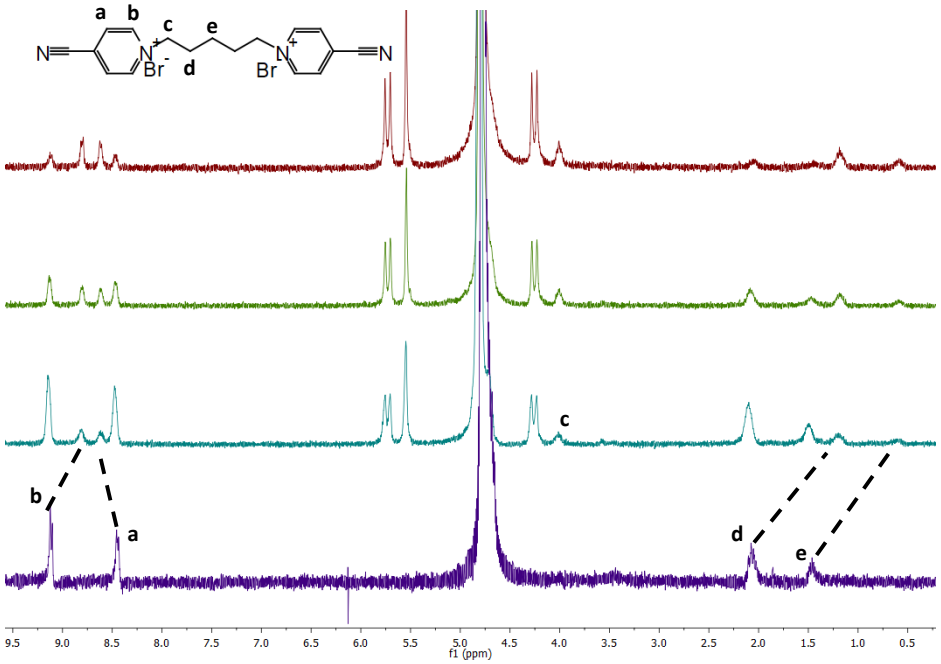

(a)

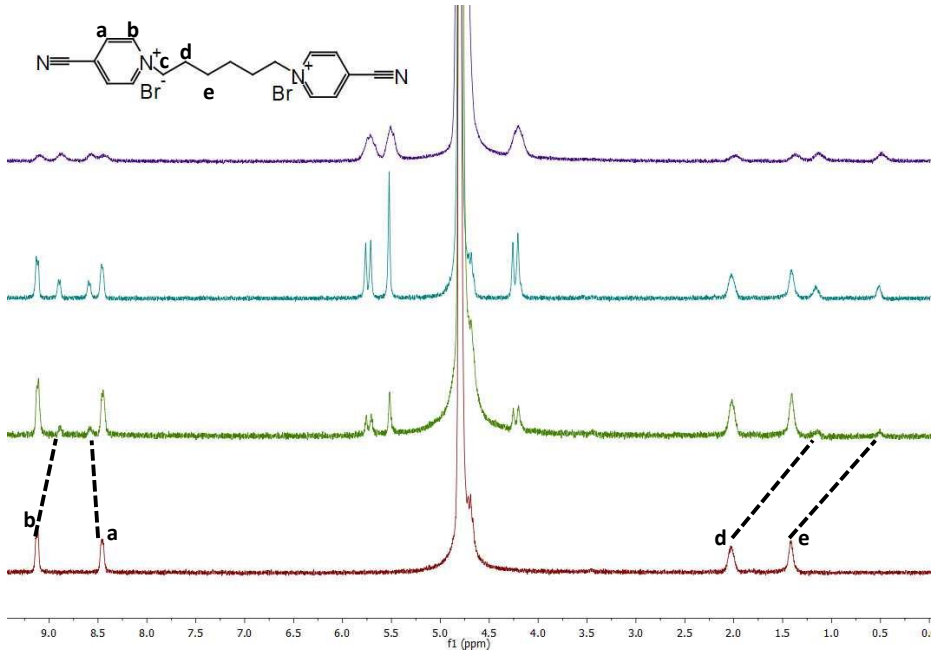

(b)

Figure 4.6: Interaction of 5 mM PyC_5Br_2 and CB[7] (a), PyC_6Br_2 and CB[7] (b). ^{1}H NMR data, from bottom to top: 0, 0.5, 1.0 and 2.0 equivalents of CB[7], respectively.

one hypothesis is that CB[7] shuttles from one side of the alkyl chain to another side in a dynamic equilibrium. Or PyC_6Br_2@CB[7] is a 1:2 complex such that two regions from CB[7] shield the proton **b** and the hexyl protons.

Based on the ^{1}H NMR information for PyC_4Br_2, PyC_5Br_2, and PyC_6Br_2, it can be expected that CB[7] can slip over the cyanopyridinium rings and is located over the butyl, pentyl, or hexyl chain of the guest. Based on the size of the CB[7] cavity, a stoichiometric complexation of 1:1 mole ratio for PyC_4Br_2@CB[7] and PyC_5Br_2@CB[7] is expected. The highest binding constant for 1,5-pentanediamine@CB[6] n-alkanediamine@CB[6] analog has been reported.[85] It's expected that PyC_5Br_2@CB[7] has the highest binding constant in this work.

4.3.2 PVC_n@CB[7] Polypseudorotaxane Electropolymerization

The PyC_nBr_2@CB[7] pseudorotaxane systems were used for electropolymerization to form polypseudorotaxanes, which are CB[7] threaded polyviologens. Cyclic voltammograms showing the polymerization processes for PyC_2Br_2 and PyC_3Br_2 are shown in Figure 4.7. Without CB[7], PyC_2Br_2 showed broad asymmetric reductive peaks at -0.68 V with a current of 30 μA, and PyC_3Br_2 also has a broad asymmetric peak at -0.75 V with a current 60 μA. The peak width at mid-height is 0.6 V for PyC_2Br_2 and 0.4 V for PyC_3Br_2. As discussed in Chapter 2, the reduction process of PyC_2Br_2 is diffusion-controlled in an aqueous solution. PyC_3Br_2 has a similar behaviour to PyC_2Br_2. After adding CB[7], both PyC_2Br_2 and PyC_3Br_2 showed a broader reductive peak with a decreased current response. After 15 cycles of successive scans, the electrodes were evaluated in a

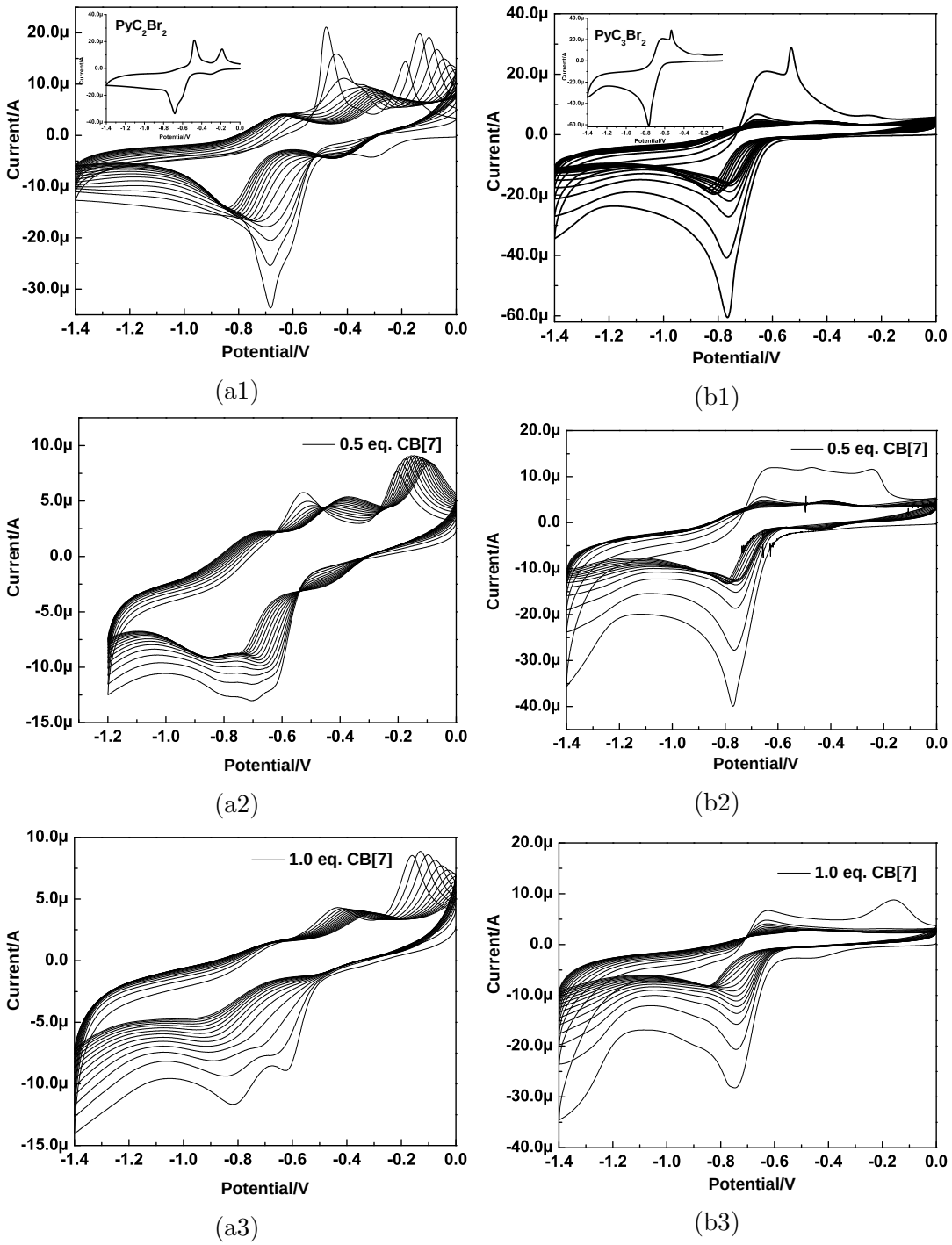

Figure 4.7: Cyclic voltammograms of the electropolymerization of 2 mM PyC_2Br_2 (a1, a2, a3) and PyC_3Br_2 (b1, b2, b3) with different equivalent of CB[7] in 0.1 M KCl electrolyte at a scan rate of 50 mV/s, 15 cycles.

Table 4.1: The current efficiencies (CEs) in 100% for precursors PyC_nBr_2 (n = 2 - 6) with varying amount of CB[7], the polymerization repeated 3 times.

Amount of CB[7]	0 eq.	0.5 eq.	1.0 eq.	1.5 eq.
PyC_2Br_2	7.3±4.1	8.3±5.6	6.9±7.1	-
PyC_3Br_2	12.5±2.0	5.7±6.7	3.4±5.4	-
PyC_4Br_2	30.4±1.6	22.8±2.9	22.1±2.1	27.5±3.2
PyC_5Br_2	34.6±3.5	43.4±5.0	77.1±6.5	15.0±4.2
PyC_6Br_2	40.6±2.1	39.4±3.4	22.3±4.8	16.4±3.5

monomer-free 0.1 M KCl solution. Compared with PyC_nBr_2 (n = 2 and 3), the PyC_nBr_2@CB[7] (n = 2 and 3) complexes had a low polymerization efficiency. (The polymerization efficiencies were calculated as described in Chapter 3 and are listed in Table 4.1.) This might be because PyC_2Br_2 or PyC_3Br_2 was entirely included by CB[7]. The reduced pyridyl ring is also included in the cavity of CB[7] and cannot couple efficiently to form viologen units. After adding 1 equivalent of CB[7] to PyC_2Br_2 and PyC_3Br_2 solutions, the two typical redox pairs of viologen unit almost disappeared on the CV. Given the low polymerization efficiency of PyC_2Br_2@CB[7] or PyC_3Br_2@CB[7] pseudorotaxanes, no more CB[7] was added for testing.

Figure 4.8 shows cyclic voltammograms for the electropolymerization processes using PyC_nBr_2 (n = 4, 5, and 6) with different amounts of CB[7] as monomers. Without CB[7], all three monomers PyC_nBr_2 were reduced at ca. −0.75 V with currents around 60 μA, as shown in Figures 4.8 (a1) - (c1). Figures 4.8 (a2) - (c2) show the polymerization results of adding 1.0 equivalent of CB[7] to 2 mM PyC_nBr_2 (n = 4, 5, and 6) solutions. The reductive currents for all three free monomers decreased to 30 μA. At the same time, a new current peak at the potential of −0.89 V grew. This new peak is assigned to PyC_nBr_2@CB[7]

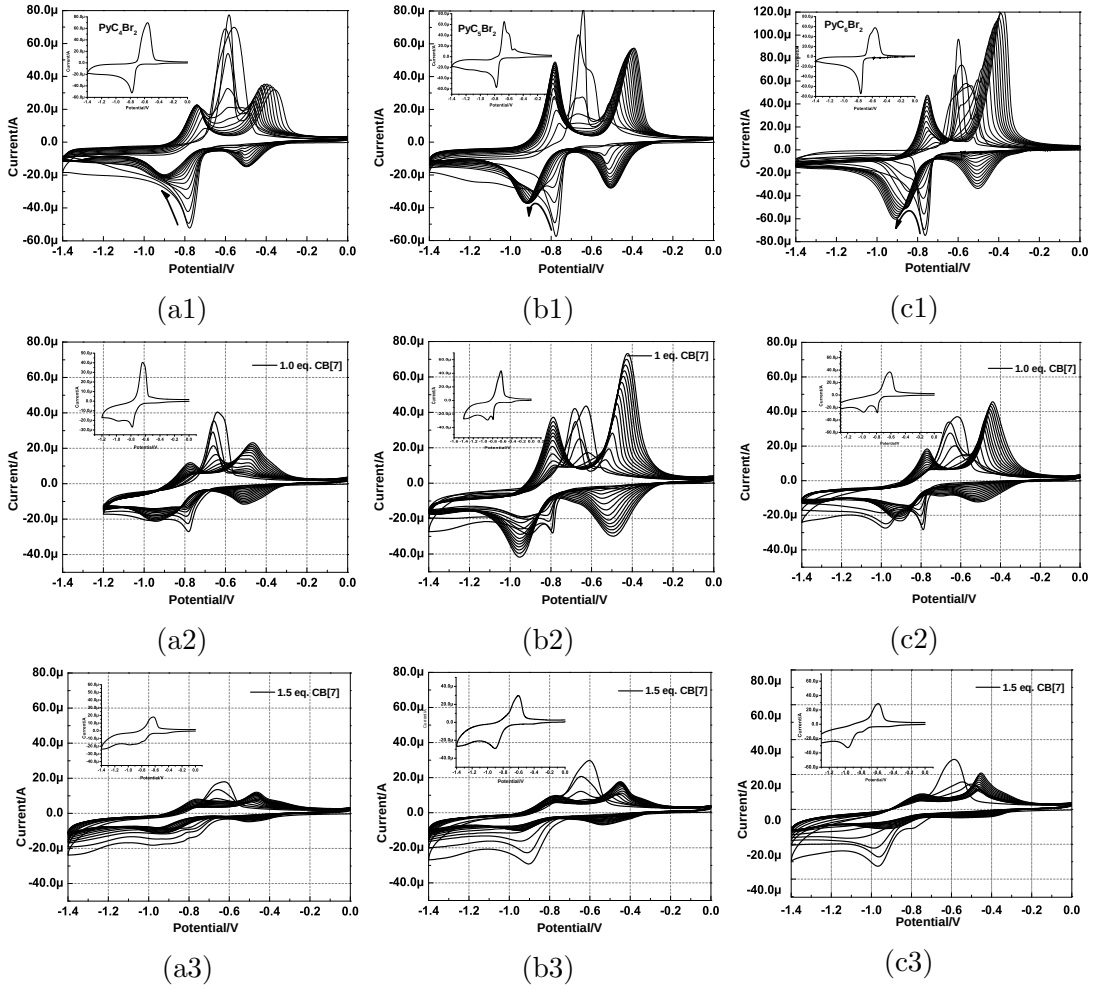

Figure 4.8: Cyclic voltammograms of the electropolymerization of 2 mM PyC_4Br_2 (a1, a2, a3), PyC_5Br_2 (b1, b2, b3) and PyC_6Br_2 (c1, c2, c3) with different equivalents of CB[7] in 0.1 M KCl electrolyte at a scan rate of 50 mV/s.

pseudorotaxane reduction. Since PyC_nBr_2 is included into the cavity of CB[7], the formed pseudorotaxanes are harder to reduce than free PyC_nBr_2. After adding 1.5 equivalent of CB[7], the current responses of PyC_5Br_2 nearly disappeared, as Figures 4.8 (b3) shows. Since little reductive current of free PyC_5Br_2 is observed, it was assumed that nearly all PyC_5Br_2 was included by CB[7] and little PyC_5Br_2 guest remains in solution. It has been reported that the binding constants of bis(pyridinium)alkane dications to CB[7] are around 3×10^6 M^{-1}.[86] Assuming the

binding constant of PyC_5Br_2 to CB[7] is similar to that of bis(pyridinium)alkane dications to CB[7], the calculated concentration of PyC_5Br_2@CB[7] is 1.999 mM in solution of 2 mM PyC_5Br_2 and 3 mM CB[7]. Therefore, the concentration of PyC_5Br_2@CB[7] was roughly 2 mM when 1.5 equivalents of CB[7] added into 2 mM PyC_nBr_2. While PVC_n (n = 4, 5, and 6) have a polymerization process that occurs as reductive adsorption, coupling, and elimination to form polyviologen, the adding of CB[7] changed this polymerization process to reduction, coupling, elimination to PVC_n@CB[7] (n = 4, 5, and 6) oligomers, deposition. The broad reductive process at −0.89 V for PyC_nBr_2@CB[7] (n = 4, 5, and 6) is reductive diffusion-controlled in the KCl solution. The diffusion coefficients (D) for the pseudorotaxane and free PyC_5Br_2 reduction at −0.89 V and −0.75 V were calculated using the Randles–Ševčík Equation,

$$C\sqrt{D} = \frac{i_p}{2.69 \times 10^5 \cdot n^{1.5} \cdot A \cdot v^{0.5}}$$

where C is the redox species concentration, D is the diffusion coefficient, i_p is the peak current, n is the electron involved, A is the electrode surface, and v is 50 mV/s. The D of PyC_5Br_2@CB[7] is 1.07×10^{-6} cm^2/s, which is 5 fold less than D of PyC_5Br_2 with 5.25×10^{-6} cm^2/s.

The polymerization efficiencies for PyC_nBr_2@CB[7] (n = 2 - 6) were listed in Table 4.1. CB[7] inclusion has little effect on the low polymerization efficiency of PyC_2Br_2, PyC_3Br_2 or PyC_4Br_2. This might because these polymers are formed from free PyC_nBr_2 (n = 2, 3, and 4) in monomer solutions. As can be seen in Figure 4.8 (a3), even on adding 1.5 equivalents of CB[7], the redox currents from free PyC_4Br_2 can be detected. PyC_nBr_2@CB[7] (n = 2 - 4) may not participate the polymerization process due to the coupling sites (cyano group positions)

encapsulated by CB[7].

As PyC_5Br_2 has a long alkyl chain, cyano groups on PyC_5Br_2@CB[7] are more accessible to couple and eliminate than PyC_nBr_2@CB[7] (n = 2 - 4). Since CB[7] has low solubility in solution, after absorbing on the electrode surface, PyC_5Br_2@CB[7] won't desorb into aqueous solutions. Therefore, the monomer solutions with 1.0 equivalent of PyC_5Br_2@CB[7] has a higher polymerization efficiency. After adding 1.5 equivalents of CB[7], more PyC_5Br_2@CB[7] complex was formed in solution. Since PyC_5Br_2@CB[7] has a low diffusion coefficient, the amount of reduced PyC_5Br_2@CB[7] radical or PVC_5@CB[7] oligomers is decreased.

In the case of PyC_6Br_2, a PyC_6Br_2@CB[7] complex with 1:2 ratio might be formed at high CB[7] concentration. The coupling sites on PyC_6Br_2@CB[7] might be blocked by CB[7]. Decreasing polymerization efficiency is observed by adding CB[7] into PyC_6Br_2 solution.

The electropolymerized PVC_n@CB[7] (n = 4, 5, and 6) films were tested in 0.1 M KCl solution. As shown in Figure 4.9, all PVC_n@CB[7] (n = 4, 5, and 6) polymers exhibit two typical redox pairs. Compared with PVC_n, the redox potentials of PVC_n@CB[7] have slightly negative shifts, indicating the polypseudorotaxanes are harder to be reduced. With more CB[7] in precursor solutions, the formed PVC_n@CB[7] (n = 4, 5, and 6) have decreased redox currents, except PVC_5@CB[7], which are related to their polymerization efficiencies.

The redox responses of polypseudorotaxane systems PVCn@CB[7] (n = 4, 5, and 6) prepared from 1 equivalent of CB[7] and PyC_nBr_2 (n = 4, 5, and 6) were measured at different scan rates. Figures 4.10 (a) - (c) show the relationship of log(current) vs. log(scan rate). The slopes of each are listed in Figure 4.10 (d). As investigated in Chapter 3, PVC_4 has an adsorption-controlled redox behavior

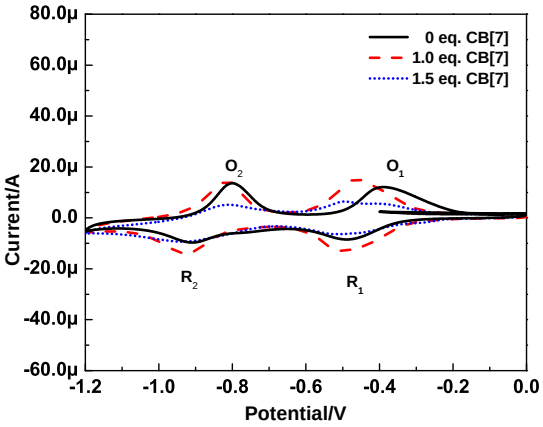

(a)

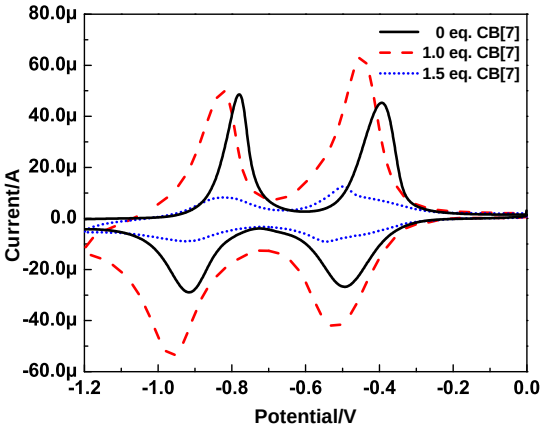

(b)

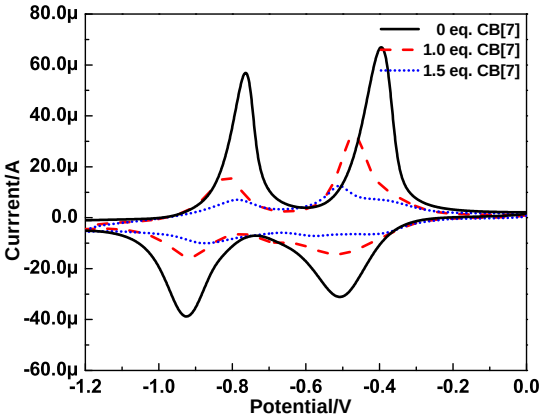

(c)

Figure 4.9: Cyclic voltammograms of the PVC_n@CB[7], (a) n = 4, (b) n = 5, and (c) n = 6 formed in different equivalent of CB[7] and 2 mM PyC_nBr_2 (n = 4, 5, and 6). The films were tested in 0.1 M KCl solution, scan rate 50 mV/s.

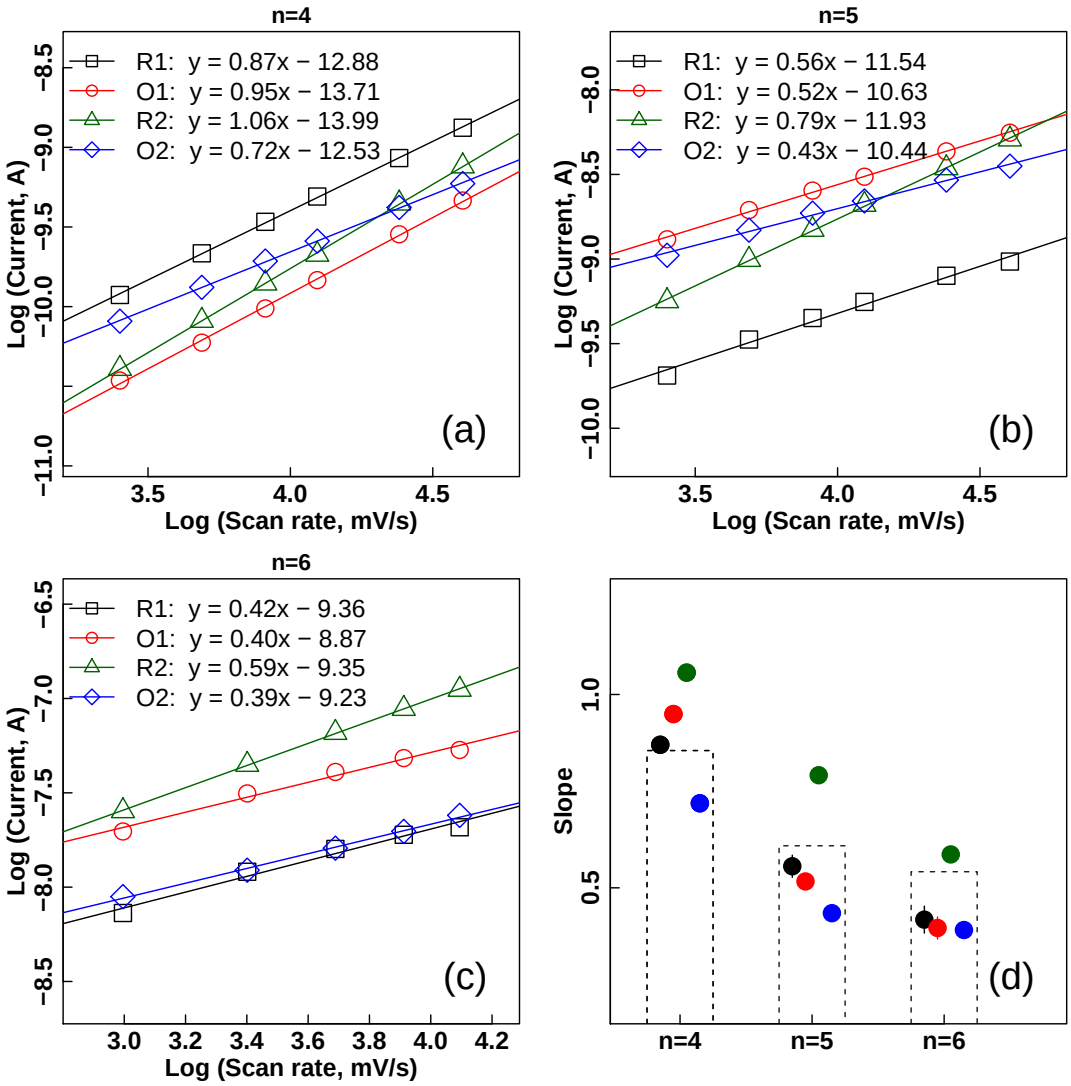

Figure 4.10: Plots of log (oxidation/reduction peak currents) vs. log (scan rates) of PVC_4@CB[7] (a), PVC_5@CB[7] (b) and PVC_6@CB[7] (c), the slopes of each fitting (d). The PVC_n@CB[7] film deposited on GCE was scanned three times from 0 to 1.2 V consecutively, at different scan rates of 20, 40, 60, 80 and 100 mV/s in monomer free 0.1 M KCl solution. The redox currents measured for the third scan at each scan rate were used for plotting.

with slopes of redox peaks around 1. PVC_4@CB[7] has a lower slope between $0.5 \sim 1.0$ for its redox peaks, indicating that CB[7] changed the morphology of PVC_4 and PVC_4@CB[7] has some open structure. Slopes near 0.5 indicate that PVC_5 and PVC_6 film structures consist of flexible open structures allowing the counterions in and out. Since PVC_5@CB[7] prepared from 2 mM of PyC_5Br_2 and 1 equivalent of CB[7] has a high polymerization efficiency, it was chosen for further study.

4.3.3 PVC_5@CB[7] Characterization

PVC_5@CB[7] was characterized using IR spectroscopy, as shown in Figure 4.11. Since the monomer PyC_5Br_2 is cyanopyridine-based, it shows a C≡N stretching absorption at 2242 cm^{-1}, which is characteristically absent in the polymer. PVC_5@CB[7] polymer did not show the absorption at 2242 cm^{-1}. Instead, it has a strong absorption at 1735 cm^{-1} which is assigned to C=O stretching of the CB[7],[87] indicating the polypseudorotaxane compound formation.

The electron transfer between PVC_5@CB[7] and the electrode surface was further investigated by cyclic voltammetry, as shown in Figure 4.12. Without CB[7], the redox peak potentials for PVC_5 are relatively invariant with increasing scan rate. The polypseudorotaxane PVC_5@CB[7] shows a different behavior. Its reductive peak potentials shift to being more negative and the oxidative peak potentials shift to become more positive. This indicates the reductions/oxidations are more difficult because of the CB[7] acting as an additional barrier to electron transfer. Similar electron transfer retardations have been reported for MV@CB[7].[84]

The stabilities of PVC_5@CB[7] films were tested in alkaline pH 12 0.1 M

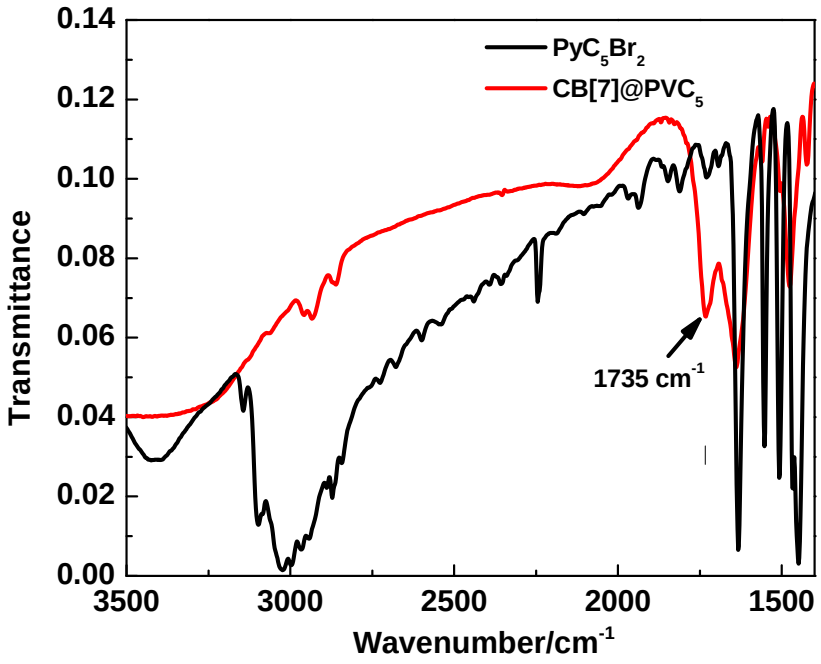

Figure 4.11: FTIR spectra of monomer PyC_5Br_2 and polymer PVC_5@CB[7].

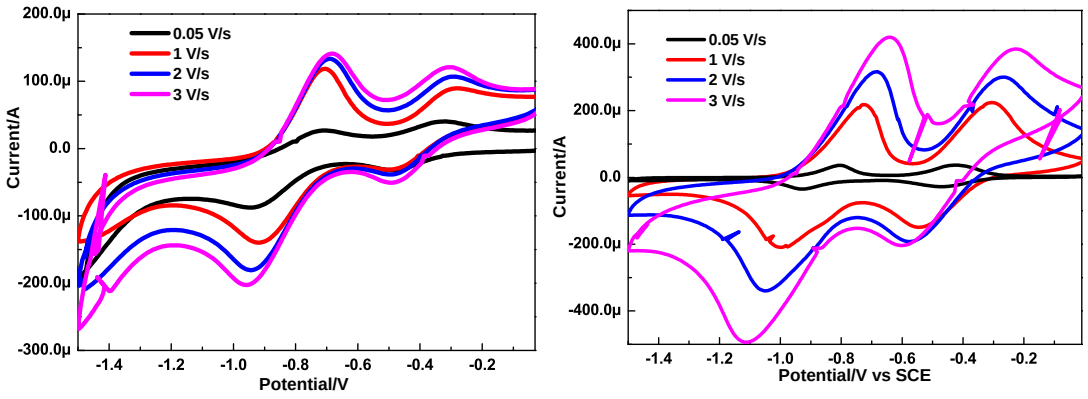

(a) (b)

Figure 4.12: Cyclic voltammograms of the PVC_5 (a) and PVC_5@CB[7] (b) at different scan rates.

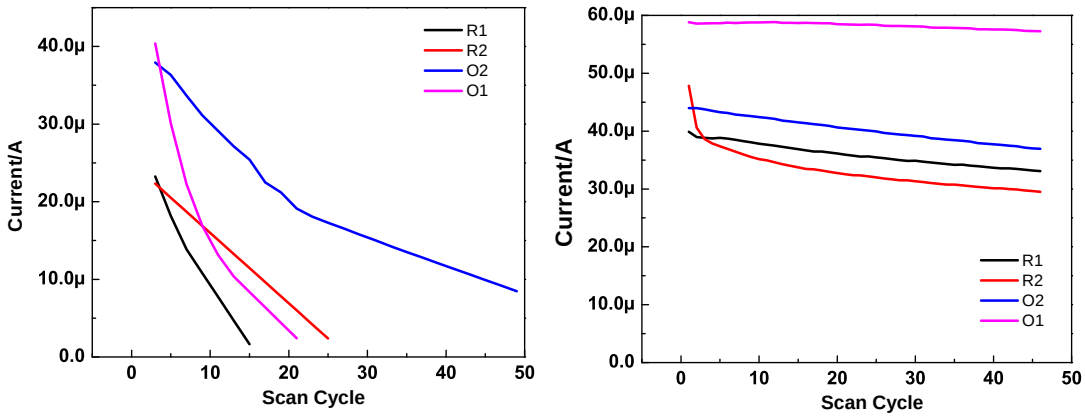

Figure 4.13: Redox peak currents (R1, R2, O2 and O1) of PVC_5 (a) and PVC_5@CB[7] (b) in pH 12 0.1 M KCl solution vs. scan cycle numbers.

KCl solution. The results are shown in Figure 4.13. After 50 successive cycles, the redox current of PVC_5 cation radical to PVC_5 dication vanished gradually, while the redox responses of PVC_5@CB[7] changed much less. This confirms the hypothesis that CB[7] encapsulates PVC_5 into its cavity and improves its chemical stability in basic media.

4.3.4 Polypseudorotaxane PVC_5@CB[7] Catalyzed Glucose Fuel Cells

To determine the effectiveness of the "protected" polyviologen in a glucose/O_2 alkaline fuel cell, PVC_5@CB[7] was electropolymerized on GCE and carbon felt anodes using a ratio of 1:1 PyC_5Br_2:CB[7] monomer solution.

By using a Pt/Nafion cathode and a 0.1 M KCl solution with 5 mM glucose as fuel cell solution, the current production by PVC_5@CB[7] formed on different anodes shows further improvements over that of PVC_5. The PVC_5@CB[7] GCE (3 mm diameter) anode generated a maximum current of 0.28 μA, which is com-

parable to the 0.21 μA generated by copolyviologen on GCE (3 mm diameter), which has been in Chapter 3.

To load more catalyst, PVC_5@CB[7] was deposited on a carbon felt anode. PVC_5@CB[7] carbon felt anodes showed an improvement in output power, the current is as high as 585 μA and the power is 122 μW (0.35 V, 348 μA). This current and power are comparable or higher than that produced by copolyviologen which was investigated in Chapter 3. Compared with 2.5 μA generated by polyviologen on graphite anode,[74] this PVC_5@CB[7] system showed a high catalytic oxidation ability for glucose.

4.4 Conclusion

PyC_nBr_2@CB[7] (n = 2 -6) was synthesized using a series of PyC_nBr_2 guests engulfed by the using of CB[7] host different equivalences. The inclusion complex was characterized by ^{1}H NMR. PyC_nBr_2@CB[7] (n = 4 and 5) likely exhibit 1:1 stoichiometric complexation.

A series of PVC_n@CB[7] complexes were electrosynthesized by using 2 mM PyC_nBr_2 and different equivalents of CB[7] as monomer solutions. CB[7] inclusion has little influence on PyC_nBr_2 (n = 2, 3, and 4) polymerization efficiency. CB[7] facilitates PyC_5Br_2 polymerization efficiency, due to its lower solubility in aqueous solution but decreases PyC_6Br_2 polymerization efficiency at high CB[7] concentrations, possibly because a 1:2 PyC_6Br_2@CB[7] complex is formed at high CB[7] concentrations. Compared to PVC_5, PVC_5@CB[7] is extremely stable in an alkaline solution at pH 12.

PVC_5@CB[7] modified GCE and carbon felt electrodes were used as anodes for glucose fuel cells. PVC_5@CB[7] on carbon felt anodes showed impressive max-

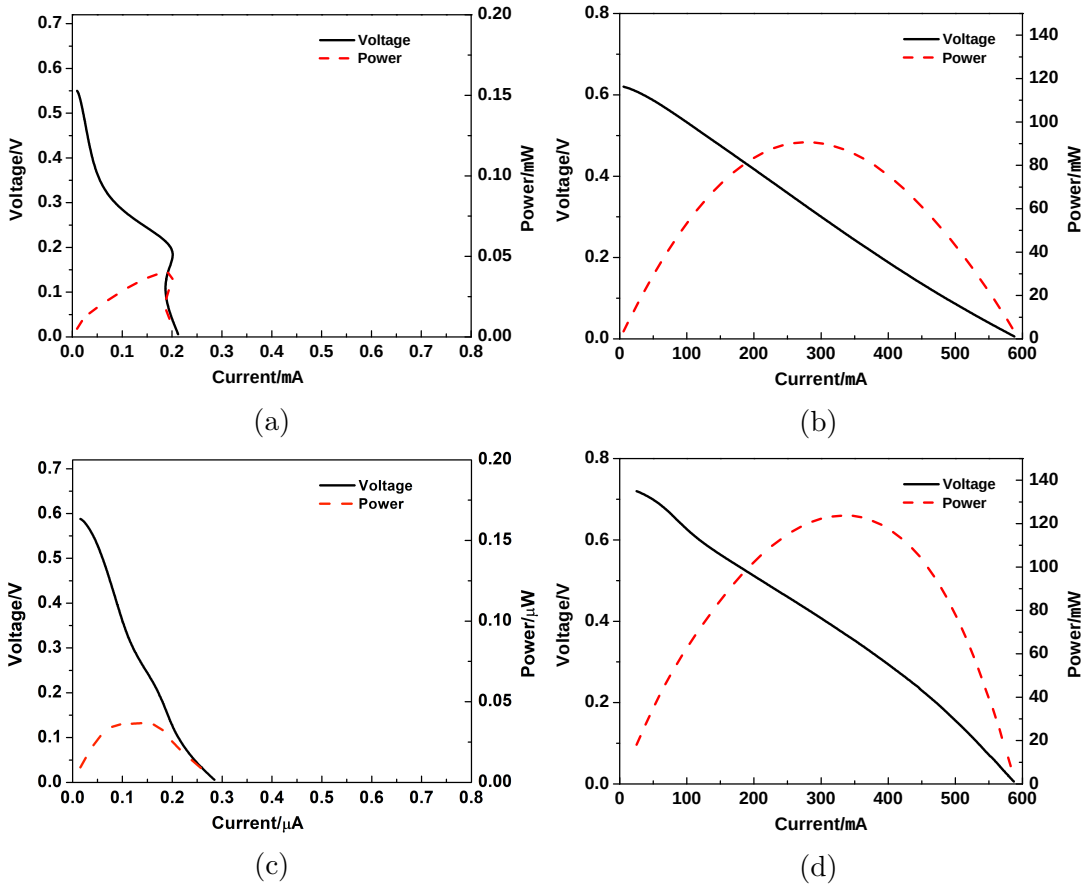

Figure 4.14: Power curves for fuel cells with Pt/Nafion film as the cathode and copolyviologen GCE (a), copolyviologen carbon felt (b) PVC_5@CB[7] GCE (c), PVC_5@CB[7] carbon felt (d) as the anode. The fuel cell solution is pH 9.7 0.1 M KCl.

imum currents as high as 585 μA, which is comparable with the copolyviologen carbon felt anode, which has been investigated in Chapter 3.

Chapter 5

Conclusions and Future Directions

5.1 Conclusions

This work has mainly focused on the electrosynthesis of viologen polymers. The prepared viologen polymers were designed to be used as catalysts for glucose oxidation in glucose alkaline fuel cells. To improve viologen polymers' utility and stability in high pH solution, two different kinds of polyviologen films were developed used as anodes in fuel cells.

The first is a copolymer which includes linear alkyl viologen units (PVC_n) and crosslinking polybezylviologen units (PVBenMe). The ratios of monomers for the electropolymerization were partially optimized. The copolyviologen films were characterized using cyclic voltammetry. They behave as crosslinked structures and show improved electrochemical stability in pH 12 solution compared to non-crosslinked PVC_5. The copolyviologen was also deposited on CNT@GCE and carbon felt electrodes, which were used as anodes for glucose alkaline fuel cells.

Using a Pt/Nafion film cathodes, the copolymer on carbon felt anodes produced an OCV as 0.62 V and a maximum current of 588 μA, with a power of 90.6 μW (0.325 V, 279 μA) in 5 mM glucose in 0.1 M KCl solution at pH 9.7. The polyviologen coated on graphite electrode reported in the literature[74] generated 2 μA with 10 mM DHA in 0.25 M phosphate buffer solution at pH 11. The polyviologen reported here showed a highly improved carbohydrate oxidation performance.

The second polyviologen developed was a kind of polypseudorotaxane. CB[7] was used as the host, and linear polyalkylviologen units were the guests. These films were electrosynthesized by using PyC_nBr_2@CB[7] complexes as monomers. The pseudorotaxane viologen polymers were characterized by cyclic voltammetry and IR. The pseudorotaxane polymer PVC_5@CB[7], is extremely stable in pH 12 solution. PVC_5@CB[7] was deposited on the carbon felt electrode, it produced a maximum current of 585 μA and a power of 122 μW (0.35 V, 348 μA) in a glucose fuel cell with a Pt/Nafion film cathode. As a glucose fuel cell catalyst, PVC_5@CB[7] shows a comparable catalytic ability to the copolyviologens investigated in this project, but with somewhat improved power generation.

5.2 Future Directions

Lifetime stability is an important property of fuel cells. However, it was not investigated in detail in this thesis or reported in other viologen-catalyzed carbohydrate fuel cell papers. The lifetime of biofuel cells is several weeks using glucose oxidase as the catalyst.[88] Since viologen is more environmentally stable than glucose oxidase, it is expected viologen fuel cells have a longer lifetime than glucose oxidase fuel cells. Compared with PVC_5, the electrochemical stability of

the copolyviologen or the CB[7] encapsulated polyviologen is improved in alkaline solution. Therefore, it is expected that the lifetime of the copolyviologen or CB[7] encapsulated polyviologen catalyzed glucose fuel cells are increased than that of PVC_5 glucose fuel cells, but this needs to be evaluated.

As investigated in Chapter 3, both PVC_5 and PVC_6 have a cross-linked structure. In Chapter 3, PVC_5 was cross-linked with PVBenMe to formed the copolymer as the fuel cell catalyst. In the future, new copolymers composed of PVC_6, or larger carbon spacers, and PVBenMe are worthwhile to make and study. Since PVC_6 has a longer alkyl chain, the new copolymers may have larger cavities which allow larger size carbohydrate fuels to be used.

To improve the fuel cell performance, loading more materials on anodes is necessary. Even though the copolymer and polyseudorotaxane polymer can be polymerized on the GCE electrode successfully, the polymer formed from 20 scan cycles reached its maximum loading. Based on the improved performance of polyviologen deposited carbon felt anodes, ultrahigh surface area three-dimensional porous materials, such as graphitic carbon, can be used as an anode.

Bibliography

[1] J. D. Shakun, P. U. Clark, F. He, S. A. Marcott, A. C. Mix, Z. Liu, B. Otto-Bliesner, A. Schmittner, and E. Bard. Global warming preceded by increasing carbon dioxide concentrations during the last deglaciation. *Nature*, 484(7392):49–54, 2012.

[2] A. Kirubakaran, S. Jain, and R. Nema. A review on fuel cell technologies and power electronic interface. *Renewable and Sustainable Energy Reviews*, 13(9):2430–2440, 2009.

[3] J. J. Hwang. Review on development and demonstration of hydrogen fuel cell scooters. *Renewable and Sustainable Energy Reviews*, 16(6):3803–3815, 2012.

[4] O.-J. Ohm and D. Danilovic. Improvements in pacemaker energy consumption and functional capability: four decades of progress. *Pacing and Clinical Electrophysiology*, 20(1):2–9, 1997.

[5] J. H. Lee, W.-Y. Jeon, H.-H. Kim, E.-J. Lee, and H. Kim. Electrical stimulation by enzymatic biofuel cell to promote proliferation, migration and differentiation of muscle precursor cells. *Biomaterials*, 53:358–369, 2015.

[6] V. Vishnyakov. Proton exchange membrane fuel cells. *Vacuum*, 80(10):1053 – 1065, 2006.

[7] L. Mor, Z. Rubin, and P. Schechner. Measuring open circuit voltage in a glucose alkaline fuel cell operated as a continuous stirred tank reactor. *Journal of Fuel Cell Science and Technology*, 5(1):0145031–0145034, 2008.

[8] R. Escobar Yonoff, G. Valencia Ochoa, Y. Cardenas-Escorcia, J. I. Silva-Ortega, and L. Meriño-Stand. Research trends in proton exchange membrane fuel cells during 2008–2018: A bibliometric analysis. *Heliyon*, 5:1–7, 2018.

[9] H. A. Gasteiger, S. S. Kocha, B. Sompalli, and F. T. Wagner. Activity benchmarks and requirements for Pt, Pt-alloy, and non-Pt oxygen reduction catalysts for PEMFCs. *Applied Catalysis B: Environmental*, 56(1-2):9–35, 2005.

[10] R. A. Bullen, T. Arnot, J. Lakeman, and F. Walsh. Biofuel cells and their development. *Biosensors and Bioelectronics*, 21(11):2015–2045, 2006.

[11] L. Ariyanfar, H. Ghadamian, and R. Roshandel. Alkaline fuel cell (AFC) engineering design: modeling and simulation for UPS provide in laboratory application. *World Renewable Energy Congress-Sweden*, 1(057):1227–1234, 2011.

[12] D. Scott and B. Y. Liaw. Harnessing electric power from monosaccharides–a carbohydrate–air alkaline fuel cell mediated by redox dyes. *Energy & Environmental Science*, 2(9):965–969, 2009.

[13] T. Saika, T. Iyoda, and T. Shimidzu. Electropolymerization of bis(4-cyano-1-pyridinio) derivatives for the preparation of polyviologen films on electrodes. *Bulletin of the Chemical Society of Japan*, 66(7):2054–2060, 1993.

[14] A. Yahiro, S. Lee, and D. Kimble. Bioelectrochemistry: I. Enzyme utilizing bio-fuel cell studies. *Biochimica et Biophysica Acta (BBA)-Specialized Section on Biophysical Subjects*, 88(2):375–383, 1964.

[15] N. P. Godman, J. L. DeLuca, S. R. McCollum, D. W. Schmidtke, and D. T. Glatzhofer. Electrochemical characterization of layer-by-layer assembled ferrocene-modified linear poly(ethylenimine)/enzyme bioanodes for glucose sensor and biofuel cell applications. *Langmuir*, 32(14):3541–3551, 2016.

[16] J. Chen, D. Bamper, D. T. Glatzhofer, and D. W. Schmidtke. Development of fructose dehydrogenase-ferrocene redox polymer films for biofuel cell anodes. *Journal of the Electrochemical Society*, 162(3):F258, 2014.

[17] G. Slaughter and T. Kulkarni. Highly selective and sensitive self-powered glucose sensor based on capacitor circuit. *Scientific Reports*, 7(1):1–9, 2017.

[18] A. C. Luna, A. Bolzan, M. De Mele, and A. Arvia. The voltammetric electrooxidation of glucose and glucose residues formed on electrodispersed platinum electrodes in acid electrolytes. *Pure and Applied Chemistry*, 63(11):1599–1608, 1991.

[19] M. Tominaga, T. Shimazoe, M. Nagashima, and I. Taniguchi. Electrocatalytic oxidation of glucose at gold nanoparticle-modified carbon electrodes in alkaline and neutral solutions. *Electrochemistry Communications*, 7(2):189–193, 2005.

[20] K. Kokoh, J.-M. Léger, B. Beden, and C. Lamy. On line chromatographic analysis of the products resulting from the electrocatalytic oxidation of d-glucose on Pt, Au and adatoms modified Pt electrodes—Part I. Acid and neutral media. *Electrochimica Acta*, 37(8):1333–1342, 1992.

[21] A. Appleby and C. Van Drunen. Anodic oxidation of carbohydrates and related compounds in neutral saline solution. *Journal of the Electrochemical Society*, 118(1):95, 1971.

[22] J. Chen, H. Zheng, J. Kang, F. Yang, Y. Cao, and M. Xiang. An alkaline direct oxidation glucose fuel cell using three-dimensional structural Au/Ni-foam as catalytic electrodes. *RSC Advances*, 7(5):3035–3042, 2017.

[23] K. Torigoe, M. Takahashi, K. Tsuchiya, K. Iwabata, T. Ichihashi, K. Sakaguchi, F. Sugawara, and M. Abe. High-power abiotic direct glucose fuel cell using a gold–platinum bimetallic anode catalyst. *ACS Omega*, 3(12):18323–18333, 2018.

[24] R. Larsson, B. Folkesson, P. M. Spaziante, W. Veerasai, and R. H. Exell. A high-power carbohydrate fuel cell. *Renewable Energy*, 31(4):549–552, 2006.

[25] R. Eustis, T. M. Tsang, B. Yang, D. Scott, and B. Y. Liaw. Seeking effective dyes for a mediated glucose–air alkaline battery/fuel cell. *Journal of Power Sources*, 248:1133–1140, 2014.

[26] D. Orton and D. Scott. Temperature dependence of an abiotic glucose/air alkaline fuel cell. *Journal of Power Sources*, 295:92–98, 2015.

[27] D. C. Hansen, Y. Pan, J. Stockton, W. G. Pitt, and D. R. Wheeler. Cyclic voltammetry investigation of organic species considered for use as catalysts in direct-carbohydrate fuel cells. *Journal of the Electrochemical Society*, 159(11):H834, 2012.

[28] A. A. Sagade, K. V. Rao, U. Mogera, S. J. George, A. Datta, and G. U. Kulkarni. High-mobility field effect transistors based on supramolecular charge transfer nanofibres. *Advanced Materials*, 25(4):559–564, 2013.

[29] B. Hu, C. DeBruler, Z. Rhodes, and T. L. Liu. Long-cycling aqueous organic redox flow battery (AORFB) toward sustainable and safe energy storage. *Journal of the American Chemical Society*, 139(3):1207–1214, 2017.

[30] M. Suzuka, S. Hara, T. Sekiguchi, K. Oyaizu, and H. Nishide. Polyviologen as the charge-storage electrode of an aqueous electrolyte-and organic-based dye-sensitized solar cell. *Polymer*, 68:353–357, 2015.

[31] G. D. Watt, D. Hansen, D. Dodson, M. Andrus, and D. Wheeler. Electrical energy from carbohydrate oxidation during viologen-catalyzed O_2-oxidation: Mechanistic insights. *Renewable Energy*, 36(5):1523–1528, 2011.

[32] D. Kiriya, M. Tosun, P. Zhao, J. S. Kang, and A. Javey. Air-stable surface charge transfer doping of MoS_2 by benzyl viologen. *Journal of the American Chemical Society*, 136(22):7853–7856, 2014.

[33] R. Kannappan, C. Bucher, E. Saint-Aman, J. Moutet, A. Milet, M. Oltean, E. Métay, S. Pellet-Rostaing, M. Lemaire, and C. Chaix. Viologen-based redox-switchable anion-binding receptors. *New Journal of Chemistry*, 34(7):1373–1386, 2010.

[34] A. Read, D. Hansen, S. Aloi, W. G. Pitt, D. R. Wheeler, and G. D. Watt. Monoalkyl viologens are effective carbohydrate O_2-oxidation catalysts for electrical energy generation by fuel cells. *Renewable Energy*, 46:218–223, 2012.

[35] M. Bahari, M. A. Malmberg, D. M. Brown, S. H. Nazari, R. S. Lewis, G. D. Watt, and J. N. Harb. Oxidation efficiency of glucose using viologen mediators for glucose fuel cell applications with non-precious anodes. *Applied Energy*, 261:114382, 2020.

[36] H. Yi, A. Jutand, and A. Lei. Evidence for the interaction between t BuOK and 1, 10-phenanthroline to form the 1,10-phenanthroline radical anion: a key step for the activation of aryl bromides by electron transfer. *Chemical Communications*, 51(3):545–548, 2015.

[37] L. Eberson and M. Nilsson. One-electron oxidation of carboxylates by hexachloroosmate (V) ion. *Journal of the Chemical Society, Chemical Communications*, 15:1041–1042, 1992.

[38] D. R. Wheeler, J. Nichols, D. Hansen, M. Andrus, S. Choi, and G. D. Watt. Viologen catalysts for a direct carbohydrate fuel cell. *Journal of the Electrochemical Society*, 156(10):B1201, 2009.

[39] J. Bus, S. Aust, and J. Gibson. Superoxide-and singlet oxygen-catalyzed lipid peroxidation as a possible mechanism for paraquat (methyl viologen) toxicity. *Biochemical and Biophysical Research Communications*, 58(3):749–755, 1974.

[40] C. R. Rigby, H. Han, P. K. Bhowmik, M. Bahari, A. Chang, J. N. Harb, R. S. Lewis, and G. D. Watt. Soluble viologen polymers as carbohydrate oxidation catalysts for alkaline carbohydrate fuel cells. *Journal of Electroanalytical Chemistry*, 823:416–421, 2018.

[41] Y. Pan, J. Stockton, R. Urie, W. Pitt, and D. R. Wheeler. Immobilized viologen polymers for carbohydrate fuel cells. *ECS Transactions*, 50(2):819, 2013.

[42] J. H. Ross and R. I. Krieger. Synthesis and properties of paraquat (methyl viologen) and other herbicidal alkyl homologs. *Journal of Agricultural and Food Chemistry*, 28(5):1026–1031, 1980.

[43] A. Factor and G. Heinsohn. Polyviologens–a novel class of cationic polyelectrolyte redox polymers. *Journal of Polymer Science Part B: Polymer Letters*, 9(4):289–295, 1971.

[44] K. Ageishi, T. Endo, and M. Okawara. Preparation of viologen polymers from alkylene dipyridinium salts by cyanide ion. *Journal of Polymer Science: Polymer Chemistry Edition*, 21(1):293–300, 1983.

[45] K. Cheng and P. Chen. Polyviologen modified glassy carbon electrode employed for anodic stripping voltammetric determination of mercury (II). *Electroanalysis: An International Journal Devoted to Fundamental and Practical Aspects of Electroanalysis*, 20(2):207–210, 2008.

[46] E. M. Kosower and J. L. Cotter. Stable free radicals. II. The reduction of 1-methyl-4-cyanopyridinium ion to methylviologen cation radical. *Journal of the American Chemical Society*, 86(24):5524–5527, 1964.

[47] M. Bai, Y. Wang, C. Hsiao, S. Li, H. Chang, and S. Cheng. Monitoring bioactivity in hydrogen fermentation by an amperometric method with polyviologen modified working electrode. *International Journal of Hydrogen Energy*, 31(10):1357–1364, 2006.

[48] N. Kitamura, Y. Nambu, and T. Endo. Preparation of a polymeric membrane crosslinked by the viologen structure from a cyanopyridinium salt polymer. *Journal of Polymer Science Part A: Polymer Chemistry*, 26(4):993–1001, 1988.

[49] L. Coche and J.-C. Moutet. Catalysis of 1,2-dibromo-1,2-diphenylethane reduction on platinum and carbon felt electrodes coated by polypyrrole films containing 4,4$^{p}rime$-bipyridinium groups: Effects of film thickness, film composition and comparison with homogeneous catalysis. *Journal of Electroanalytical Chemistry and Interfacial Electrochemistry*, 224(1-2):111–122, 1987.

[50] I. Carelli and M. Emilio Cardinali. Electrochemical reduction of 4-cyano-1-methylpyridinium ion. *Journal of Electroanalytical Chemistry and Interfacial Electrochemistry*, 124(1-2):147–153, 1981.

[51] M. N. Zhidkova, K. E. Aysina, V. Y. Kotov, V. K. Ivanov, Y. V. Nelyubina, I. V. Ananyev, and V. K. Laurinavichyute. Synthesis and electropolymerization of bis(4-cyano-1-pyridino) alkanes: Effect of co-and counter-ions. *Electrochimica Acta*, 219:673–681, 2016.

[52] J. Iehl, M. Frasconi, H.-P. Jacquot de Rouville, N. Renaud, S. M. Dyar, N. L. Strutt, R. Carmieli, M. R. Wasielewski, M. A. Ratner, J.-F. Nierengarten, and J. F. Stoddart. π-Dimerization of viologen subunits around the core of C_{60} from twelve to six directions. *Chem. Sci.*, 4:1462–1469, 2013.

[53] C. Bird and A. Kuhn. Electrochemistry of the viologens. *Chemical Society Reviews*, 10(1):49–82, 1981.

[54] J. Farrington, A. Ledwith, and M. Stam. Cation–radicals: oxidation of methoxide ion with 1,1$^{p}rime$-dimethyl-4,4$^{p}rime$-bipyridylium dichloride (paraquat dichloride). *Journal of the Chemical Society D: Chemical Communications*, 1(6):259–260, 1969.

[55] K. Kamata, T. Kawai, and T. Iyoda. Anion-controlled redox process in a cross-linked polyviologen film toward electrochemical anion recognition. *Langmuir*, 17(1):155–163, 2001.

[56] N. Wang, P. Damlin, B. M. Esteban, T. Ääritalo, J. Kankare, and C. Kvarnström. Electrochemical synthesis and characterization of copolyviologen films. *Electrochimica Acta*, 90:171–178, 2013.

[57] H.-C. Lu, S.-Y. Kao, T.-H. Chang, C.-W. Kung, and K.-C. Ho. An electrochromic device based on Prussian blue, self-immobilized vinyl benzyl viologen, and ferrocene. *Solar Energy Materials and Solar Cells*, 147:75–84, 2016.

[58] L. Zhu, H. Yan, X. Wang, and Y. Zhao. Light-controllable cucurbit [7] uril-based molecular shuttle. *The Journal of Organic Chemistry*, 77(22):10168–10175, 2012.

[59] J. Ding, C. Zheng, L. Wang, C. Lu, B. Zhang, Y. Chen, M. Li, G. Zhai, and X. Zhuang. Viologen-inspired functional materials: synthetic strategies and applications. *Journal of Materials Chemistry A*, 7(41):23337–23360, 2019.

[60] F. Kitamura, T. Ohsaka, and K. Tokuda. Adsorption behavior of viologen derivatives on hanging mercury electrode surfaces. *Journal of Electroanalytical Chemistry*, 347(1-2):371–381, 1993.

[61] K. Arihara, F. Kitamura, K. Nukanobu, T. Ohsaka, and K. Tokuda. Voltammetric and spectroscopic study of the adsorption of alkyl viologens on a HOPG electrode. *Journal of Electroanalytical Chemistry*, 473(1-2):138–144, 1999.

[62] K. Moon and A. E. Kaifer. Modes of binding interaction between viologen guests and the cucurbit[7]uril host. *Organic Letters*, 6(2):185–188, 2004.

[63] R. Fujita, M. Hoshino, Y. Tojyo, A. Kimura, and H. Hongo. Reaction of pyridinium and quinolinium salts having the leaving group at the 2-or 4-position with active methylene compounds. *Yakugaku Zasshi: Journal of the Pharmaceutical Society of Japan*, 126(2):99, 2006.

[64] J. Shen, C. Zhang, T. Yu, L. An, and Y. Fu. Structural and functional modulation of five 4-cyanopyridinium iodoargentates built up from cubane-like Ag_4I_4 nodes. *Crystal Growth & Design*, 14(12):6337–6342, 2014.

[65] Y. Chen, Z. Yang, C. Guo, C. Ni, H. Li, Z. Ren, and J. Lang. Using alcohols as alkylation reagents for 4-cyanopyridinium and N, N'-dialkyl-4, 4'-bipyridinium and their one-dimensional iodoplumbates. *CrystEngComm*, 13(1):243–250, 2011.

[66] T. Hui and M. D. Baker. Redox processes of methyl viologen cation radicals at zeolite Y-modified electrodes. *The Journal of Physical Chemistry B*, 106(4):827–832, 2002.

[67] F. Marken, A. Neudeck, and A. M. Bond. *Cyclic Voltammetry*, pages 57–106. Springer Berlin Heidelberg, Berlin, Heidelberg, 2010.

[68] D. C. Hansen, G. Watt, J. Nichols, M. B. Andrus, D. R. Wheeler, and S. H. Choi. Viologen catalyst for direct-carbohydrate fuel cell. *Ecs Transactions*, 16(2):2057, 2008.

[69] G. Watt. A new future for carbohydrate fuel cells. *Renewable Energy*, 72:99–104, 2014.

[70] K. Kamata, T. Suzuki, T. Kawai, and T. Iyoda. Voltammetric anion recognition by a highly cross-linked polyviologen film. *Journal of Electroanalytical Chemistry*, 473(1-2):145–155, 1999.

[71] N. Wang, A. Kähkönen, P. Damlin, T. Ääritalo, J. Kankare, and C. Kvarnström. Electrochemical synthesis and characterization of branched viologen derivatives. *Electrochimica Acta*, 154:361–369, 2015.

[72] J. Iehl, M. Frasconi, H.-P. J. de Rouville, N. Renaud, S. M. Dyar, N. L. Strutt, R. Carmieli, M. R. Wasielewski, M. A. Ratner, J.-F. Nierengarten, et al. π-Dimerization of viologen subunits around the core of C 60 from twelve to six directions. *Chemical Science*, 4(4):1462–1469, 2013.

[73] D. Nečas and P. Klapetek. Gwyddion: an open-source software for SPM data analysis. *Open Physics*, 10(1):181–188, 2012.

[74] Y. Pan, J. Stockton, R. Urie, W. Pitt, and D. R. Wheeler. Immobilized Viologen Polymers for Carbohydrate Fuel Cells. *ECS Transactions*, 50(2):819, 2013.

[75] S. Walker, R. Oun, F. J. McInnes, and N. J. Wheate. The potential of cucurbit[n]urils in drug delivery. *Israel Journal of Chemistry*, 51(5-6):616–624, 2011.

[76] A. A. Elbashir and H. Y. Aboul-Enein. Supramolecular analytical application of cucurbit[n]urils using fluorescence spectroscopy. *Critical Reviews in Analytical Chemistry*, 45(1):52–61, 2015.

[77] B. C. Pemberton, R. K. Singh, A. C. Johnson, S. Jockusch, J. P. Da Silva, A. Ugrinov, N. J. Turro, D. Srivastava, and J. Sivaguru. Supramolecular photocatalysis: insights into cucurbit[8]uril catalyzed photodimerization of 6-methylcoumarin. *Chemical Communications*, 47(22):6323–6325, 2011.

[78] H. Li and Y. Yang. Gold nanoparticles functionalized with supramolecular macrocycles. *Chinese Chemical Letters*, 24(7):545–552, 2013.

[79] J. Lagona, P. Mukhopadhyay, S. Chakrabarti, and L. Isaacs. The cucurbit[n]uril family. *Angewandte Chemie International Edition*, 44(31):4844–4870, 2005.

[80] W. Xu, J. Kan, B. Yang, T. J. Prior, B. Bian, X. Xiao, Z. Tao, and C. Redshaw. A Study of the interaction between cucurbit[8]uril and alkyl-substituted 4-pyrrolidinopyridinium salts. *Chemistry–An Asian Journal*, 14(1):235–242, 2019.

[81] H. Tang, D. Fuentealba, Y. H. Ko, N. Selvapalam, K. Kim, and C. Bohne. Guest binding dynamics with cucurbit[7]uril in the presence of cations. *Journal of the American Chemical Society*, 133(50):20623–20633, 2011. PMID: 22073977.

[82] E. Kovalenko and D. Mainichev. Supramolecular system of aminoacids and cucurbit[7]uril: NMR studies in solution. *Applied Magnetic Resonance*, 46(3):281–293, 2015.

[83] S. B. Ellis. Advances toward the utilization of cucurbit[7]uril and selected viologens in molecular machines and devices. 2013.

[84] H. Kim, W. S. Jeon, Y. H. Ko, and K. Kim. Inclusion of methylviologen in cucurbit[7]uril. *Proceedings of the National Academy of Sciences*, 99(8):5007–5011, 2002.

[85] W. L. Mock and N. Y. Shih. Structure and selectivity in host-guest complexes of cucurbituril. *The Journal of Organic Chemistry*, 51(23):4440–4446, 1986.

[86] N. A. Tcyrulnikov, R. Varadharajan, A. A. Tikhomirova, M. Pattabiraman, V. Ramamurthy, and R. M. Wilson. Modulation of Reduction Potentials of Bis(pyridinium)alkane Dications through Encapsulation within Cucurbit[7]uril. *The Journal of Organic Chemistry*, 84(13):8759–8765, 2019. PMID: 31187624.

[87] D. Mohanan, N. Sumina, R. T. Thomas, A. Mohamed, U. Hareesh, A. K. Ray, and S. Pillai. Cucurbit[7]uril encapsulated dye-sensitized enhanced solar photocatalysis using positively charged sheet-like anatase TiO_2 mesocrystals. *Applied Surface Science*, 488:911–920, 2019.

[88] C. Wang, E. Shim, H. K. Chang, N. Lee, H. R. Kim, and J. Park. Sustainable and high-power wearable glucose biofuel cell using long-term and high-speed flow in sportswear fabrics. *Biosensors and Bioelectronics*, 169:112652, 2020.

Appendix A

^{1}H NMR Data

The respective compounds were placed in NMR tubes and dissolved in 0.5 mL D_2O or DMSO$-d_6$. Measurements were made using a Mercury VX-300 NMR Spectrometer, operating with a 4-nuclei auto switchable PFG probe.

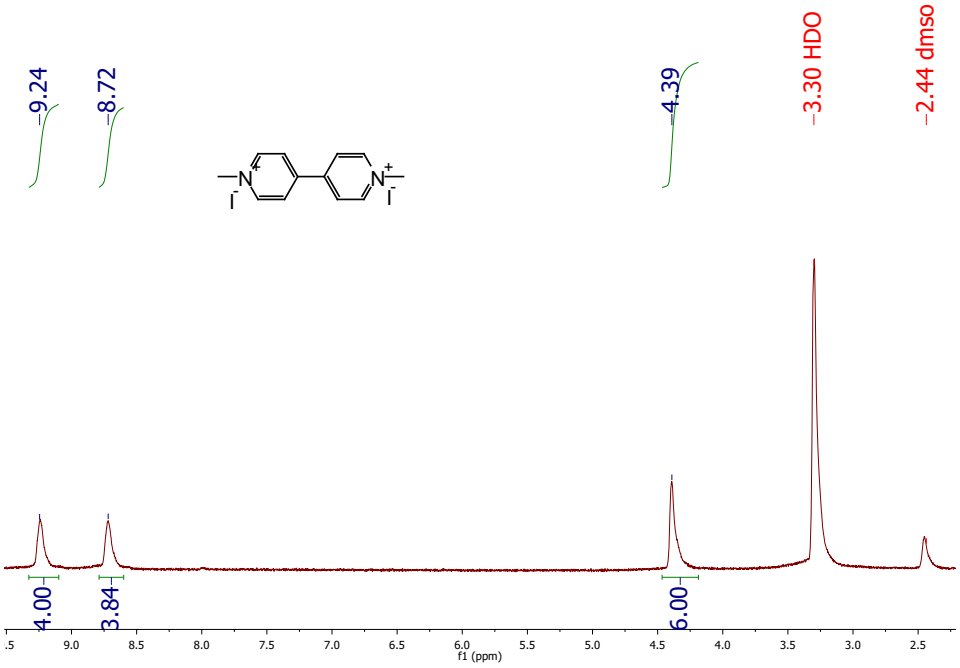

Figure A.1: Methyl viologen (DMSO−d_6).[62]

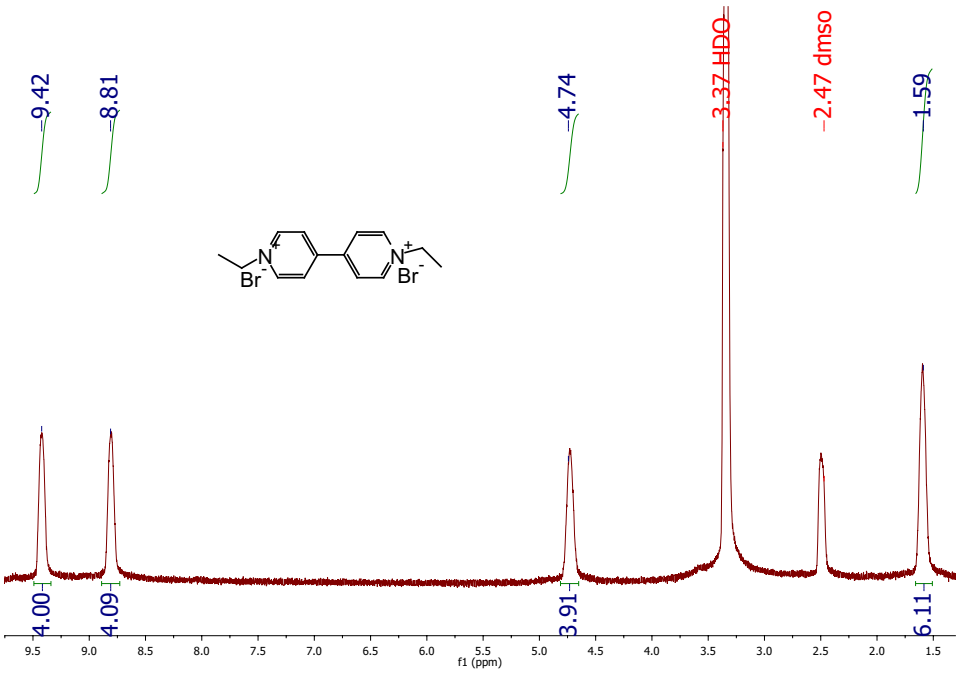

Figure A.2: Ethyl viologen (DMSO−d_6).[62]

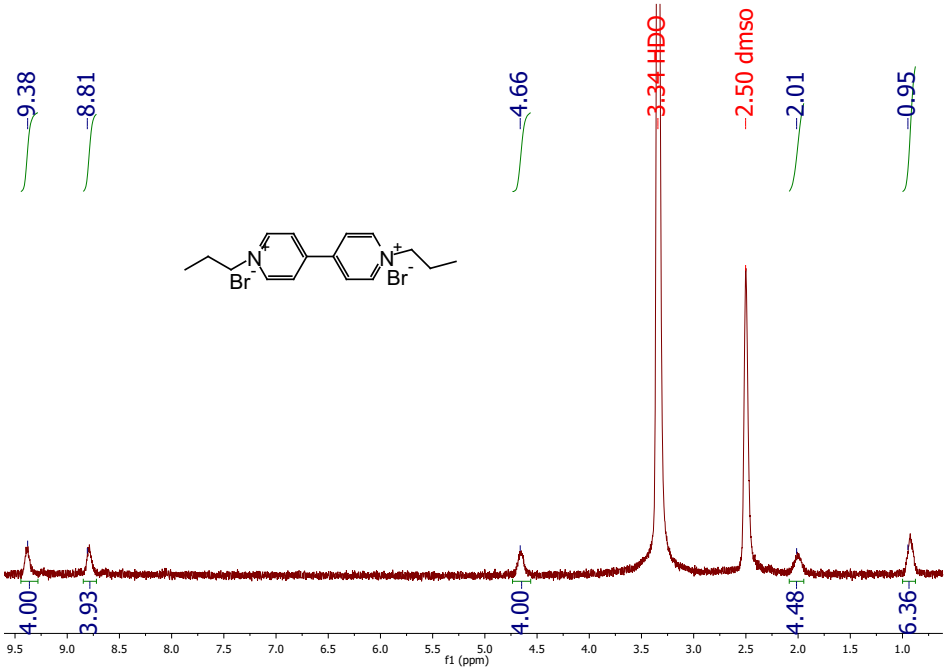

Figure A.3: Propyl viologen (DMSO−d_6).[62]

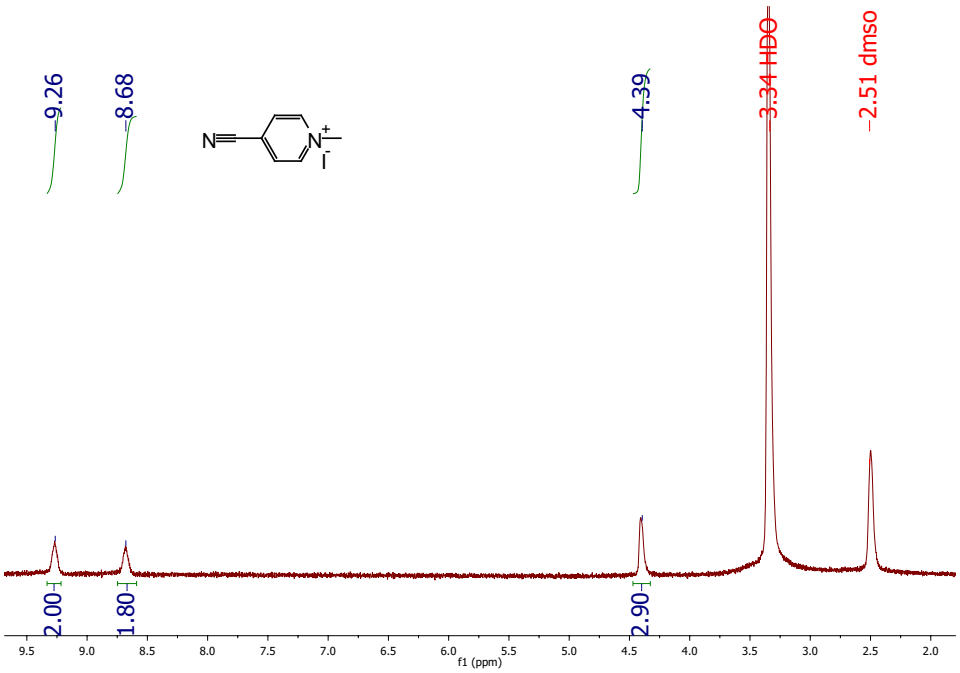

Figure A.4: PyC_1I (DMSO−d_6).[63]

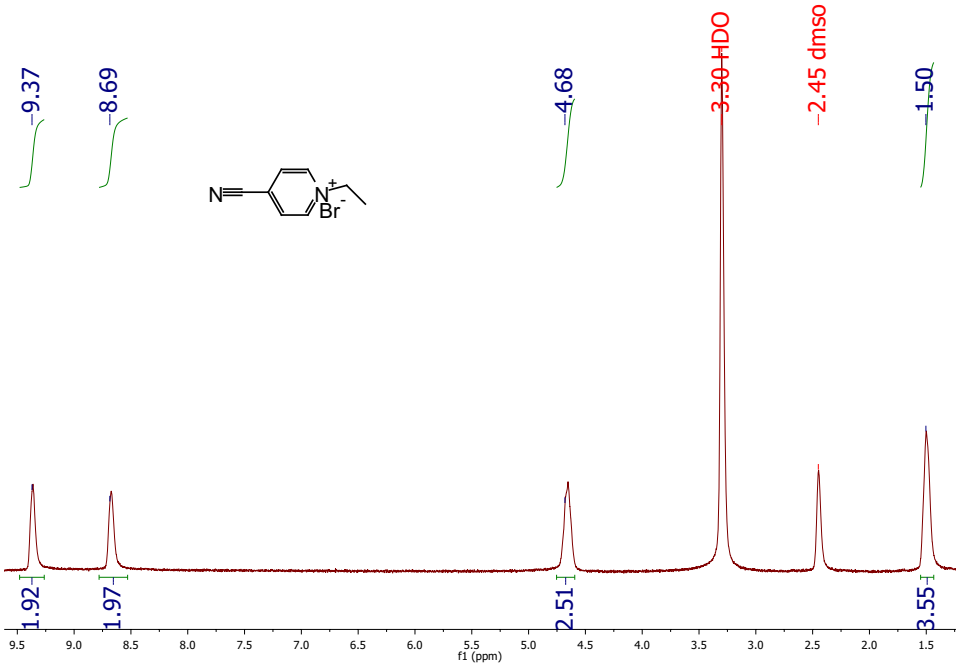

Figure A.5: PyC_2Br ($DMSO-d_6$).[64]

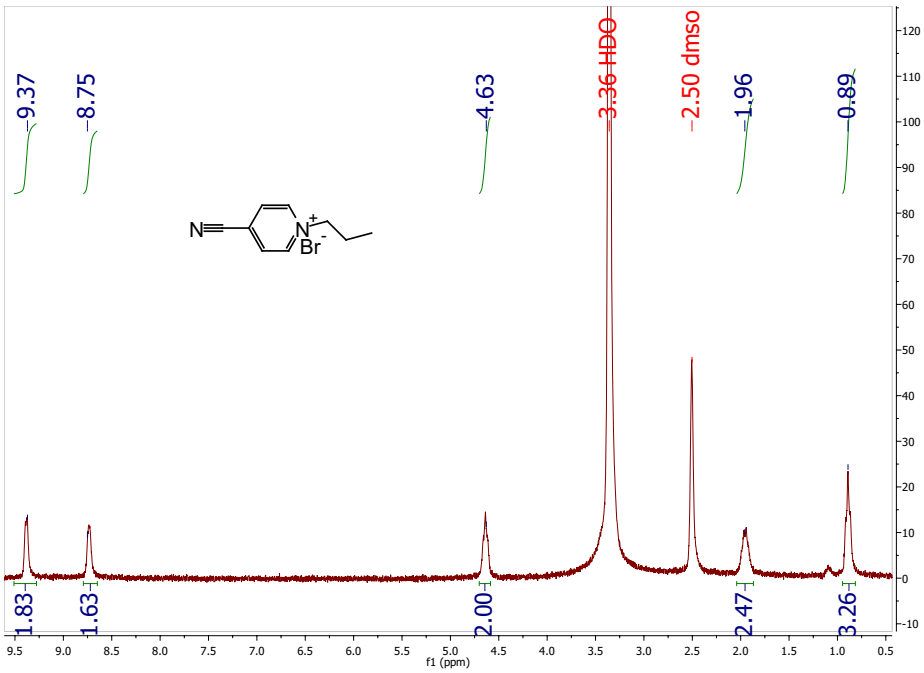

Figure A.6: PyC_3Br ($DMSO-d_6$).[65]

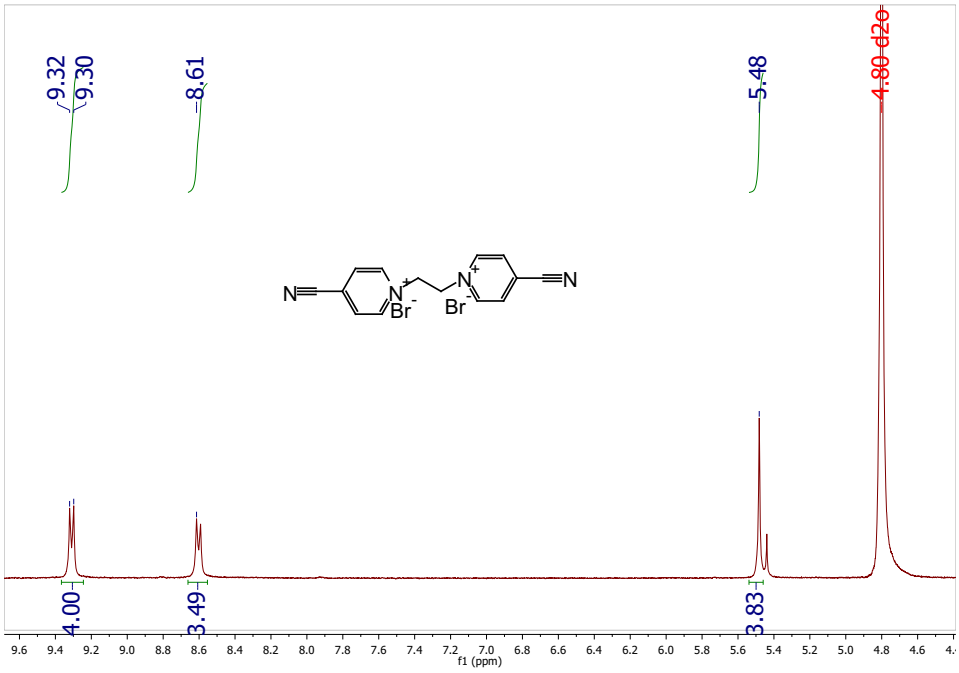

Figure A.7: PyC_2Br_2 (DMSO−d_6).[51]

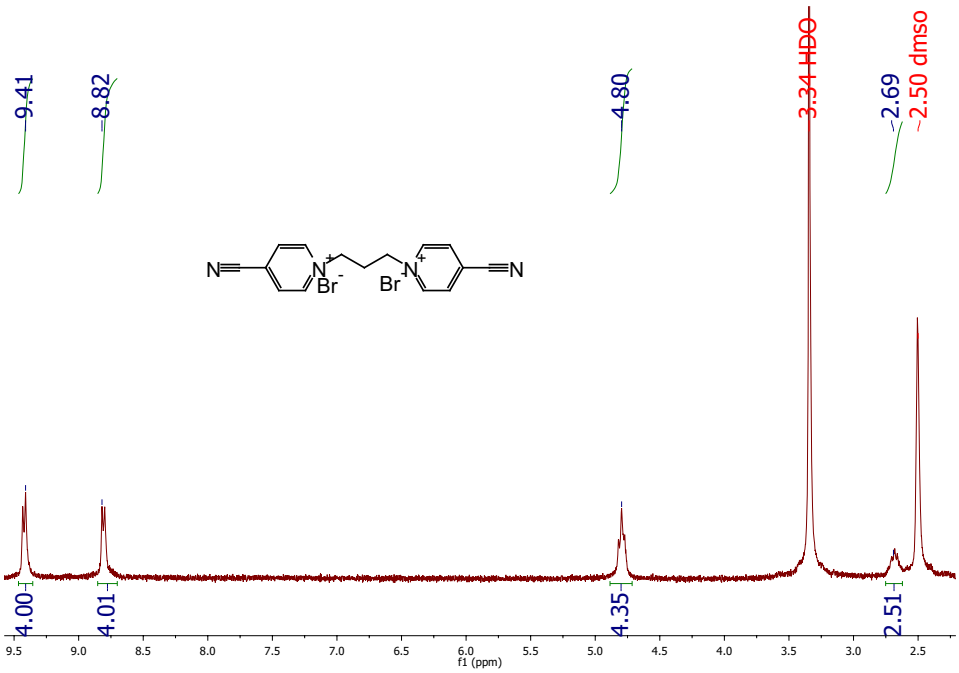

Figure A.8: PyC_3Br_2 (DMSO−d_6).[51]

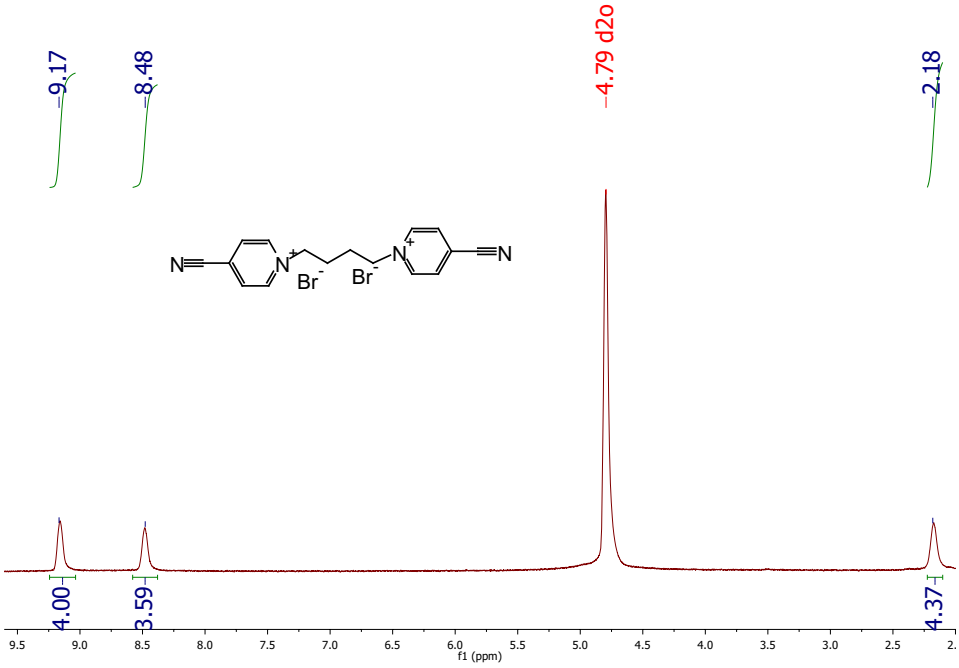

Figure A.9: PyC_4Br_2 (D_2O).[51]

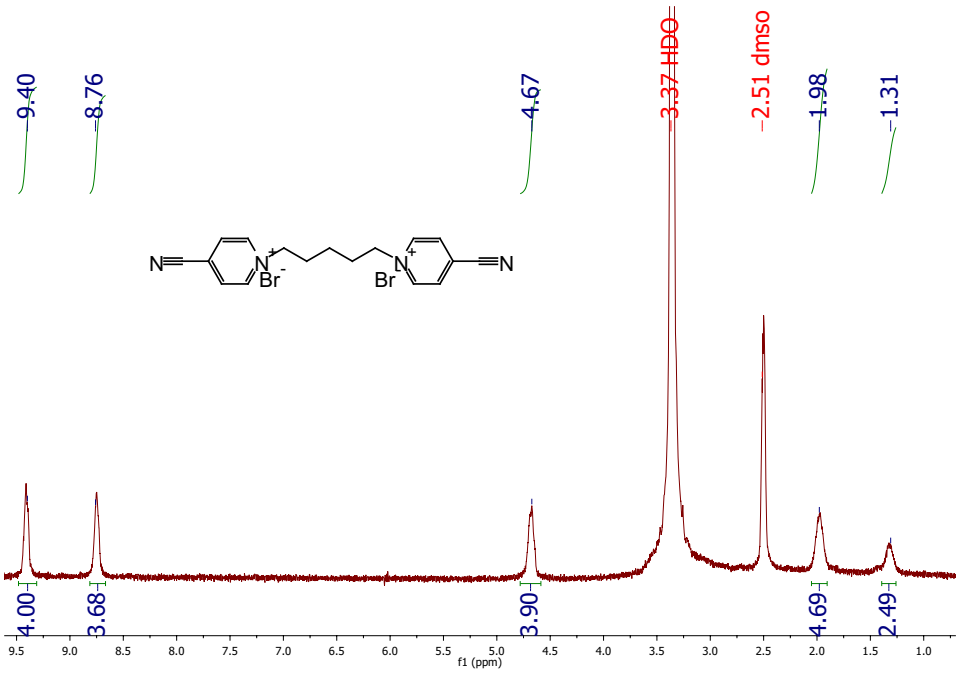

Figure A.10: PyC_5Br_2 ($DMSO-d_6$).[51]

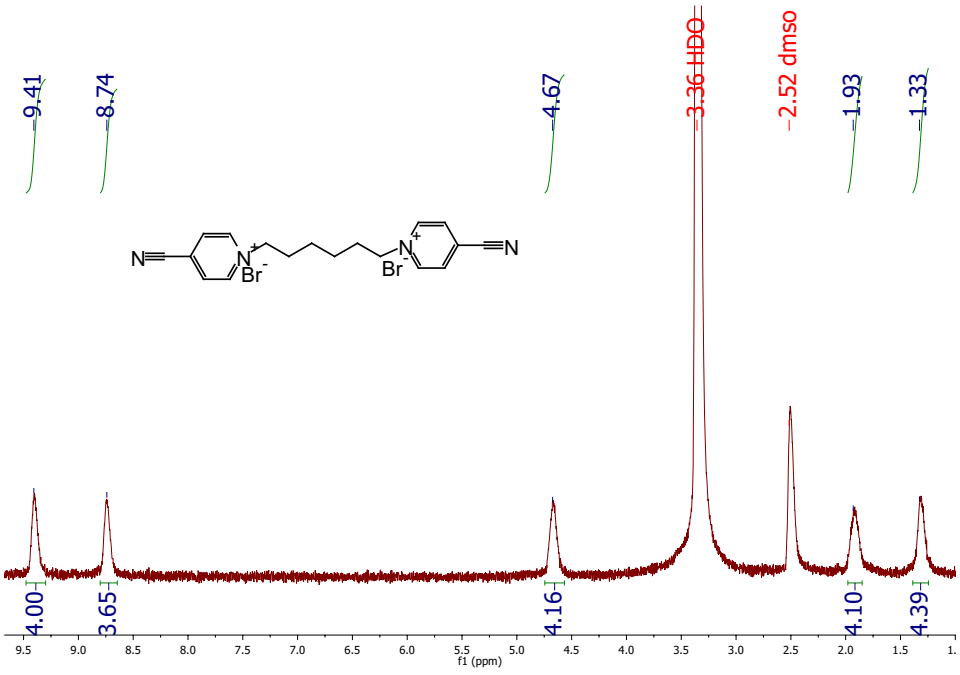

Figure A.11: PyC_6Br_2 (DMSO−d_6).[51]